2013-07-10

Large-Scale Testing of Passive Force Behavior for Skewed Abutments with High Width-Height Ratios

Katie Noel Palmer
Brigham Young University - Provo

BYU ScholarsArchive Citation

Palmer, Katie Noel, "Large-Scale Testing of Passive Force Behavior for Skewed Abutments with High Width-Height Ratios" (2013). *Theses and Dissertations*. 4176.
https://scholarsarchive.byu.edu/etd/4176

Large-Scale Testing of Passive Force Behavior for Skewed Abutments with High Width-Height Ratios

Katie Noel Palmer

A thesis submitted to the faculty of
Brigham Young University
in partial fulfillment of the requirements for the degree of

Master of Science

Kyle M. Rollins, Chair
Kevin W. Franke
Fernando S. Fonseca

Department of Civil Engineering

Brigham Young University

July 2013

ABSTRACT

Large-Scale Testing of Passive Force Behavior for Skewed Abutments with High Width-Height Ratios

Katie Noel Palmer
Department of Civil Engineering, BYU
Master of Science

The effects of seismic forces and thermal expansion on bridge performance necessitate an accurate understanding of the relationship between passive force and backwall deflection. In past case studies, skewed bridges exhibited significantly more damage than non-skewed bridges. These findings prompted studies involving numerical modeling, lab-scale tests, and large-scale tests that each showed a dramatic reduction in passive force with increased skew. Using these results, a correlation was developed between peak passive force and backwall skew angle. The majority of these tests had length to height ratios of 2.0; however, for several abutments in the field, the length to height ratio might be considerably higher than 2.0. This change in geometry could potentially affect the validity of the previously found passive force reduction correlation.

To explore this issue, laterally loaded, large-scale pile cap tests were performed with densely compacted sand at a length of 11 ft (3.35 m) and a height of 3 ft (0.91 m), resulting in a length to height ratio of 3.7. The backwall interface was adjusted to fit three various skew angles including: 0°, 15° and 30°. The behavior of both the pile cap and adjacent soil backfill were monitored under these conditions. The peak passive force for the 15° and 30° tests were found to be 71% and 45%, respectively, of the peak passive force for the 0° skew test. These findings are relatively consistent with previously performed tests. Passive forces peaked at deflections between 2% and 5% of the backwall height, decreasing with skew angle. All skews exhibited a log spiral failure plane that transitioned into a linear plane. These results also agreed with previously reported values for large-scale passive force-deflection tests. Rotation of the pile cap was detected in the direction opposite to the skew. Higher pressures were found to be on both corners of the pile cap than in the middle portion, as is suggested by the elastic theory.

Keywords: passive force, bridge abutment, large-scale, skew, pile cap, lateral resistance, backwall pressure, inclinometer, shape array

ACKNOWLEDGEMENTS

I would like to express my sincere appreciation to my chair, Dr. Kyle M. Rollins, for all of his time, patience, and support, as well as his example of integrity, dedication, and professionalism. He has instilled a sense of confidence in me that will be taken to my future endeavors within the field of engineering. I would also like to express my appreciation to the other members of my graduate committee, Dr. Kevin W. Franke, and Dr. Fernando S. Fonseca for their time, encouragement, input, and sincere concern for my successfulness. I also thank my fellow graduate school classmates Bryan Franke, Aaron Marsh, and Jaycee Smith (my partner in crime) who helped to make this experience both fun and successful.

Most of all, I wish to thank my family, specifically my parents and four sisters, for their continual support throughout my studies and in all other aspects of my life. The immeasurable love and joy that they bring to my life makes all of my efforts and accomplishments worthwhile.

Funding for this study was provided by an FHWA pooled fund supported by the Departments of Transportation from the states of California, Minnesota, Montana, New York, Oregon, and Utah. Utah served as the lead agency with David Stevens as the project manager. This support is gratefully acknowledged; however, the conclusions and recommendations in this thesis do not necessarily represent those of the sponsoring organizations. I also express my appreciation to the Salt Lake City Airport Department for providing access to the test site used for this study.

TABLE OF CONTENTS

LIST OF TABLES

LIST OF FIGURES

1 INTRODUCTION

Thermal expansion and seismic forces cause passive forces to develop behind bridge abutments that can greatly affect the performance of the structure. These forces must be properly accounted for in design to ensure adequate bridge performance. Several large scale tests have been done in the past that have helped to understand these forces on non-skewed abutments (Duncan & Mokwa, 2001a; Lemnitzer et al., 2009; Rollins & Cole, 2006; Rollins & Sparks, 2002). However, when a bridge abutment interacts with soil backfill at a skewed angle, the passive forces may be significantly different. Bridges with skewed abutments have performed much worse than non-skewed bridges in recent earthquakes. For example, in the 2010 Chilean earthquake skewed bridges experienced about twice the damage rate of non-skewed bridges and repair costs were about four times higher than for non-skewed bridge (Toro et al., 2013).

The Department of Transportation has reported that about 41% of the 605,000 bridges in the United States bridge database are skewed (Nichols, 2012). Since bridges with skewed abutments are so prevalent, it is important to develop a relationship between skew angle and passive resistance. However, this relationship has not been fully identified and the majority of engineers completely disregard skew effects with respect to soil pressure during bridge design (Caltrans, 2010; Kunin & Alampalli, 1999). Instead, most agencies limit the skew of an integral structure to 30° or less (Kunin & Alampalli, 1999), but by this point the backfill has already lost a significant amount of passive strength.

Varying backwall width to height ratios should also be considered during this process. This correlation can then be used for bridge design calculations to improve accuracy and save money on construction costs.

Recently, Rollins and Jessee (2012) conducted a series of laboratory tests to investigate the passive force on an abutment as a function of skew angle. The test wall interface was 2 ft (0.61 m) high by 4 ft (1.22 m) wide. Based on these tests, the passive force was found to decrease significantly as a function of skew angle and a reduction factor, R_{skew} was proposed by the equation

$$R_{skew} = \frac{P_{P-skew}}{P_{P-no\ skew}} = 8.0 * 10^{-5}\theta - 0.018\theta + 1.0 \tag{1-1}$$

where $P_{P\text{-}skew}$ and $P_{P\text{-}no\ skew}$ are the peak passive forces for a skewed and a non-skewed abutment, and θ is the skew angle.

To validate this equation for walls closer to field conditions, a series of large scale tests were undertaken in 2012. Marsh (2013) reported results for a 5.5 ft (1.68 m) high wall 11 ft (3.35 m) wide with wingwalls transverse to the direction of loading. Franke (2013) reported results for the same wall but with MSE wingwalls running parallel to the direction of loading. Both of these studies generally confirmed the validity of Equation 1-1; however, the walls tested by Rollins and Jessee (2012), Marsh (2013), and Franke (2013) all had length to height ratios of 2.0. For many abutments in the field, the length to height ratio might be considerably higher than 2.0 and this change in geometry could potentially affect the validity of Equation (1-1) for these conditions.

When an abutment displaces into the backfill, the failure surface extends beyond the end of the abutment, increasing the effective width of the abutment. This increase in effective width owing to 3D edge shear has been defined by Ovesen (1964). According to Ovesen (1964), the 3D failure geometry for non-skewed abutments and anchors is directly dependent upon the width to height ratio of the loaded area. As this L/H ratio increases, the effective width decreases and 3D effects lose significance. Currently, the impact of 3D effects on skewed anchors still remains unknown. Since these effects have the capacity to alter passive pressures by as much as double their magnitudes, it is important to investigate this relationship in greater depth.

1.1 **Research Objectives**

The primary objectives of this experiment are:

1. To determine the passive force-displacement curves for skewed abutments with larger length to width ratios from large scale tests
2. To provide comparisons of the passive force of skewed abutments relative to normal abutments with these larger L/H ratios.
3. To develop simple procedures for calculating passive force-displacement curves for skewed abutments.

1.2 **Scope of Research**

Large-scale testing was performed on a sand backfill behind a pile cap to simulate the horizontal movement of a bridge abutment into the backfill. Since a typical highway bridge abutment is wider than it is tall, (Shamsabadi et al., 2006) three tests were performed on the pile cap with an interface width of 11 ft (3.35 m) and a depth of 3 ft (0.91 m) for skew angles of 0°, 15°, and 30°. The backfill consisted of dense poorly graded sand. Two actuators pushed the pile cap longitudinally and measurements were taken for the passive force deflection curves, backfill heave, shear failure surface, and the movement and rotation of the pile cap. Test results were then compared with previous lab test results performed by (Jessee, 2012) in which they developed an equation for computing the passive force for a given skew angle. Additionally, pressure plates installed on the interface of the 30° skew wedge provided data to assess the progression of horizontal pressure distribution during pile cap movement. Computer software models PYCAP and ABUTMENT were later used to provide passive force calculations for comparison purposes.

2 LITERATURE REVIEW

2.1 Introduction

Results obtained from previous research studies provide the basis of our current understanding regarding soil-structure interaction. This valuable information was developed using computer analysis, lab-scale experiments, large-scale experiments, and fully-functioning bridges in the field. Case studies were also performed on post-earthquake structures. These results not only increase our understanding, but also generate the development of theories, methods, and codes for the improvement of bridge design. Research incorporated both skewed and normal bridges within the studies.

Since multiple passive earth pressure theories exist in the geotechnical realm, studies were performed to determine which of these provided the most accurate predictions in comparison to actual test data. A proper understanding of these theories along with a basic knowledge of the forces acting on the backfill soil wedge during bridge movement improves accuracy of passive earth pressure predictions for design purposes. Explanations of these forces, earth pressures, and related theories for skewed and normal bridges as well as pertinent studies are presented in this portion.

2.2 Forces due to Skewed Bridges

The longitudinal movement of a bridge causes a force to be exerted on the supporting abutments. When a bridge is skewed, the total longitudinal force, P_L can be separated into two components—one that is parallel to the skewed backwall and one that is normal to it. For equilibrium of the bridge to be maintained, opposing forces from the backfill at the soil-wall interface must counteract these two components. These forces within the soil backfill are known as the shearing resistance P_R, and passive force P_P. Figure 2-1 illustrates the geometry of force distributions that occur on a skewed bridge when longitudinal forces are applied.

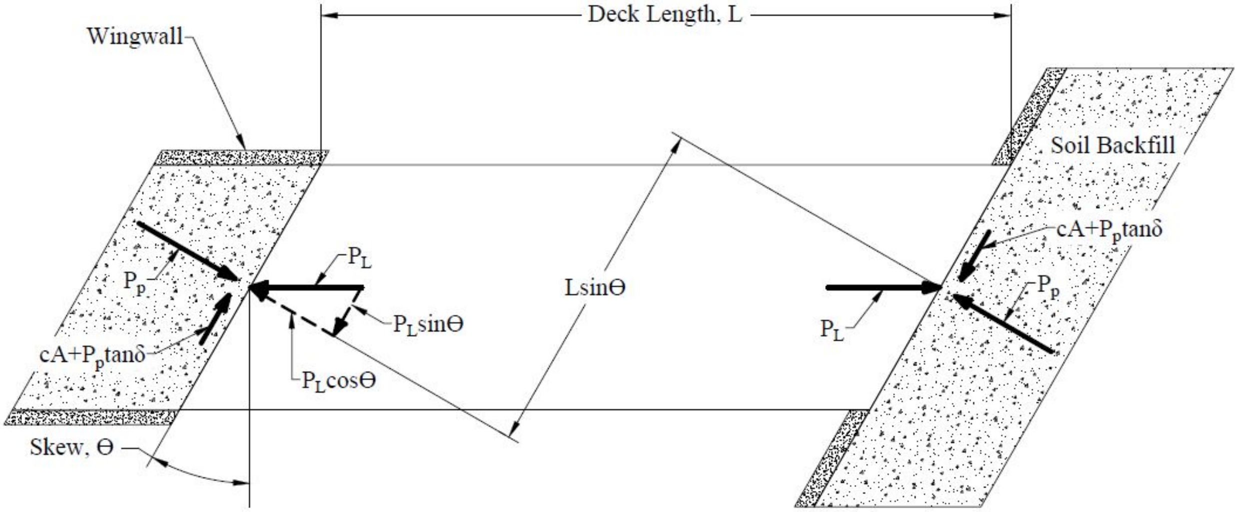

Figure 2-1: Typical distribution of forces on a bridge with skewed abutments.

The passive force, shear resistance, and the applied shear force component of the longitudinal force can all be equated in terms of the longitudinal force as seen in Equations (2-1), (2-2), and (2-3) (Burke Jr., 1996). The abutment will slide against the soil backfill if Equation (2-4) is not satisfied. Additionally, the external forces acting on both ends of the superstructure will cause the bridge to rotate towards the acute corners of the structure (counterclockwise direction in Figure 2-1) if the inequality in Equation (2-5) is not satisfied (Burke Jr., 1996).

$$P_P = P_L \cos\theta \tag{2-1}$$

$$P_T = P_L \sin\theta \tag{2-2}$$

$$P_R = cA + P_P \tan\delta \tag{2-3}$$

$$\frac{cA + P_P \tan\delta}{F_s} \geq P_L \sin\theta \tag{2-4}$$

$$\frac{(cA + P_P \tan\delta)L\cos\theta}{F_s} \geq P_P L\sin\theta \tag{2-5}$$

where

θ = skew angle of backwall

c = soil cohesion

A = backwall area

δ = angle of friction between backfill soil and abutment wall

F_s = factor of safety

L = length of bridge

These equations are only valid if the bridge remains stable. Therefore, if the bridge rotates, the distribution of forces on the abutment backwall will likely change, rendering these equations inaccurate. During the large-scale tests that were performed for this thesis, the rotation was restrained by the actuators, allowing for any variances in the equations above to be considered negligible.

When cohesion is ignored, Equation (2-5) reveals that the potential for bridge rotation is independent of passive force and bridge length but relies solely upon the interface friction angle and the skew angle of the backwall. If a typical design interface friction angle of 22° is used, the factor of safety decreases below 1.5 (Burke Jr., 1996) . For skews of 30° and 45° the factor of safety quickly declines to 0.7 and 0.4.

Computer simulations and experimental results both show the tendency of the passive soil wedge for skewed angles to be asymmetric. Asymmetry corresponds to an uneven force distribution from the abutment on the backfill. This is partially accredited to bridge deck rotation, which generates non-uniform loading of the abutment wall (Shamsabadi et al., 2006). Also, in the case of skewed abutments, the soil wedge is narrower. This leads to less soil resistance than a soil wedge from a normal interface (Shamsabadi et al., 2006).

For dense sand, movement of less than 5% of the height of the face is needed to mobilize full passive pressure (AASHTO, 2011). Other studies show that in many instances movements of even smaller magnitudes can achieve full passive pressure (Rollins & Sparks, 2002). This leaves little room for expansion or lateral movement of bridge decks. Composite backfill-structure interaction can greatly affect the stability of these bridges as well—specifically with semi-integral bridges. This topic is therefore recommended for further research to guide future bridge designs (Burke Jr., 1996).

2.3 **Passive Earth Pressure Theories**

When a structure and the surrounding soil experience lateral movement two types of primary earth pressures develop: active and passive. Passive earth pressures accumulate as a structure moves laterally into the adjacent soil, causing a compressive strain. This can be the result of bridge expansion or earthquake ground motions. Active earth pressures occur when the structure pulls away from the soil and the passive pressures are released. Passive pressures are of much greater concern than active pressures when designing structures with high soil-structure interaction such as bridge abutments, soil retaining walls, deep foundations, and anchor blocks as illustrated in Figure 2-2 (Duncan & Mokwa, 2001b).

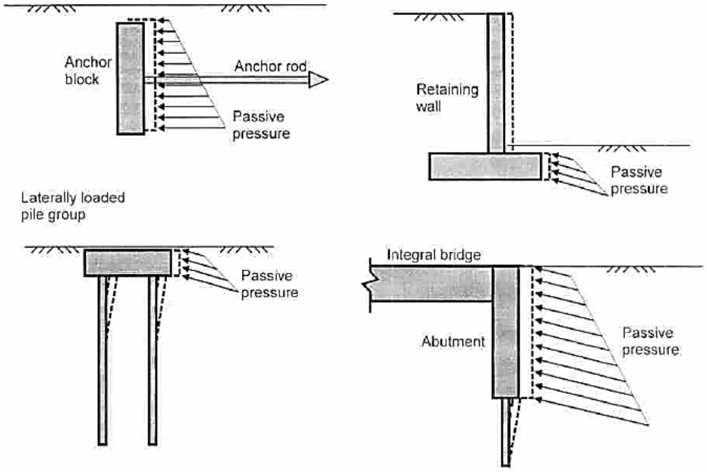

Figure 2-2: Examples of conditions where passive pressures resist displacements of structures (Duncan & Mokwa, 2001b)

During bridge movement, the force-resistance of abutments is largely provided by soil-backwall interaction and the backfill passive earth pressure. As stated previously, bridge designs often do not incorporate these important factors. Bozorgzahah (2008) stated that soil properties, abutment geometry, and the area of structure backfill all play key roles in determining the ultimate capacity and stiffness of bridge abutments (Bozorgzahah, 2008; Duncan & Mokwa, 2001b). Passive earth pressure is specifically dependent upon the soil friction angle, ϕ, soil-structure interface friction angle, δ, soil stiffness, K, and other backfill properties. It can be seen in Figure 2-3 (a) that as the abutment moves horizontally, the soil wedge moves both horizontally and vertically. This causes an upward shear force on the abutment and a downward shear force on the soil. The resultant passive force, E_p, is applied at an angle, δ_{mob}, above the normal to the soil-wall interface (Figure 2-3 (b)).

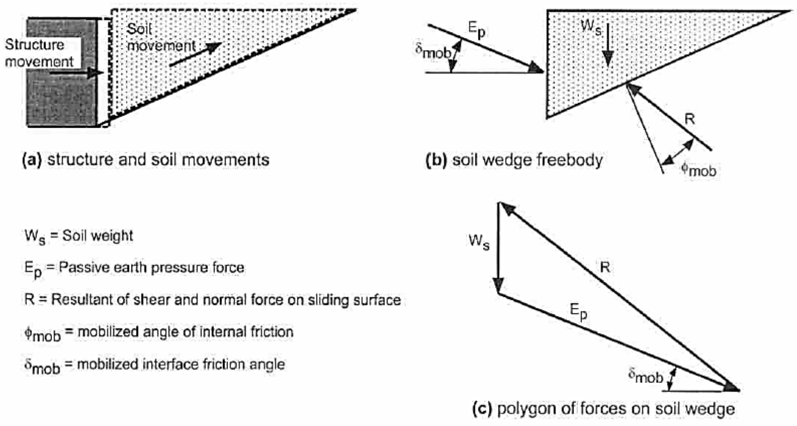

Figure 2-3: Movements, forces, and equilibrium requirements for a soil wedge during horizontal backwall movement (Duncan & Mokwa, 2001b)

In essence, interface friction directs the passive force downward. The resultant force, *R*, from the shear and normal forces satisfies static equilibrium while reacting at an internal soil friction angle, ϕ_{mob}, from the normal of the planar slip surface (Figure 2-3 (b) and (c)). When in motion, the resultant force is strong enough to force the soil wedge upward.

The magnitude of the passive force is typically estimated using the Rankine, Coulomb, or Log Spiral theories but other methods have been developed as well. These theories vary in parameters, assumptions, and limitations. Thus it is important to understand them individually so that proper application can be achieved. This is still an active branch of research.

2.3.1 Rankine & Coulomb

The Rankine and Coulomb theories were established centuries ago as the primary methods for calculating active and passive earth pressures. Even still, they are commonly being used throughout the field of geotechnical engineering. Both formulas assume a soil that is cohesionless, homogeneous, isotropic, well drained, and has a planar failure surface. The Rankine theory is a simpler method than that of Coulomb. It considers the wall to be frictionless with the soil-wall interface being vertical. The Rankine theory is better used for determining earth pressures on a vertical plane within a mass of soil, not against a wall (Hassiotis & Xiong, 2007). It is also known to be more accurate for predicting active pressures than for passive pressures. The linear variation in stress developed by the Rankine theory can be written as:

$$P_p = \frac{1}{2} K_p \gamma \mathrm{h}^2 + 2\sqrt{K_P} cH \tag{2-6}$$

in which *c* is the soil cohesion, *H* is the backwall height, and K_p is the passive earth pressure coefficient defined as:

$$K_p = cos\ \beta \left[\frac{cos\beta + [cos^2\beta - cos^2\phi]^{1/2}}{cos\beta - [cos^2\beta - cos^2\phi]^{1/2}}\right] \tag{2-7}$$

In this case, β is considered to be the embankment soil inclination above the horizontal, and ϕ is the angle of internal friction. When an embankment is not present K_p can be simplified to:

$$K_P = tan^2\left(45 + \frac{\phi}{2}\right) \tag{2-8}$$

Coulomb's theory incorporates a wall friction angle, δ, that can account for more complex conditions. It is an upper-bound theory which results in higher predictions than that of the Rankine theory. Coulomb's passive earth pressure coefficient can be seen as:

$$K_p = \frac{cos^2\phi}{cos\delta\left[1 - \sqrt{\frac{sin(\phi + \delta)\sin(\phi + \beta)}{cos\delta cos\beta}}\right]^2} \tag{2-9}$$

where β is again the angle of backfill slope, ϕ is the soil internal friction angle, and δ is the angle of wall friction. The failure surface for the Coulomb can be seen in Figure 2-4 below.

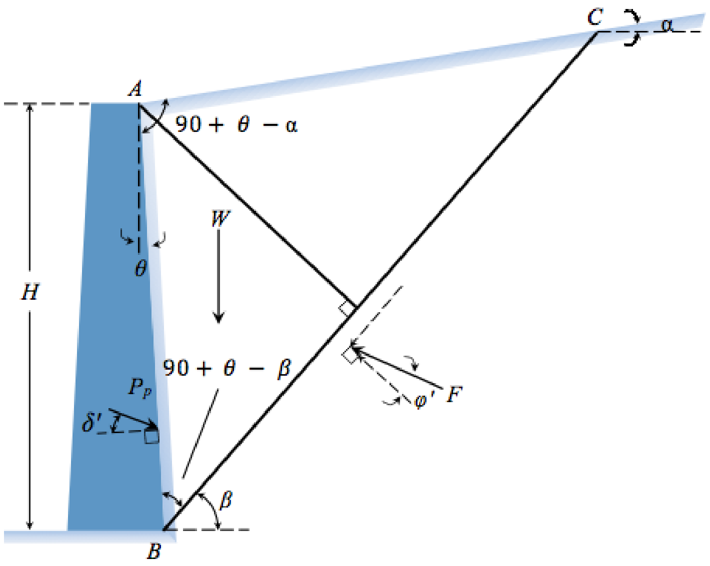

Figure 2-4: Coulomb failure wedge (Franke, 2013)

The Coulomb passive pressure predictions are relatively accurate until an interface friction angle, δ greater than 40% of the soil's internal friction angle, ϕ is addressed (Duncan & Mokwa, 2001b). At this point, values drastically over-predict the actual passive earth pressures.

2.3.2 Log Spiral

Developed by Terzaghi (1943), the logarithmic spiral (Log Spiral) theory's greater complexity causes it to be less widely used than the Rankine and Coulomb theories. It has, however, proven to be the most accurate in a greater variety of cases (Lemnitzer et al., 2009; Rollins & Sparks, 2002). It is also supported by other alternative theoretical procedures including that of Kumar and Subba Rao (1997), Soubra (2000) and Zhu and Qian (2000). Unlike the Coulomb theory, Log Spiral calculations do not have wall friction angle limitations.

The Log Spiral theory has a curved failure surface that provides a more realistic prediction of the probable behavior of the soil, including cohesion. Figure 2-5 reveals that the failure surface initially follows a logarithmic spiral plane which later transitions into a linear failure plane. This transition occurs when the soil reaches a point where the Log Spiral pressure is equivalent to a passive Rankine state.

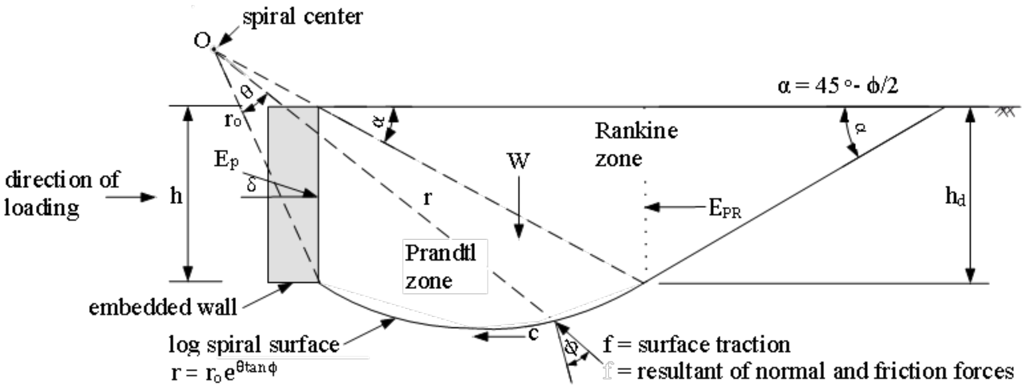

Figure 2-5: Log Spiral failure mechanism (Terzaghi, 1943)

As with the Coulomb theory, Log Spiral is an upper-bound theory. Terzaghi (1943) developed complex graphical solutions for application of the theory. To further improve the simplicity of the Log Spiral theory, charts and tables have also been established for generic cases. For example, AASHTO (2011) adopted Figure 2-6 from the U.S. Department of the Navy design manual for ease in finding the passive lateral earth pressure coefficient, K_p. This figure considers both wall friction and an accurate failure plane for a vertical or sloped wall and is designed for noncohesive soils. When parameters vary from those within these types of figures, more complex computational methods should be applied.

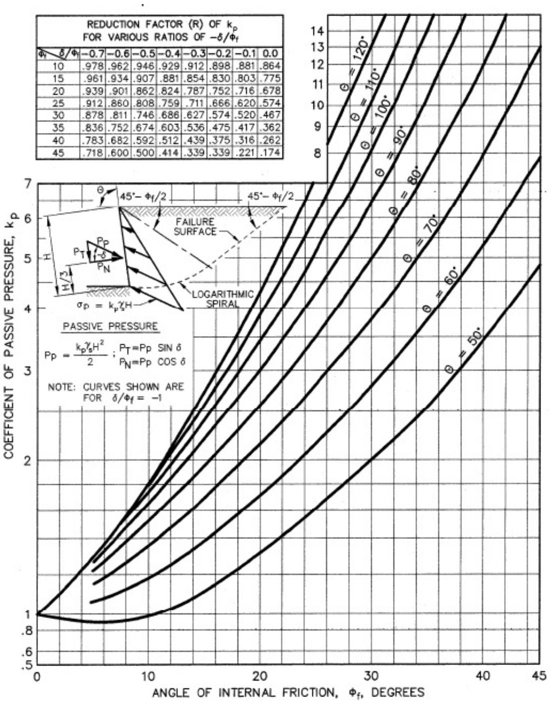

REDUCTION FACTOR (R) OF k_p
FOR VARIOUS RATIOS OF $-\delta/\phi_f$

ϕ_f \ δ/ϕ_f	−0.7	−0.6	−0.5	−0.4	−0.3	−0.2	−0.1	0.0
10	.978	.962	.946	.929	.912	.898	.881	.864
15	.961	.934	.907	.881	.854	.830	.803	.775
20	.939	.901	.862	.824	.787	.752	.716	.678
25	.912	.860	.808	.759	.711	.666	.620	.574
30	.878	.811	.746	.686	.627	.574	.520	.467
35	.836	.752	.674	.603	.536	.475	.417	.362
40	.783	.682	.592	.512	.439	.375	.316	.262
45	.718	.600	.500	.414	.339	.339	.221	.174

Figure 2-6: AASHTO computational procedures for passive earth pressures for vertical and sloping walls with horizontal backfill (AASHTO, 2011)

Computer programs have been developed specifically for application of the Log Spiral theory. Duncan and Mokwa (2001b) created the numerical model PYCAP that separates the passive pressure into three components: soil weight, surcharge, and cohesion. Ovesen's 3-D factor can also be incorporated in these calculations. This program is accurate for any values of δ but is recommended for simpler conditions (Duncan & Mokwa, 2001b). ABUTMENT is another program that was developed to simplify predictions of backfill capacities. Shamsabadi et al. (2007) created this software so that it has no soil type restrictions. The program can also be applied to seismic analysis. In 2012, Rollins and Jessee (2012) compared the two programs to measured field test results and concluded that the curves produced by both the PYCAP and ABUTMENT methods were relatively good.

2.4 Methods for Design

Determining an accurate relationship between passive force and backfill deflection can be critical in bridge design. This is typically done through passive force-deflection curves. These curves enable the prediction of soil reaction behind an abutment with bridge deck movement. Several methods have been developed with the purpose of providing simplicity over the Log Spiral theory while still maintaining accuracy in passive force-deflection predictions.

2.4.1 Method of Slices

AASHTO (2011) specifically recommends a trial procedure based on the wedge theory for complex parameters where wall friction values do not exceed one half the angle of internal friction. As can be seen in Figure 2-7 below, the method of slices incorporates the wedge theory by examining intermediate forces acting on a series of wedges along the failure plane. The mobilized horizontal passive capacity is obtained by summing these forces (Shamsabadi et al., 2007).

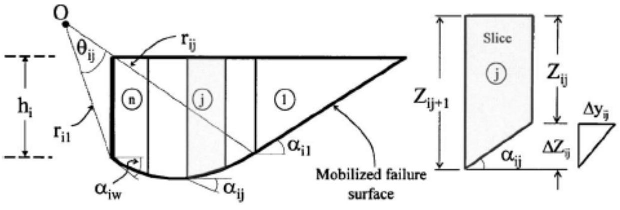

(a) **Geometry**

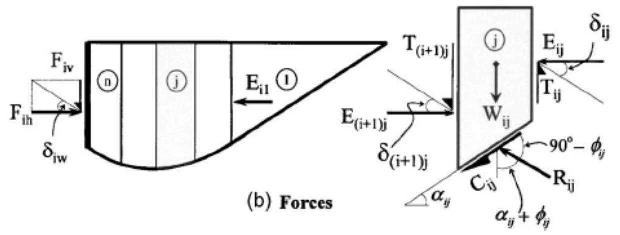

(b) **Forces**

Figure 2-7: Mobilized logarithmic-spiral passive wedge using method of slices (Shamsabadi et al., 2007)

2.4.2 Hyperbolic Model and Bilinear Method

In addition to the method of slices, the wedge theory serves as the foundation for other design methods that are also currently being used in design practices. Two of these methods include the hyperbolic model and bilinear method (Caltrans, 2001; Duncan & Mokwa, 2001b). As can be seen in Figure 2-8, passive resistance is often assumed to follow a hyperbolic trend line (Duncan & Mokwa, 2001b; Shamsabadi et al., 2007). In the hyperbolic model, the equation for this line includes parameters for the average soil stiffness, K, and the maximum abutment force, F_{ult}, developed at a maximum displacement, y_{max}.

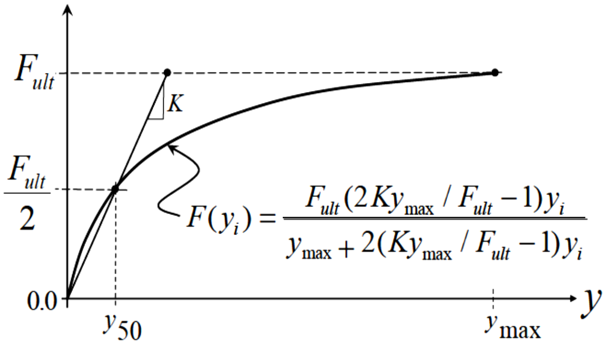

Figure 2-8: Hyperbolic force-displacement (HDF) model (Shamsabadi et al., 2006)

This is a simplified equation that has been tested and found to be in agreement with equations incorporating multiple other parameters (Shamsabadi et al., 2007). However, it does not account for the residual strength that occurs once maximum passive pressures have been achieved.

The bilinear method used by Caltrans (2010) was developed via full-scale abutment testing to determine the passive force resistance based on ultimate static force. The bilinear method is easy to apply but assumes a uniform pressure distribution instead of the hyperbolic shape that force-displacement curves typically experience (see Figure 2-9). This method also neglects variable soil strength parameters and residual strength. However, this method has still proven to produce very accurate approximations for backfill resistance capacities.

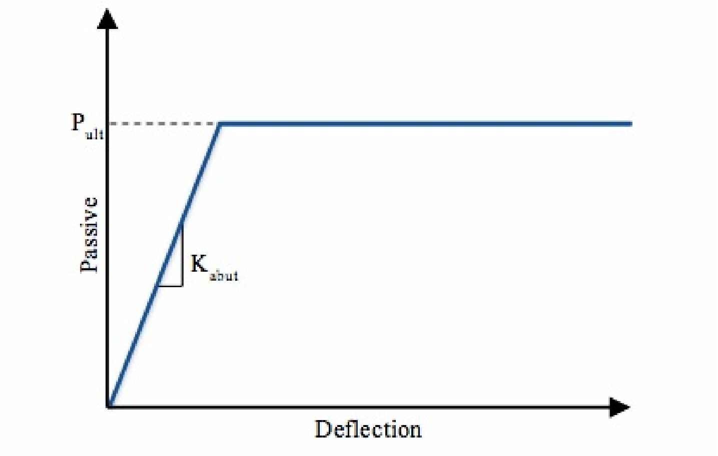

Figure 2-9: Estimated passive force-deflection curve as developed by the bilinear method

The initial stiffness, K_i, used by Caltrans (2010) can be estimated by Equation (2-10) for soil types meeting the following specifications:

- Standard penetration, upper layer [0 to 10 ft (0 to 3 m)] $N = 20$ (Granular soils)
- Standard penetration, lower layer [10 to 30 ft (3 to 9 m)] $N = 30$ (Granular soils)
- Undrained shear strength, $s_u > 1500psf \quad (72KPa)$ (Cohesive soils)
- Shear wave velocity, $v_s > 600\ ft/sec \quad (180\ m/sec)$
- Low potential for liquefaction, lateral spreading, or scour

NOTE: $N =$ The uncorrected blow count from the Standard Penetration Test (SPT)

Fill that does not meet these requirements should use the suggested stiffness in Equation (2-11). Furthermore, this stiffness must be adjusted to incorporate the ratio between the backwall width, *w*, and height, *h*.

$$K_i \approx \frac{50\mathrm{kip/in}}{\mathrm{ft}} \text{ or } \left(\frac{28.70\mathrm{kN/mm}}{\mathrm{m}}\right) \qquad (2\text{-}10)$$

$$K_i \approx \frac{25\mathrm{kip/in}}{\mathrm{ft}} \text{ or } \left(\frac{14.35\mathrm{kN/mm}}{\mathrm{m}}\right) \qquad (2\text{-}11)$$

$$\mathrm{K_{abut}} = \begin{cases} \mathrm{K_i} \times \mathrm{w} \times \left(\dfrac{\mathrm{h}}{5.5\ \mathrm{ft}}\right) & \text{US units} \\ \mathrm{K_i} \times \mathrm{w} \times \left(\dfrac{\mathrm{h}}{1.7\ \mathrm{m}}\right) & \text{SI units} \end{cases} \qquad (2\text{-}12)$$

The passive pressure, P_p, can then be estimated by incorporating the effective abutment wall area, A_e, with the maximum passive pressure 5.0 ksf (239 kPa) obtained during large-scale testing, and the height proportional to the height of the tested abutment walls.

$$\mathrm{P_P} = \begin{cases} \mathrm{A_e} \times 5.0\ \mathrm{ksf} \times \left(\dfrac{\mathrm{h}}{5.5\mathrm{ft}}\right) & (\mathrm{ft, kip}) \\ \mathrm{A_e} \times 239\ \mathrm{kPa} \times \left(\dfrac{\mathrm{h}}{1.7\mathrm{m}}\right) & (\mathrm{m, kN}) \end{cases} \qquad (2\text{-}13)$$

2.4.3 Ovesen-Brinch Hansen Method

Unfortunately, none of the previous theories account for 3D effects. They are purely planar and therefore do not incorporate the width of the pile cap and the resulting failure surface. To take this into consideration, a correction factor can be applied with the Ovesen-Brinch Hansen Method.

Ovesen (1964) performed tests on two size-varying anchor slabs with sand behind them. In these passive pressure tests, Ovesen simulated a slab of infinite length and one of a defined length. Results showed passive pressures to be higher than expected for slabs with shorter widths. This was due to the increased effective width of the failure wedge that extended beyond the edges of the slab. His calculations were based on a log-spiral failure plane and showed that the correction factor can range from 1.0 for a wall of infinite length to 2.0 for narrower structures (Duncan & Mokwa, 2001b; Shamsabadi et al., 2007). This data was used to develop Equation (2-14) for approximating the ultimate capacity, T_{ult}, of embedded anchor blocks incorporating 3D end effects using a width correction factor, M.

$$T_{ult} = M(K_P - K_a)p_0'bh \tag{2-14}$$

where

$$M = 1 + (K_P - K_a)^{0.67}\left[1.1E4 + \frac{1.6B}{1 + 5\left(\frac{b}{h}\right)} + \frac{0.4(K_P - K_a)E^3B^2}{1 + 0.05\left(\frac{b}{h}\right)}\right]$$

$K_P = \textit{coefficient of passive earth pressure}$

$K_a = \textit{coefficient of active earth pressure}$

$p_0' = effective\ overburden\ pressure\ at\ midheight\ of\ anchor\ block$

$B = 1 - \left(\frac{b}{s}\right)^2$

$E = 1 - \frac{h}{z + h}$

$b = \textit{width of anchor block}$

$s = \textit{center to center spacing of anchor blocks}\ (\textit{for only 1 block } s = 0)$

$h = \textit{height of anchor block}$

$z = \textit{depth of top of anchor block below ground surface}$

2.5 Integral and Semi-Integral Bridges

The reduction in passive earth pressure of skewed bridges has a greatest effect on integral and semi-integral bridges where the abutments are rigidly connected to the bridge deck. It is therefore important to describe the dynamics between passive force and these types of structures. Integral and semi-integral bridges contain a rigid connection that causes the abutments to be directly affected by deck movement and soil resistance. These bridges have dramatically increased in popularity in recent decades (Steinberg & Sargand, 2010) due to several advantages that have been found over a more traditional design. Cooler climates such as Canada and northern portions of the United States have even adopted integral bridges as one of their preferred bridge designs (Dicleli & Erhan, 2010; Hassiotis & Xiong, 2007; Kunin & Alampalli, 1999). An integral bridge is a design that incorporates the bridge deck, abutments, and supporting steel H piles into one rigid frame structure (see

Figure 2-10 below). This type of design has a variety of advantages including: elimination of problems and costs due to the use of joints and bearings, reduced number of foundation piles, increased load capacity and load distribution, and in-built resistance to uplift at the end of the abutment (Hassiotis & Xiong, 2007; Kunin & Alampalli, 1999).

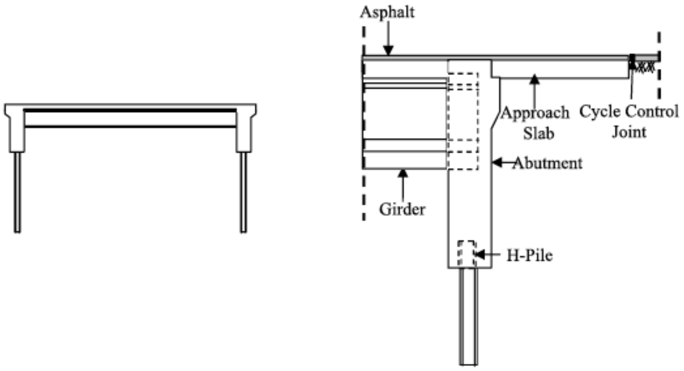

(a) (b)

Figure 2-10: (a) A typical single span integral abutment bridge, (b) details of the abutment (Dicleli & Erhan, 2010)

Abutments and foundations of integral bridges are designed to be more flexible than other bridges to account for the rigidity of the superstructure. To obtain this flexibility, often only one row of steel H piles is used in providing longitudinal support. Decreased passive earth pressures of skewed abutments would be considered an advantage for integral bridges due to the additional flexibility it provides (Dicleli & Erhan, 2010).

Engineers will often neglect the soil-bridge interaction effects of integral bridges for live load analysis (Kunin & Alampalli, 1999). In design, overestimating the passive earth pressure would lead to underestimating the bending moments on the spans, causing them to be nonconservative in design (Hassiotis & Xiong, 2007). However, completely neglecting passive pressure would result in constructing a more laterally resistant structure than is necessary. Proper calculations of passive earth resistance would decrease construction costs while maintaining the integrity of the structure.

Although integral bridges have several advantages over traditional bridges, they have their drawbacks as well. Integral bridges tend to have settlement in the approach fill that causes voids near the abutment. They can also experience cracking in the wingwalls due to rotation and lateral displacement, require strong embankments or subsoil, and are restricted in length (Hassiotis & Xiong, 2007). To account for these shortcomings, semi-integral bridges have been developed. This design achieves a more flexible bearing surface by incorporating other bridge concepts such as elastomeric pads that rest on the abutment. The bridge deck, girders, and diaphragm are still incorporated into one rigid unit (see Figure 2-11).

Semi-integral bridges are beneficial because they combine the cost-effectiveness of a jointless deck with an ability to resist lateral movement. However, a proper understanding of the soil-structure interaction is still imperative if further advancement is to be made to ensure substructure stability of semi-integral bridges (Burke Jr. & Gloyd, 1997).

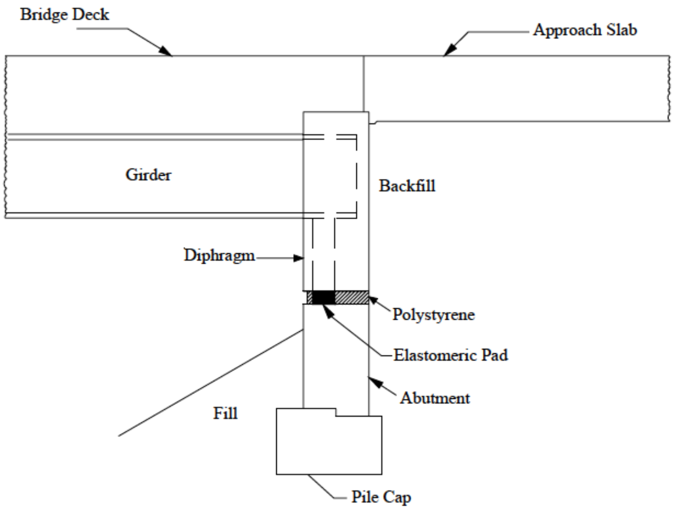

Figure 2-11: Typical semi-integral bridge abutment and diaphragm design (Shehu, 2009)

2.6 Passive Force-Displacement Tests for Non-Skewed Walls

When an abutment pushes into the adjacent backfill, the force of the resisting soil eventually reaches a maximum passive earth pressure before shearing. The passive earth pressure coefficient, K_p, can then be determined from this magnitude. The development of K_p was investigated by several laboratory and field tests (Duncan & Mokwa, 2001b; Rollins & Sparks, 2002; Terzaghi, 1943). Many of the more recent tests used their field results as a comparison for determining the accuracy of the passive earth pressure methods stated previously. Additionally, they obtained a ratio between the lateral displacement and wall height at which maximum passive earth pressures develop. When the design height of the abutment is known, this ratio can be very useful in designing allowable displacements of bridge decks. The following section consists of major studies conducted to simulate the movement of non-skewed abutments on backfill.

2.6.1 Duncan and Mokwa (2001)

Two passive pressure load tests were performed by Duncan and Mokwa (2001) on a pile group at the Virginia Polytechnic Institute. Horizontal loads were applied to a reinforced concrete anchor block with a size of 3.5 ft (1.1 m) high, 6.3 ft (1.9 m) long, and 3.0 ft (0.91 m) thick. The anchor block was first pushed against natural soil consisting of hard sandy silt (ML) and sandy clay (CL). This test was followed by a similar one containing backfill of compacted gravel with crusher run aggregate (GW-GM and SW-SM) and a relative density of 80%. The anchor block was loaded incrementally until beyond the point when failure had clearly been achieved.

Results of the passive pressure tests were then compared to calculations performed using the Rankine, Coulomb, and Log Spiral theories with and without incorporating the Ovesen-Brinch Hansen correction for 3D effects. Analysis showed the Log Spiral theory to be the most accurate when 3D effects were incorporated. The Coulomb theory and Log Spiral theory without Ovesen-Brinch Hansen correction were extremely similar due to the small interface friction angle of the two tests. They concluded that abutment load-deflection relationships are generally hyperbolic in nature as shown in Figure 2-12.

Furthermore, Duncan and Mokwa (2001) developed an equation for predicting this curve using the initial soil stiffness as the slope of the force-deflection curve.

$$P = \frac{y}{\frac{1}{K_{max}} + R_f \frac{y}{P_{ult}}} \tag{2-15}$$

where K_{max} is the initial tangent stiffness and R_f is the failure ratio.

In conjunction with this study, Duncan and Mokwa (2001) also developed the aforementioned program PYCAP, which is still being used by engineers today.

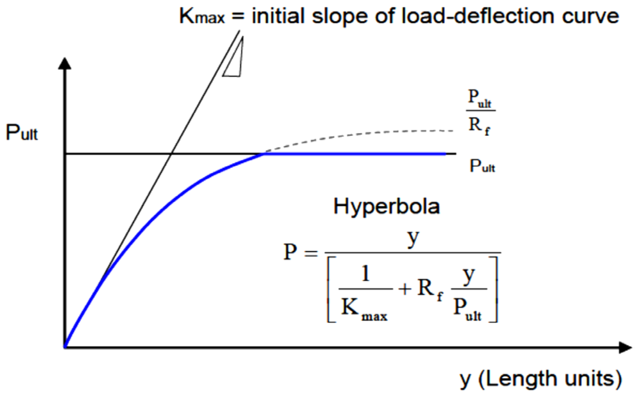

Figure 2-12: Hyperbolic force-deflection model presented by Duncan and Mokwa (2001)

2.6.2 Rollins and Sparks (2002)

Rollins and Sparks (2002) investigated the behavior of laterally loaded fixed-head pile groups along with their adjacent backfill passive pressures. This full-scale test consisted of nine steel pipe piles in a 3x3 grid, a 4.0-ft (1.22-m) thick concrete pile cap, and sandy gravel backfill. Five different methods were used to predict the passive earth pressure including the Rankine, Coulomb, Log Spiral and Caltrans methods as well as the program GROUP that is based on p-y curves. These calculations were then compared to the actual measured resistance to determine the accuracy of each method. For this study, the Log Spiral method proved to be the most accurate, agreeing well with the field test results obtained by Duncan and Mokwa (2001b). The

Coulomb method results were twice as high as those given by Log Spiral whereas Rankine, Caltrans, and GROUP all yielded very conservative results with Caltrans being the next closest to the Log Spiral method.

During this same study, Rollins and Sparks also presented a complete summary of previous experiments performed for assessing passive pressures (see Table 2-1). This table also presents ratios between wall height and displacement that were required to develop full passive pressures in each test.

Table 2-1: Chronological Summary of Medium to Large-Scale Passive Pressure Experiments and Test Results (Rollins and Sparks)

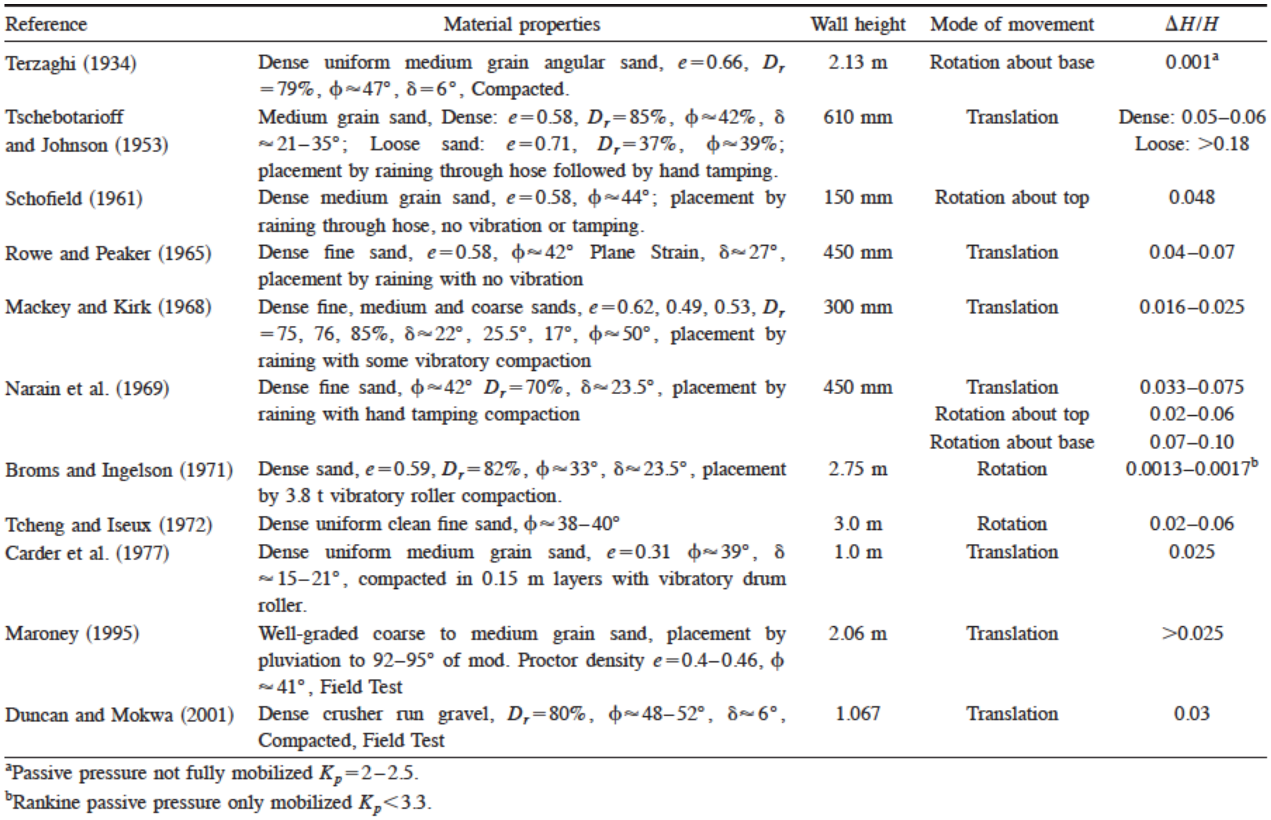

Reference	Material properties	Wall height	Mode of movement	$\Delta H/H$
Terzaghi (1934)	Dense uniform medium grain angular sand, $e=0.66$, $D_r=79\%$, $\phi\approx 47°$, $\delta=6°$, Compacted.	2.13 m	Rotation about base	0.001^a
Tschebotarioff and Johnson (1953)	Medium grain sand, Dense: $e=0.58$, $D_r=85\%$, $\phi\approx 42\%$, $\delta\approx 21-35°$; Loose sand: $e=0.71$, $D_r=37\%$, $\phi\approx 39\%$; placement by raining through hose followed by hand tamping.	610 mm	Translation	Dense: 0.05–0.06 Loose: >0.18
Schofield (1961)	Dense medium grain sand, $e=0.58$, $\phi\approx 44°$; placement by raining through hose, no vibration or tamping.	150 mm	Rotation about top	0.048
Rowe and Peaker (1965)	Dense fine sand, $e=0.58$, $\phi\approx 42°$ Plane Strain, $\delta\approx 27°$, placement by raining with no vibration	450 mm	Translation	0.04–0.07
Mackey and Kirk (1968)	Dense fine, medium and coarse sands, $e=0.62$, 0.49, 0.53, $D_r=75$, 76, 85%, $\delta\approx 22°$, 25.5°, 17°, $\phi\approx 50°$, placement by raining with some vibratory compaction	300 mm	Translation	0.016–0.025
Narain et al. (1969)	Dense fine sand, $\phi\approx 42°$ $D_r=70\%$, $\delta\approx 23.5°$, placement by raining with hand tamping compaction	450 mm	Translation Rotation about top Rotation about base	0.033–0.075 0.02–0.06 0.07–0.10
Broms and Ingelson (1971)	Dense sand, $e=0.59$, $D_r=82\%$, $\phi\approx 33°$, $\delta\approx 23.5°$, placement by 3.8 t vibratory roller compaction.	2.75 m	Rotation	$0.0013-0.0017^b$
Tcheng and Iseux (1972)	Dense uniform clean fine sand, $\phi\approx 38-40°$	3.0 m	Rotation	0.02–0.06
Carder et al. (1977)	Dense uniform medium grain sand, $e=0.31$ $\phi\approx 39°$, $\delta\approx 15-21°$, compacted in 0.15 m layers with vibratory drum roller.	1.0 m	Translation	0.025
Maroney (1995)	Well-graded coarse to medium grain sand, placement by pluviation to 92–95° of mod. Proctor density $e=0.4-0.46$, $\phi\approx 41°$, Field Test	2.06 m	Translation	>0.025
Duncan and Mokwa (2001)	Dense crusher run gravel, $D_r=80\%$, $\phi\approx 48-52°$, $\delta\approx 6°$, Compacted, Field Test	1.067	Translation	0.03

[a] Passive pressure not fully mobilized $K_p=2-2.5$.

[b] Rankine passive pressure only mobilized $K_p<3.3$.

As can be seen, displacements of approximately 2-6% of the wall height were typically needed to fully mobilize passive pressures. All tests were performed on medium to dense sands and gravels.

2.6.3 Rollins and Cole (2006)

Due to the large variety of passive force equations developed in the past, Rollins and Cole undertook a study in which they compared the predictions of these equations to actual field results of varying soil types. Their testing consisted of four different soil backfills that underwent cyclic loading behind a pile cap. These soil types included clean sand, fine gravel, course gravel, and silty sand.

Findings for cyclic loading revealed that the Rankine theory significantly underestimated the passive force while the Coulomb theory overestimated it (see Table 2-2 below). Furthermore, results indicated that the Log Spiral theory provided the most accurate estimates of the measured passive force.

Table 2-2: Comparison of Measured and Predicted Peak Passive Force (Rollins and Cole, 2006)

	Peak passive force (kN)			
Method	Clean sand	Fine gravel	Course gravel	Silty sand
Measured	1,090	774	1,997	1,428
Caltrans	914	914	914	914
Coulomb[a]	1,577 (1,577)[b]	1,149 (824)[b]	3,464 (2,224)[b]	1,575 (351)[b]
Log spiral[a]	922	817	1,688	1,210
Rankine[a]	357 (357)[b]	405 (300)[b]	719 (474)[b]	804 (194)[b]

[a] Methods includes Brinch Hansen (1996) 3D ® correction factors.

[b] Cohesion contribution computed using trial wedge for Coulomb and $2c\sqrt{K_P}$ for Rankine; numbers in parenthesis neglect cohesion contribution.

All four tests presented the same findings; hence, the accuracy of each method was not dependent upon soil type. Rollins and Cole accredited the accuracy of the Log Spiral method to the incorporation of both the cohesion of the soil and soil–structure interface friction angle within the equation.

2.6.4 Lemnitzer and Ahlberg (2009)

A full-scale cyclic lateral load test was performed on an abutment backwall with conditions simulating a typical California bridge design. Displacements occurred within a range of null to 11% of the wall height, *H* (*.11H*). The backwall was 8.5 ft (2.6 m) high by 14.75 ft (4.50 m) wide. The backfill consisted of silty sand (SE 30) with a depth that extended 2 ft (0.61 m) below the base of the pile cap. Gypsum columns were inserted into the backfill to examine the shear failure plane. Results indicated that maximum earth pressures occurred at a wall displacement of *0.03H*. Despite this being a dynamic test, results agreed very well with the range presented for static loading given by Rollins and Sparks (2002). The passive force resistance was underestimated by the Rankine and Coulomb methods but coincided well with the Log Spiral method and a method-of-slices approach. The gypsum columns also indicated a Log Spiral principal shear failure surface of the backfill.

2.6.5 Nasr and Rollins (2010)

Nasr and Rollins (2010) conducted a study in which they developed equations for predicting backfill passive resistance in 2D and 3D conditions. The computer software program PLAXIS was used for this study with soil parameters calibrated using PYCAP (Duncan & Mokwa, 2001a) and ABUTMENT (Shamsabadi et al., 2007). Results were compared to large-scale tests performed by Rollins et al. (2010).

Models were performed for loose silty sand and dense fine gravel behind a pile cap with depths of 3.67 ft (1.12 m) and 5.5 ft (1.68 m). The shear strain profile obtained for the homogenous sand backfill can be seen in Figure 2-13.

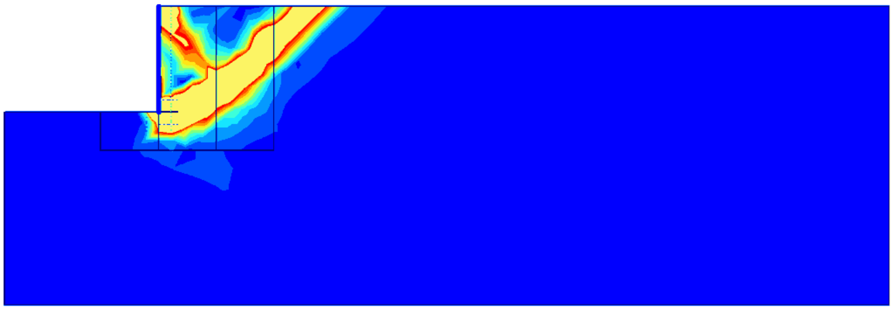

Figure 2-13: Observed shear strain profile obtained from PLAXIS 2D finite element model for homogeneous sand backfill (Nasr & Rollins, 2010)

This figure indicates a shear failure plane with a log spiral trend. Another shear plane can also be seen descending from the soil surface at the top of the pile cap interface to a location diagonally downward to the lower shear plane. This second shear plane failure separates the Prandtl zone from the Rankine zone (see Figure 2-5). The gravel backfill also indicated similar failure planes with the log spiral portion of the lower failure plane being slightly more defined.

2.7 Passive Force-Displacement Tests for Skewed Walls

Due to the uneven pressure distribution of skewed bridges, 3D effects must be considered in addition to the generic passive pressure behaviors that normal bridges present. When considering the effects of skew on integral bridges, force resistance by backfill soil pressures is greater on the obtuse side of the structure (Sandford & Elgaaly, 1993). This is also the case for cyclic loading due to earthquakes (Hassiotis & Xiong, 2007). The following studies all show these characteristics as well as other behaviors beneficial to gaining a clearer understanding of skewed abutment backfill.

2.7.1 Sandford & Elgaaly (1993)

Instrumentation was installed on an integral bridge with a 20° skew to monitor the effects of skew on lateral soil pressure distribution. Pressure cells were mounted on the back of the concrete abutments and temperature indicators were installed near the cite to monitor the air temperature. Recordings were taken for 33 months, accounting for bridge contraction during winter months and expansion during warmer weather. Results exhibited average pressures on both sides of the abutments to be relatively the same during winter months. However, by the middle of July the pressure on the obtuse side of the abutment was significantly greater than on the acute side. (Sandford & Elgaaly, 1993) used his findings to design a lateral pressure distribution for skewed abutments (Figure 2-14).

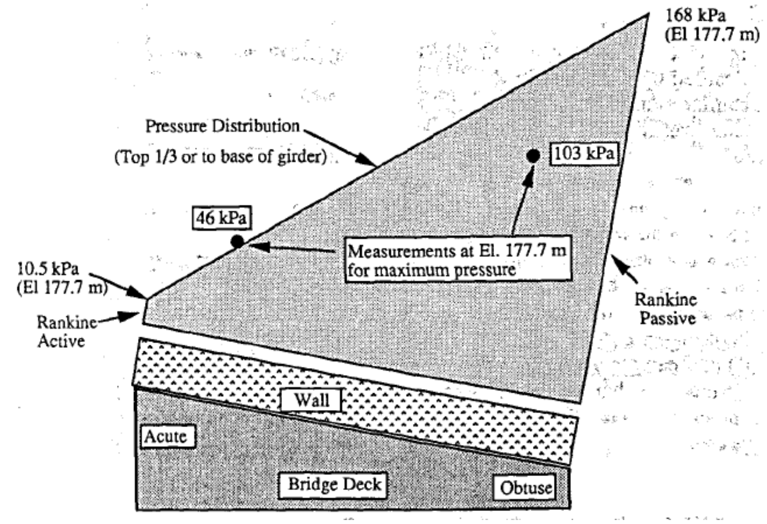

Figure 2-14: Design lateral pressure distribution for skewed abutments (Sandford & Elgaaly, 1993)

Sandford and Elgaaly obtained this design by combining actual measured data with both interpolated and linearly extrapolated values. Rotation of the abutment was predicted to be the cause for the higher pressures that developed on the obtuse side.

2.7.2 Shamsabadi et al. (2006)

Shamsabadi et al. (2006) identified passive force resistance behind a skewed abutment as a three-dimensional problem that incorporates bridge deck rotation with its lateral force-displacement capacity. Images such as the one presented in Figure 2-15 were used to portray the failure wedge adjacent to a damaged skewed bridge abutment.

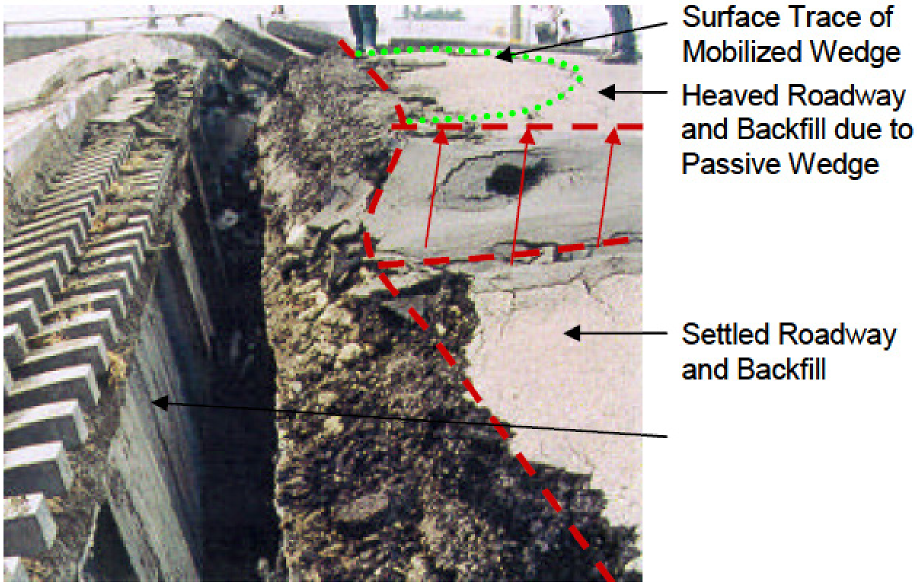

Figure 2-15: Passive wedge behind failed skewed abutment (Shamsabadi et al., 2006)

Shamsabadi analyzed both skewed and non-skewed abutments through observation and computer-simulated responses created by PLAXIS. In their findings, they were able to develop

3D nonlinear finite-element models that estimate soil capacities based on varying skewed abutments and their longitudinal displacement, as shown in Figure 2-16 (a) and (b).

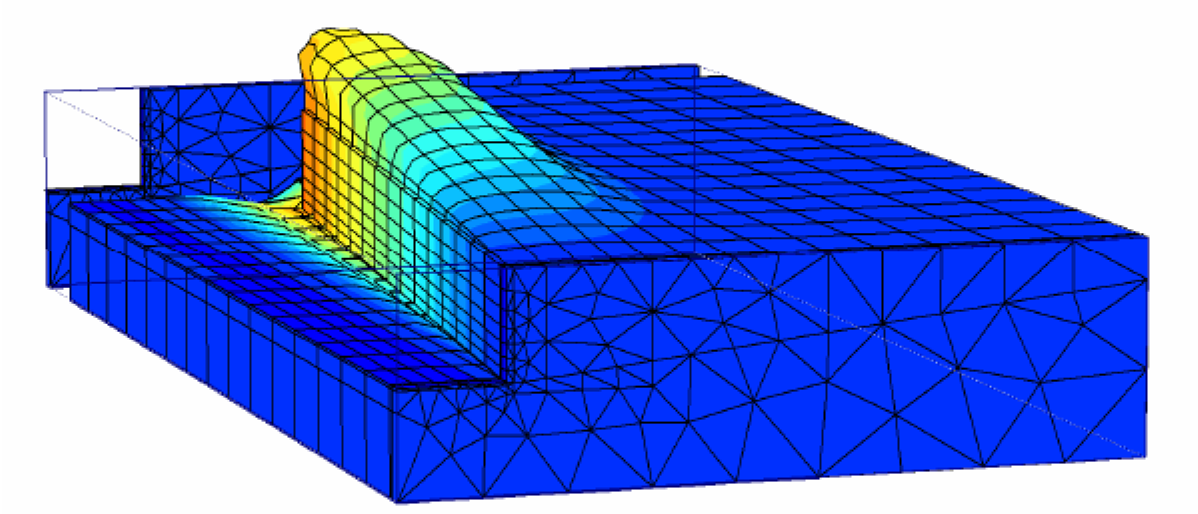

(a)

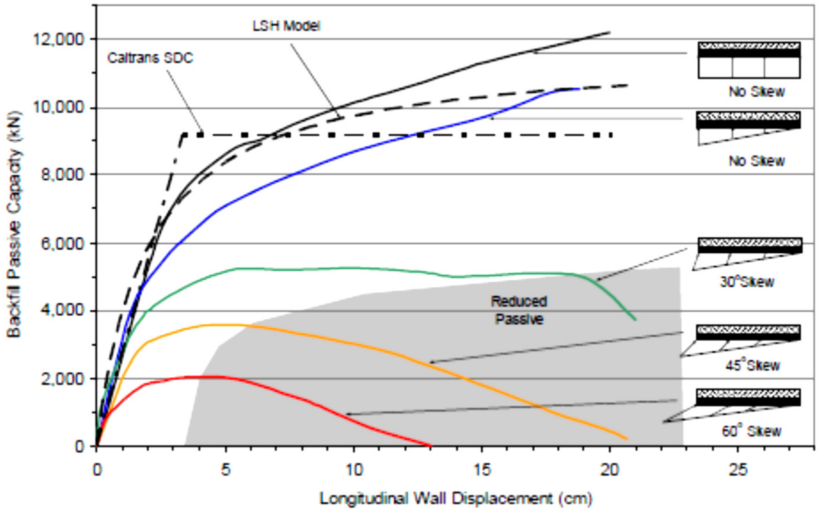

(b)

Figure 2-16: (a) 3D finite-element model of backfill displacement behind a 45° skew based on PLAXIS and (b) effect of skew angle on passive backfill capacity based on computer model PLAXIS (Shamsabadi et al., 2006)

They determined passive force resistance to decrease as the skew angle increased. They also concluded that the bridge rotates during movement, generating a non-uniform loading of the abutment wall. This creates an asymmetric passive soil wedge in which heave is greatest in the soil near the acute side of the abutment.

This study was performed with a length to height ratio of 13.6, but results still agreed with tests performed with a L/H of 2.0, suggesting that L/H geometry may not be important. However, this is still a numerical study result not yet confirmed by physical testing.

2.7.3 Rollins and Jessee (2012)

A small-scale test was performed by Rollins and Jessee (2012) to determine the effect of increased skew on passive resistance. The test layout consisted of a concrete wall 4.13 ft (1.26 m) wide and 2 ft (0.61 m) high that was pushed into confined dense sand backfill 3 ft (0.91 m) thick, extending 1 ft (0.30 m) below the wall to incorporate a possible log-spiral shear plane. Tests were performed with skew angles of 0°, 15°, 30°, and 45°.

As can be seen in Figure 2-17, the passive resistance significantly decreased with increased skew angle. Additionally, the passive resistance curves of the skewed angles experienced a plateau before receding. All tests experienced very similar initial stiffness values despite their variance in ultimate passive strengths.

Using results from this study, Rollins and Jessee (2012) developed the reduction factor mentioned in Chapter 1 Equation (1-1) for passive strength predictions of backfill adjacent to skewed bridge abutments. These results were also compared to those predicted by Shamsabadi et al. (2006) during his numerical analysis. Figure 2-18 shows these findings to be very similar.

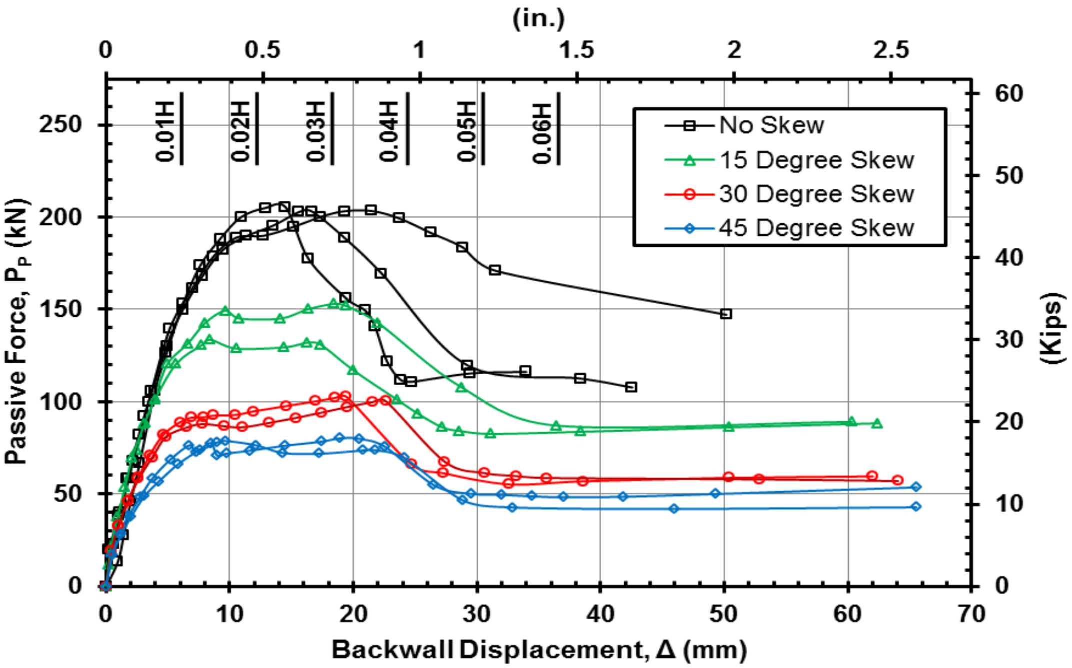

Figure 2-17: Force-deflection curve test results for skewed angles of 0°, 15°, 30°, and 45° Rollins and Jessee (2012)

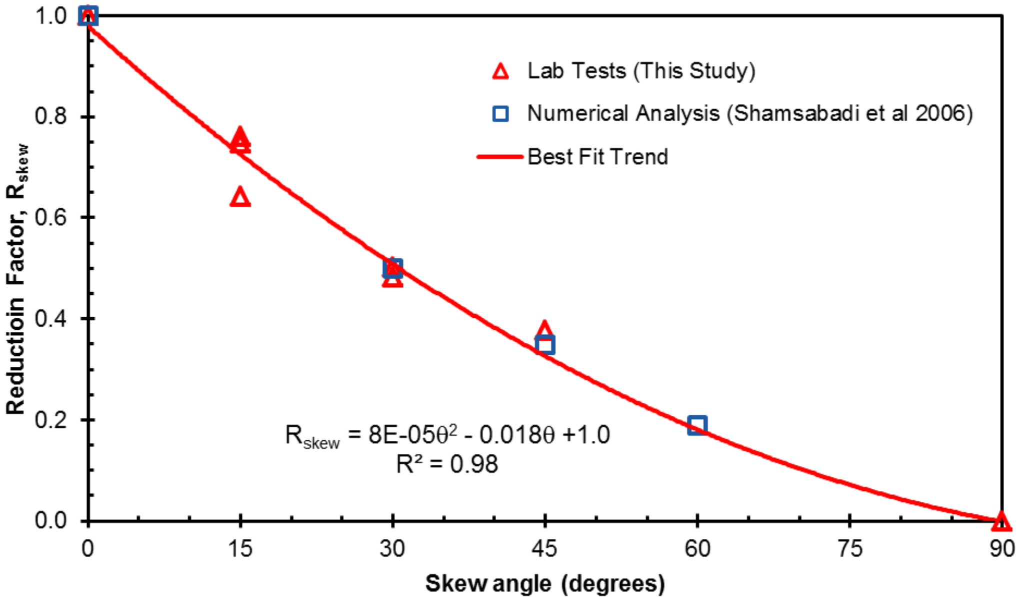

Figure 2-18: Reduction factor for bridge abutments presented by Rollins and Jessee (2012)

2.7.4 Rollins and Marsh (2013)

A large-scale test was performed by Rollins and Marsh (2013) to confirm the findings of Rollins and Jessee (2012). This study was accomplished by conducting tests at skew angles of 0°, 15°, and 30° at a backfill width of 11 ft (3.35 m) and a height of 5.5 ft (1.68 m)—a width to height ratio of 2.0. Results were found to generally agree with the reduction factor proposed by Rollins and Jessee (2012) given in Equation (1-1). The deflection required to obtain peak passive resistance decreased with increased skew angle. Skew was also shown to have an impact on pile cap rotation, backfill heave, and other behaviors. The shear failure planes resembled a log-spiral shape at the base that transitioned into a linear plane, and the Log Spiral method appeared to produce the most accurate peak passive force predictions.

2.8 Earthquake Case Studies

During an earthquake, bridge decks have a tendency to rotate away from the acute corner and towards the obtuse corner. This rotation decreases the length supported by the abutment, resulting in unseating of the bridge deck as can be represented by Figure 2-19 (Watanabe & Kawashima, 2004).

These outcomes have been seen in several case studies around the world and have resulted in damaged and collapsed bridge structures. Skewed bridges also induce other factors that lead to a weakened and damaged structure. The following case studies portray these detrimental outcomes.

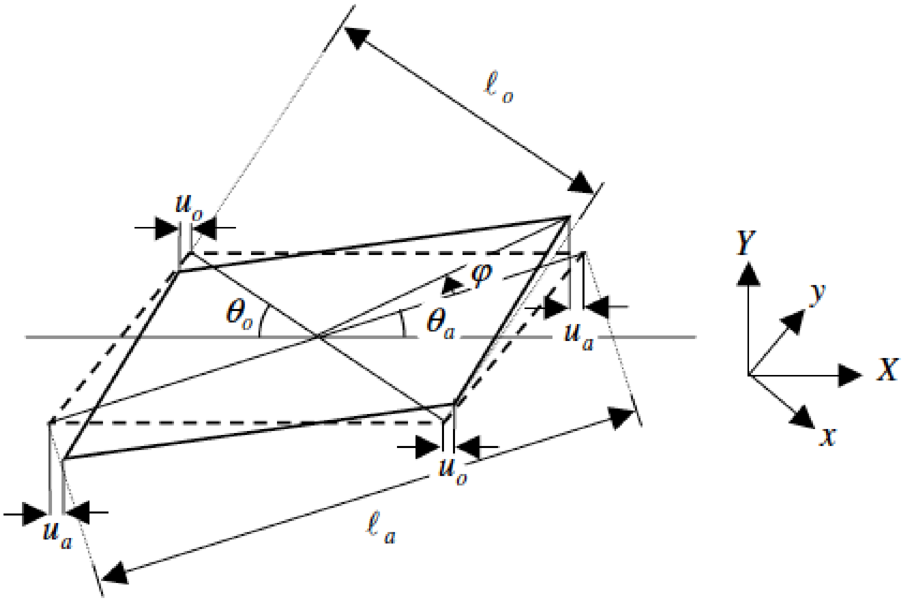

Figure 2-19: Decrease of Length Supported by Abutment due to Rotation of Deck (Watanabe & Kawashima, 2004)

2.8.1 Apirakvorapinit et al. (2012)

Following the 1994 Northridge earthquake in California, a case study was performed on the Pico-Lyons Bridge near Newhall, California. This bridge had a skew angle of 40°. Nonlinear finite-element modeling and push-over modeling were used to simulate the superstructure. A coinciding non-skewed bridge model was also analyzed to use as a baseline. Stresses in the girders were compared between the 0° and 40° skew simulations as can be seen in Figure 2-20.

Results from computer analysis agreed with field reports for locations of maximum damage and stress. These results revealed that the end girders for the skewed bridge model experienced 50% greater stress than in the non-skewed analysis. The girders on the obtuse corners experienced the greatest stress, agreeing with results from previously mentioned tests.

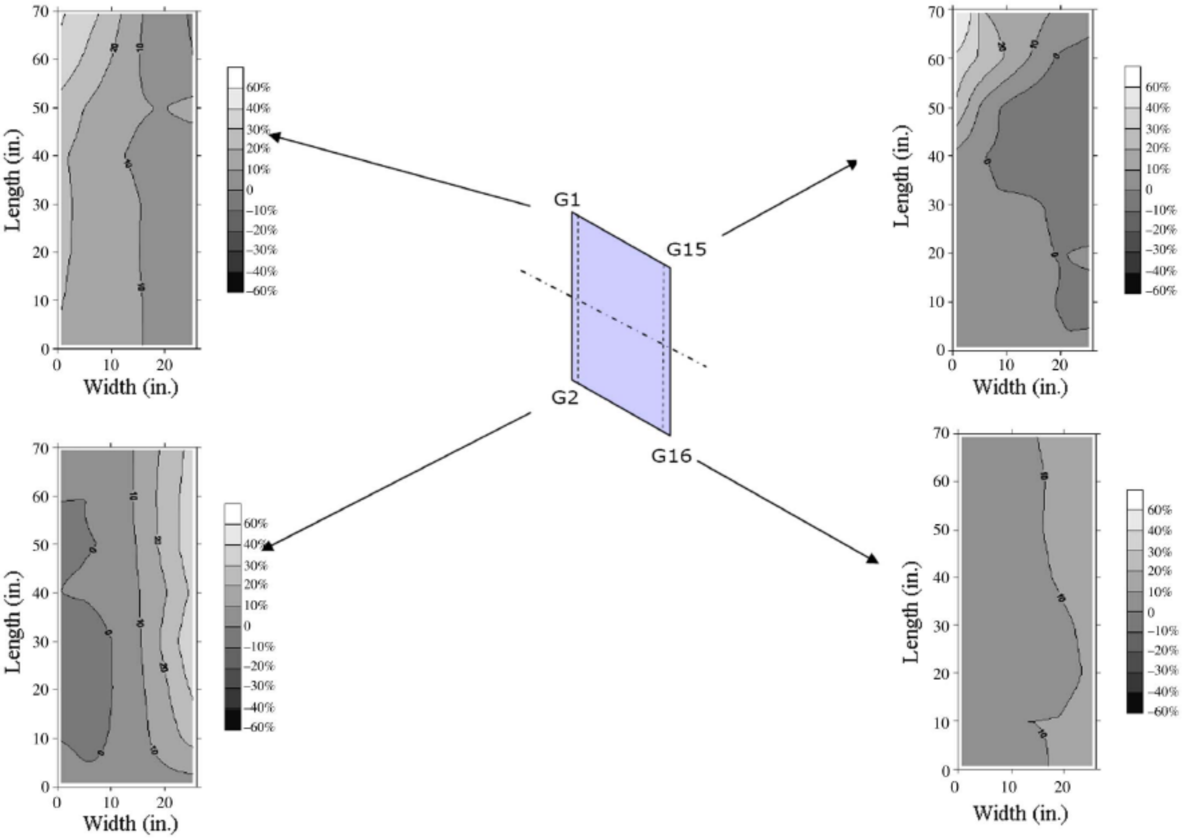

Figure 2-20: Maximum principal stresses on girders of skewed bridge (Apirakyorapinit et al., 2012)

Watanabe and Kawashima (2004) stated in the 2004 World Conference of Earthquake Engineering that unseating generally starts to occur at the acute edges. This connects with Apirakvorapinit et al. (2012) because as the obtuse corner of the bridge deck rotates into the backfill, the stress increases on that side and the acute corner is pushed outward. These results would be beneficial to consider when designing for seismic forces on a skewed bridge.

2.8.2 Maule, Chile Earthquake (2010)

In 2010, an earthquake struck Maule, Chile with a magnitude of 8.8. Teams of engineers from across the globe performed investigations throughout the affected region to assess damage and determine probable failure mechanisms. The majority of the bridges examined were designed using prestressed concrete girders supported by rubber pad bearings without stiff connections, including anchors. Recent Chilean design practices also omitted diaphragms, resulting in reduced in-plane stiffness and connectivity. This omission has shown to cause increased pounding on the shear keys as seen in Figure 2-21 below (Elnashai et al., 2010).

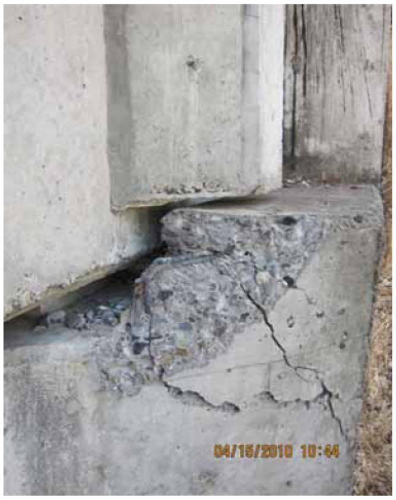

Figure 2-21: Damaged shear key at abutment. Chile Maule earthquake, 2010 (Elnashai et al., 2010)

At the conclusion of their investigations, engineers identified in-plane rotation of skewed bridges to be one of the most common causes of damage during the Maule earthquake (Unjohn, 2012). The skew caused an unbalanced effect between the superstructure and abutment that forced the rotation. Combining this with a reduced deck stiffness and weaker connections proved to be detrimental in some cases.

In one specific case study, two overpasses stood side by side but experienced dramatically different results. The north-bound overpass was a recently designed bridge with a skew angle of 45° whereas the south-bound bridge was older, included diaphragms and stopper mechanisms, and was not skewed (Unjohn, 2012). As a result of the earthquake, the skewed bridge completely collapsed while the non-skewed bridge suffered almost no damage at all as can be seen in Figure 2-22. This example demonstrates the harmful impact that rotation has on skewed bridges where inertial forces cause the deck to be unseated.

Figure 2-22: Collapse of skewed bridge deck adjacent to a functioning normal bridge. Chile Maule earthquake, 2010 (Unjohn, 2012)

In another case, a typical highway overpass from Route 5 was analyzed for a two-span bridge that was highly skewed. Major damage was shown due to a lateral shift of 11.8 in. (0.3 m) of the bridge deck. Cracks in the east embankment soil portrayed the soil deformation that occurred within the backfill (Figure 2-23). This deformation was later attributed to the passive pressure of the abutment with the embankment.

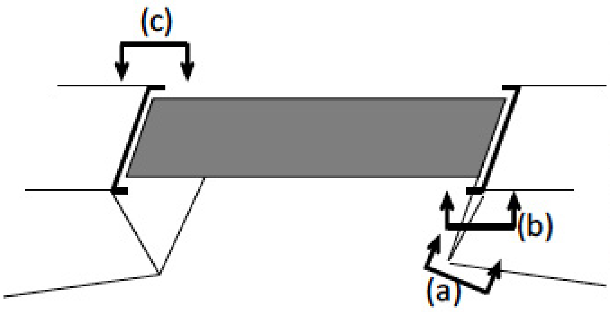

(a) Cracks on bridge embankment

(b) 41 cm gap at east abutment

(c) 25 cm gap at west abutment

Figure 2-23: (a) Cracks in embankment soil, (b) gap in west abutment, and (c) gap in east abutment of bridge due to large skew during the Chile Maule earthquake, 2010 (Unjohn, 2012).

In addition to the Maule earthquake studies mentioned previously, Toro et al. (2013) performed an assessment on 88 overpasses along Route 5. The average repair costs for skewed bridges were found to be 26% of their original construction costs whereas costs were only 7% for non-skewed bridges. Furthermore, skewed bridges were two times more likely to experience displacement or rotation of the superstructure than for non-skewed bridges. Their final conclusion was that skewed bridges are more vulnerable than non-skewed bridges and that current Chilean design provisions should be revised to account for this additional factor.

2.9 **Literature Review Summary**

As can be seen in the above studies, skewed abutments can dramatically affect how a bridge structure and adjacent fill behave. If these factors aren't properly considered, damage and even complete bridge failure can occur. Integral and semi-integral bridges are especially susceptible to damage due to skew but other bridge types have shown to be impacted by skew as well.

The Log Spiral theory has shown to be the most accurate predictor of passive pressures. Several methods have been created to increase the usability of this method. However, these methods do not take into account the dramatic reduction in passive pressures skew causes on backfill. This reduction can be estimated using Equation (1-1) developed by Rollins and Jessee (2012).

Although recent large scale field tests suggest that Equation (1-1) may be appropriate for typical conditions, the abutment wall length to height ratios for these tests are considerably smaller than would be expected for many abutments used in engineering practice. The results from the numerical analyses conducted by Shamsabadi et al (2006) with an L/H ratio of 13.6 suggest that this factor may not have a significant impact on the equation. Nevertheless, additional large scale physical testing is necessary to determine how significant the length to height ratio may be on the skew reduction factor.

Results from Rollins and Jessee (2012) also show a significant decrease in passive force for large displacements. Because the backfill in these tests was compacted to approximately 98% of the modified Proctor maximum density, it is unclear if this reduction in passive resistance will be typical for backfills compacted closer to the 95% standard.

3 FIELD TEST SETUP

This chapter contains information regarding the test location, geotechnical characteristics of the test site, layout of the test setup, geotechnical properties of the backfill material, and general testing procedures.

3.1 Site Description

Testing was performed at the Salt Lake City International Airport (SLC), approximately 1000 ft (305 m) north of the airport control tower. An aerial photograph of the test area location in relation to the airport control tower is shown in Figure 3-1.

The land was unused by the airport and conditions were favorable due to the flat topography and lack of vegetation. The local water table was located at a depth of 5 to 5.5 ft (1.52 to 1.68 m) below the ground surface. No utility lines ran above ground or below ground to conflict with testing. Also, no problems were encountered regarding the close proximity of the testing site to the airport control tower.

Figure 3-1: Aerial photo of testing site directly north of airport control tower (adapted from Google Earth)

3.2 Geotechnical Site Characterization

Over the past 17 years, several large-scale lateral load tests of drilled shafts and driven pile groups have been conducted at the SLC location (Christensen, 2006; Johnson, 2003; Nasr & Rollins, 2010; Rollins et al., 2005; Taylor, 2006). During these previous tests, the necessary subsurface site characteristics needed for this study were obtained through in-situ and laboratory testing. These results were used to produce the soil profile shown in Figure 3-2, which extended below the piles to a depth of 50 ft (15 m) below the ground surface (Christensen, 2006). Results showed that the upper 5 ft (1.5 m) of the soil profile consisted of imported gravel fill. The underlying sub layers consisted of alternating lean clay, sandy silt, and silty sand layers down to a depth of about 50 ft (15 m). Prior to this series of tests, the gravel fill was excavated and imported clean sand was compacted around the drilled shaft and pile groups. Additional soil characteristics are provided in Christensen (2006).

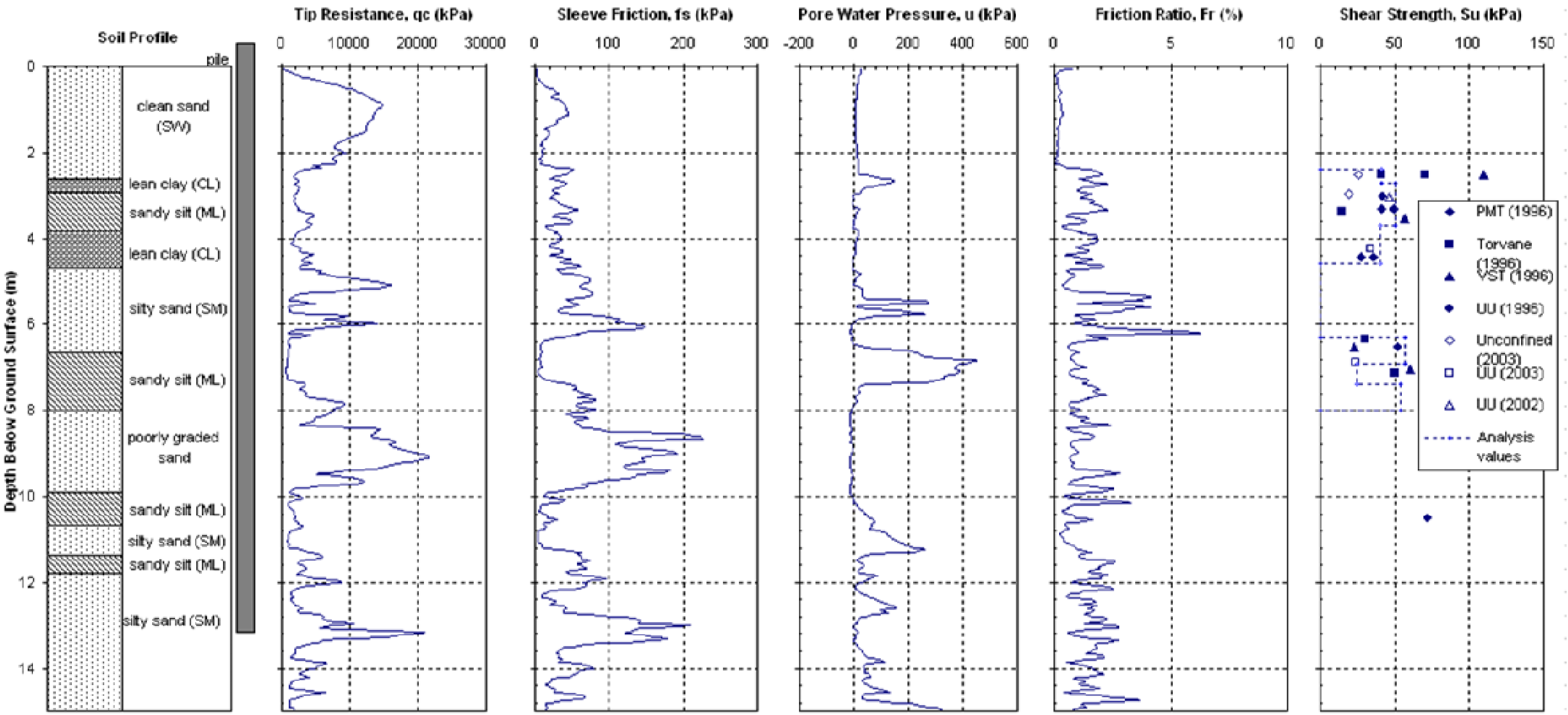

Figure 3-2: Idealized soil profile constructed from laboratory and in-situ test data (Christensen, 2006)

3.3 **Test Layout**

The test layout for each of the tests consisted of four primary components: the reaction foundation, a rectangular pile cap with 15° and 30° concrete wedge attachments, the loading apparatus, and the backfill zone. All components of the test setup were designed and used for previous tests except the newly installed 15° and 30° wedges. Plan and elevation views of the complete test setup are shown in Figure 3-3.

3.3.1 Reaction Foundation

Two 4-ft (1.22-m) diameter drilled shafts installed 12 ft (3.66 m) apart on center provided the base of the support for the reaction foundation. The east shaft extended 70 ft (21.35 m) into the soil and the west shaft extended to 55.2 ft (16.82 m). Alignment was in the east-west direction. Reinforcement of the shafts consisted of 18 #11 (#36) vertical bars with a #5 (#16) bar spiral at a pitch of 3 in (75 mm) for the first 35 ft (10.7 m) and then 9 #11 (#36) vertical bars with the spiral reinforcement at a pitch of 12 in (300 mm) for the remaining depths. Concrete cover was approximately 4.75 inches (120 mm) throughout the shafts. Concrete compressive strength was 6,000 psi (41 MPa). These shafts were also capped with 4-ft (1.22-m) square by 2-ft (0.61-m) thick concrete caps.

A sheet pile wall made of ASTM A-572 Grade 50 steel was installed on the north side of the two drilled shafts using a vibratory hammer. This AZ-18 sheet piling was driven to depths ranging from 33.6 to 35.6 ft (10.24 to 10.85 m) below the excavated ground surface. Both the north and south sides of the drilled-shaft/sheet-pile wall had a steel I-beam spanning the east-west direction with the strong axis oriented in the north-south direction. I-beams provided the foundation with additional lateral rigidity and were supported by additional stiffeners parallel to the strong axis. The I-beams had dimensions of 64 in (162.6 cm) high by 16 in (40.6 cm) wide by 28 ft (8.53 m) long. They were secured to the sheet pile wall and drilled shafts using eight 1.75 in (44 mm) diameter threaded “DYWIDAG” bars with minimal post-tensioning.

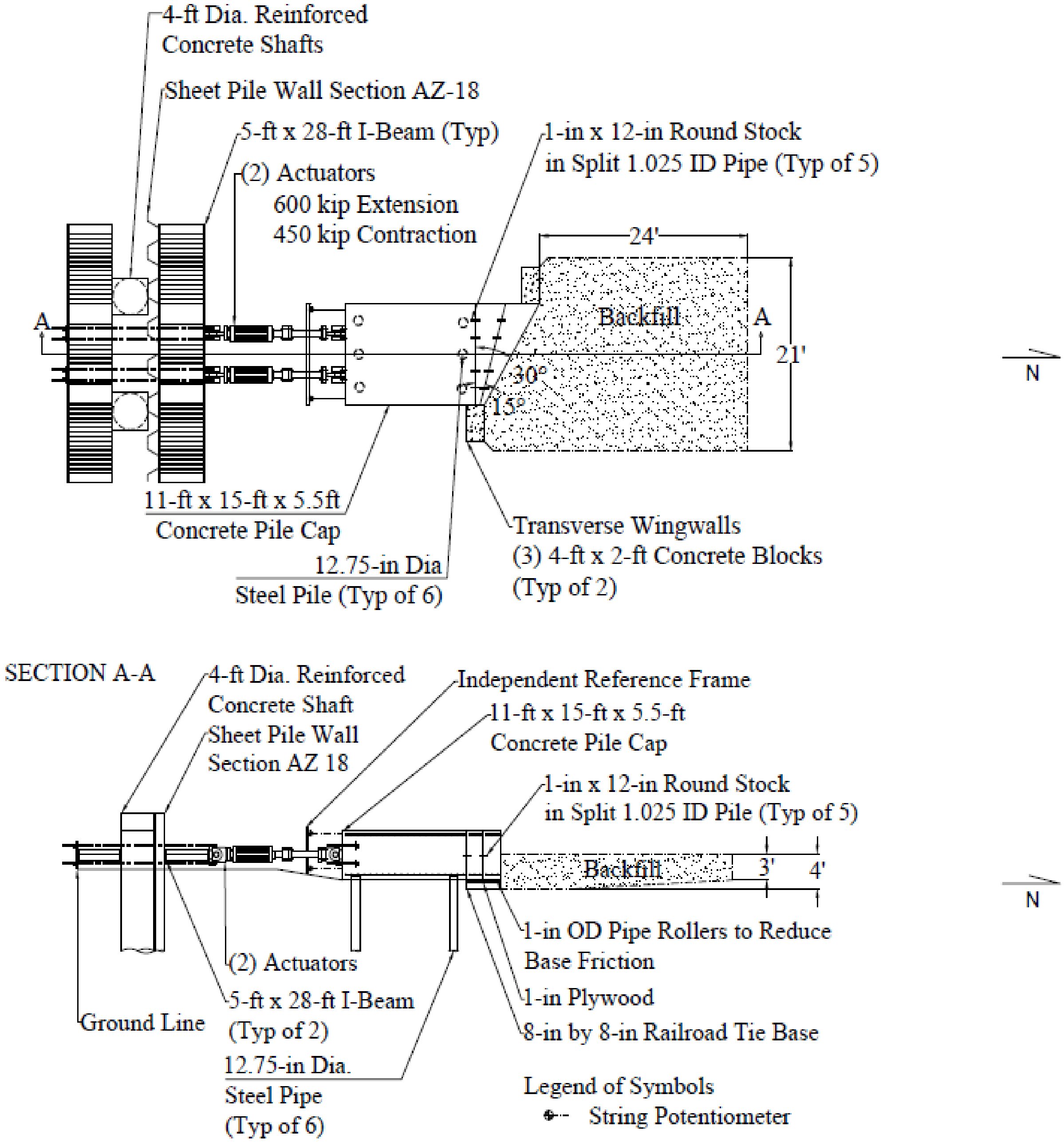

Figure 3-3 Plan and cross section views of general test layout

3.3.2 Pile Cap and Piles

A pile cap was used in this study to simulate lateral bridge abutment movement. It was situated 16.4 ft (5.0 m) north of the reaction foundation and had dimensions of 5.5 ft (1.68 m) high by 11 ft (3.35 m) wide by 15 ft (4.57 m) long. The pile cap was supported by a group of six-12.75 in (32.39 cm) diameter steel pipe piles with a wall thickness of 0.375 in (9.5 mm). All piles were constructed using ASTM A252 Grade 3 steel pipe with average yield strength of 57 ksi (393 MPa). These piles were located in two rows of three piles each in the east-west direction with a spacing of 12 ft (3.66 m) on center between the rows and 3.5 ft between piles on center. They were driven closed-ended and extended to a depth of approximately 43 ft (13.1 m) below the filled ground surface. A third row of piles once existed between the other two rows for use in a previous study, but this row was removed before the pile cap was installed to decrease resistance on the actuators.

The piles were attached to the pile cap by rebar cages set 13.2 ft (4.02 m) within the piles and extending upward 4.8 ft (1.47 m) into the pile cap. These cages were comprised of 6 #8 (#25) vertical bars and a #4 (#13) spiral at a pitch of 6 in (152 mm). The piles themselves were embedded 6 in (150 mm) into the base of the pile cap. Inclinometer and shape array pipes were installed within the center pile on both the north and south ends for data recording purposes. Eight threaded "DYWIDAG" anchor bars were also cast horizontally into the south end of the pile cap for attachment of the loading apparatus.

The pile cap itself contained reinforcement mats on both the upper and lower portions that consisted of #5 (#19) bars in both the longitudinal and transverse directions spaced at 8 in (203 mm) on center. Concrete with a compressive strength of 6,000 psi (41.37 MPa) was used for both the pile cap and pile fill.

3.3.3 Concrete Wedges

For this study, varying interface angles were needed to simulate various skewed bridge abutment angles in the field. To achieve this, concrete wedges were attached to the face of the existing pile cap. Construction and setup time were minimized by casting both the 15° and 30° wedges simultaneously together against the pile cap interface as shown in Figure 3-4. This was done at the completion of the 0° skew tests. Once the concrete reached sufficient compressive strength, the 30° skew tests were conducted and the outer 30° wedge was removed. The 15° skew tests were then conducted.

Figure 3-4: Casting of 15° and 30° wedges

The concrete wedges required high strength reinforcing and concrete to ensure that crushing did not occur, especially on the acute corner on the wedges. Therefore, designs were made considering worst-case conditions. The 15° wedge was reinforced with #4 (#13) bars throughout the entire segment. Both the top and bottom grids were oriented parallel and perpendicular to the face of the wedge and had spacings of 11 in (280 mm) on center. The face of the wedge had horizontal reinforcement oriented at 3, 15, 27, 45, and 64 in (0.08, 0.38, 0.69, 1.14, and 1.63 m) from the base of the wedge with limited horizontal reinforcement on the backside. Vertical reinforcement was placed only sporadically as needed to hold the horizontal bars in position. A model of the 15° wedge reinforcement grid is shown in Figure 3-5 below.

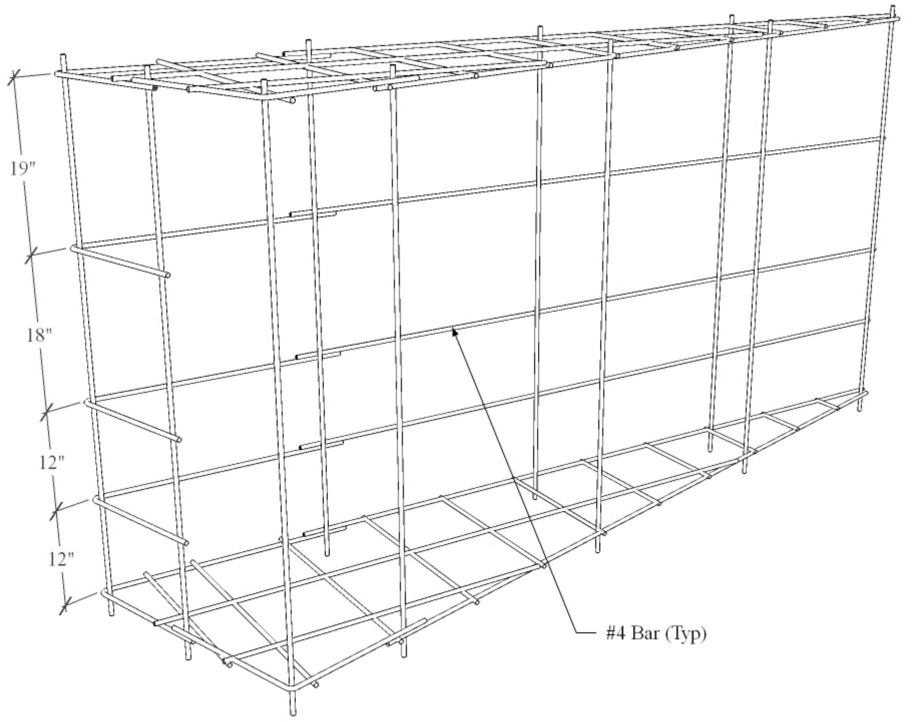

Figure 3-5: Reinforcing grid for 15° wedge (Marsh, 2013)

The 30° wedge was reinforced with #5 (#16) bars on both the top and bottom grids oriented parallel and perpendicular to the face of the wedge and spaced at 11 in (280 mm) on center. Three of the horizontal reinforcement bars on the face of the wedge were oriented at 3, 9, and 15 in (76, 230, and 380 mm) from the base of the wedge and consisted of #6 (#19) bars. These bars extended 56 in (1.42 m) from the acute end towards the obtuse end. Five #5 (#16) bars were also placed at 21, 27, 37, 49, and 63 in (0.53, 0.69, 0.94, 1.24, and 1.60 m) up from the base and extended 50 in (1.27 m) along the face. Limited horizontal reinforcement was also used on the backside. Vertical reinforcement was placed only sporadically as needed to hold the horizontal bars in position. A model of the 30° wedge reinforcement grid is shown in Figure 3-6.

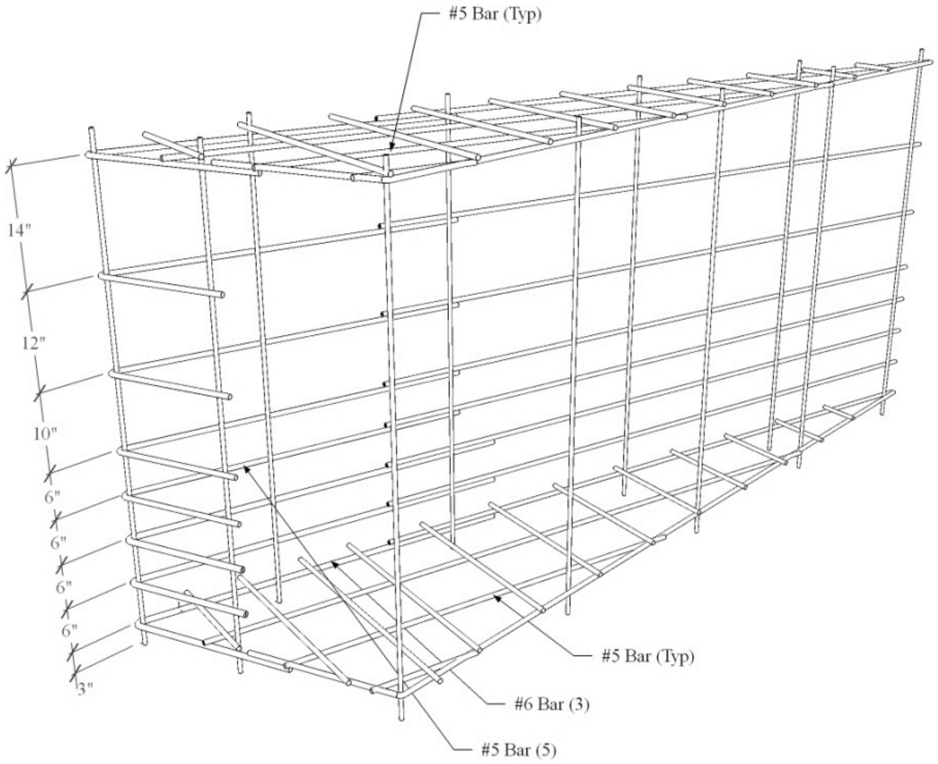

Figure 3-6: Reinforcing grid for 30° skew wedge (Marsh, 2013)

A strong connection between wedges was imperative to eliminating possible complications. However, these wedges also needed to be easily removed for alteration of the skew angle. To accomplish this, metal slip connections were poured 6 in (15.2 cm) into the concrete of both wedges. These connections consisted of 1-in (25.4-mm) diameter by 11-in (279 mm) long pieces of round stock inserted into 1.0625-in (26.99 mm) inside-diameter pipe as shown in Figure 3-7. To secure the 15° wedge to the existing pile cap, the pipe extended from the wedge and slid into 1-1/8-in (28.58 mm) diameter, 6-in (152 mm) deep holes that were drilled in the concrete. The interface between the pile cap and 15° wedge was lined with a double layer of plastic sheeting while the two skew wedges were separated by a double layer of ¾-in (1.90 cm) plywood for easier removal.

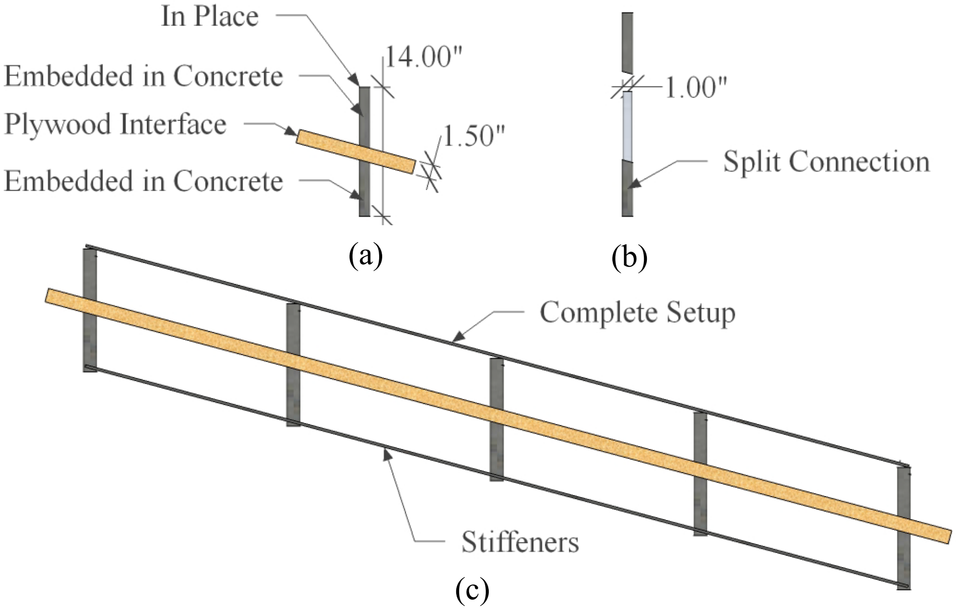

Figure 3-7: Interface connection details: (a) plan view detail of individual split connection, (b) plan view detail with bars extended out of pipe, and (c) plan view layout of the entire assembly with five split bar connections arranged across width of pile cap (Marsh, 2013)

The second precaution taken was to externally install side and top plates between the wedges and the original pile cap, as shown in Figure 3-8. These plates ensured that the wedges did not move relative to the existing pile cap. The plates were attached to the cap segments using cast-in-place anchors, 1-in (25.4 mm) in diameter and 8-in (203 mm) in length, for all newly poured concrete. Otherwise 1-in (25.4 mm) diameter, 7-in (177.8 mm) long wedge-type anchors (Redheads) were used to attach the side and top plates to the pile cap and wedges.

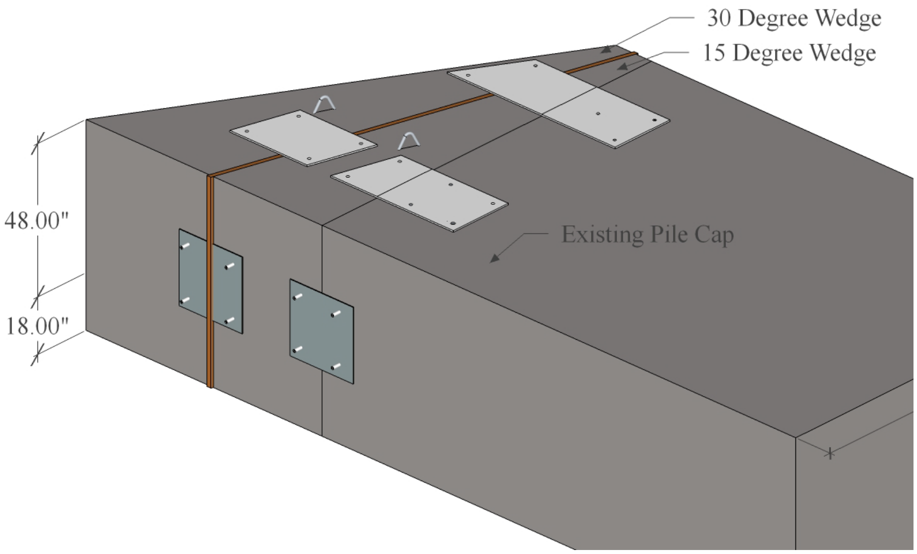

Figure 3-8: Plate interface connections (Marsh, 2013)

Additional consideration was given to the base of the concrete wedges where friction could possibly develop during testing. This factor was reduced by installing rollers underneath the wedges. The rollers were supported by railroad ties as a foundation with a layer of plywood sheeting above and below the metal rollers as shown in Figure 3-9 and Figure 3-10. Sand was kept out of this zone by placing filter fabric over the gap between the wedge segment and the underlying foundation. This wedge base also provided additional restraint against forward rotation of the pile cap.

At the completion of the 30° skew tests, the 30° skew wedge was removed to enable testing at a 15° skew. This process is shown in Figure 3-11 below. Removal of the wedge went very smoothly with no damage occurring on the remaining 15° skew wedge or pile cap. The underlying rollers were cut off with a cutting torch to fit the new skew angle and the extruding plywood was also cut to fit the 15° skew wedge.

Figure 3-9: Railroad tie foundation for 15° and 30° wedges with sand compacted between ties (Marsh, 2013)

Figure 3-10: Roller foundation for 15° and 30° wedges (Marsh, 2013)

Figure 3-11: 30° wedge removal (Marsh, 2013)

3.3.4 Loading Apparatus

Movement of the pile cap was made possible through loads provided by two MTS actuators attached to the front of the reaction foundation and the backwall of the pile cap in the north-south direction as shown in Figure 3-12. These actuators each had an extensional capacity of 600 kips (2.67 MN) and a contractive capacity of 450 kips (2.00 MN). The DYWIDAGs from the reaction foundation found in Section 3.3.1 were used as connections for the actuators. Eight DYWIDAGs embedded 2.5 ft (0.76 m) above the base of the pile cap connected the actuators to the backwall of the pile cap. Both ends of the actuators were attached to these connections with swivel heads to protect the equipment from bending moments Also, the actuators required two 4-ft (1.22-m) long extensions to provide sufficient length to reach both ends.

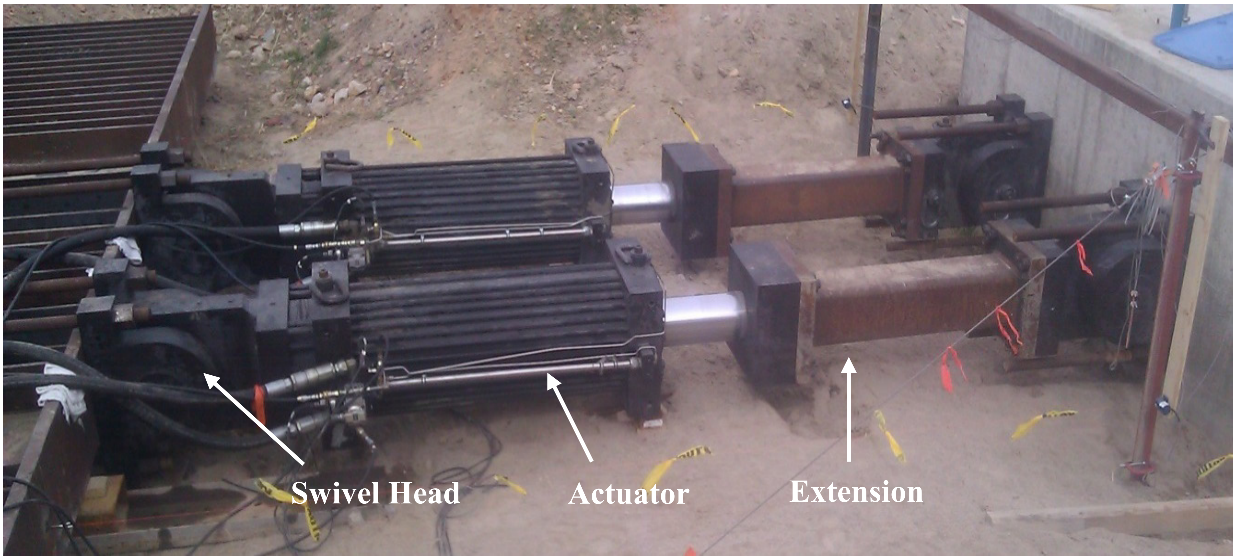

Figure 3-12: MTS Hydraulic Actuators

3.3.5 Backfill Zone

The unconfined backfill test required sufficient room for the failure soil wedge to develop in all directions so that 3D effects could be examined. To accomplish this task, the backfill zone had a width of approximately 24 ft (7.32 m) and a length of 24 ft (7.32 m). The backfill also extended to a depth approximately 1 to 2 ft (0.30 to 0.61 m) below the base of the pile cap for the first 8 ft (2.44 m) before gradually inclining to allow for log-spiral failure surfaces to develop. This zone was located on the north end of the pile cap.

Two submersible pumps were installed on the east and west sides of the pile cap approximately 2 ft (0.60 m) below the bottom of the cap to make certain that water levels never rose above the base of the backfill zone.

3.3.6 General Instrumentation and Measurements

Several forms of instrumentation were used to measure movement of the pile cap, piles, and the adjacent soil backfill. These devices detected pile cap and pile movement in both the longitudinal and transverse directions and measured backfill behavior in all three dimensions.

Referring to Figure 3-13, an independent reference frame was placed between the reaction foundation and the pile cap. A total of six string pots were attached to this reference frame. Four of these string pots were connected to the pile cap for detection of longitudinal movement and rotation. Out of these four, two string pots were located 3 in (76.2 mm) below the top of the pile cap while the lower two were at 51 in (1295 mm) from the top. They were installed 3 in (76.2 mm) and 129 in (3.28 m) from the west side of the pile cap. The remaining two string pots were positioned on the large I-beam of the reaction foundation, directly in front of the center of the drilled shafts. These string pots measured the southern displacement of the reaction foundation as the actuators pushed away from the pile cap.

Both string pots and Linear Variable Differential Transformers (LVDTs) measured transverse movement of the pile cap during the 15° and 30° skew tests along with inclinometers and shape arrays. A total of four LVDTs were mounted on the west side of the pile cap to external supports, as is shown in Figure 3-15 and Figure 3-16. These devices slid along metal plates attached to the side wall of the pile cap.

Unfortunately, the LVDTs did not perform properly, especially on the bottom locations. Since the base of the hanging metal stakes weren't fixed to a support, insufficient connections were likely the source of the inaccuracy. Also, if the sidewall of the pile cap had any flaws or curvature, the LVDT results would have detected this in conjunction with pile cap displacement and increased the error. Results produced by this instrumentation were therefore omitted from data analysis, and other forms of measurement were used in place of the LVDTs for calculations.

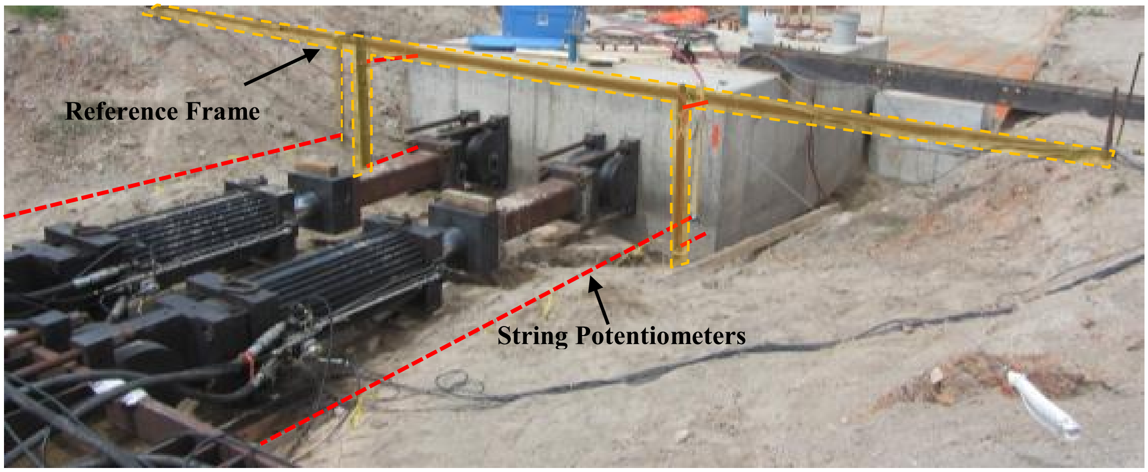

Figure 3-13: String potentiometer locations on south end of pile cap

Figure 3-14: String potentiometer setup for backfill movement and strain measurements

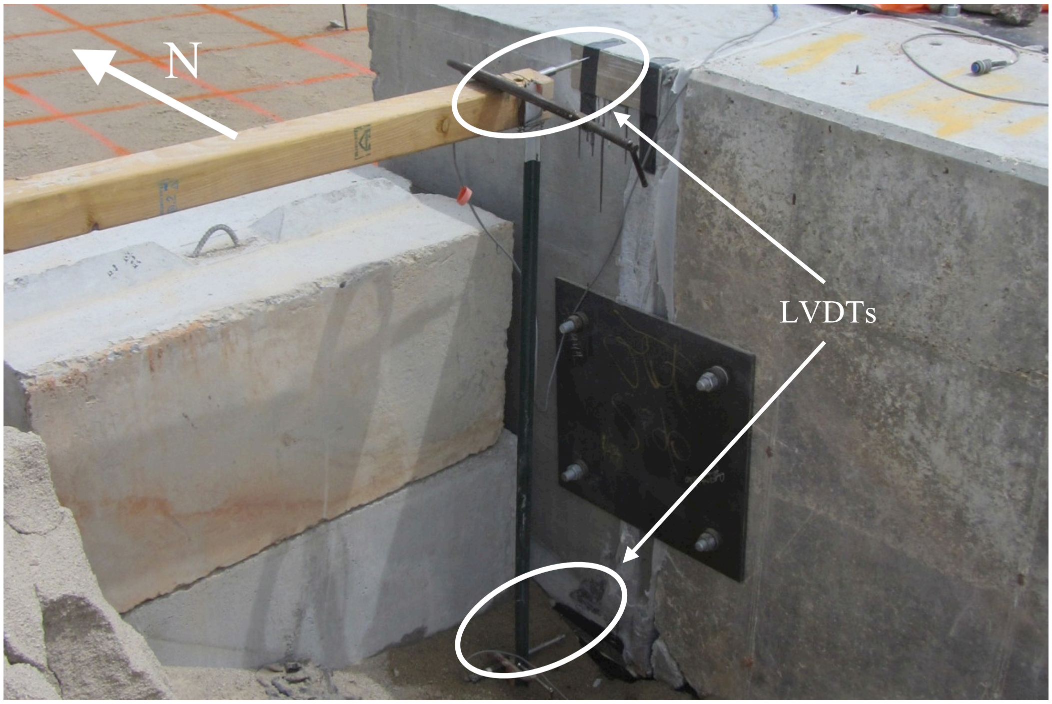

Figure 3-15: LVDTs for measuring transverse cap movement (north end)

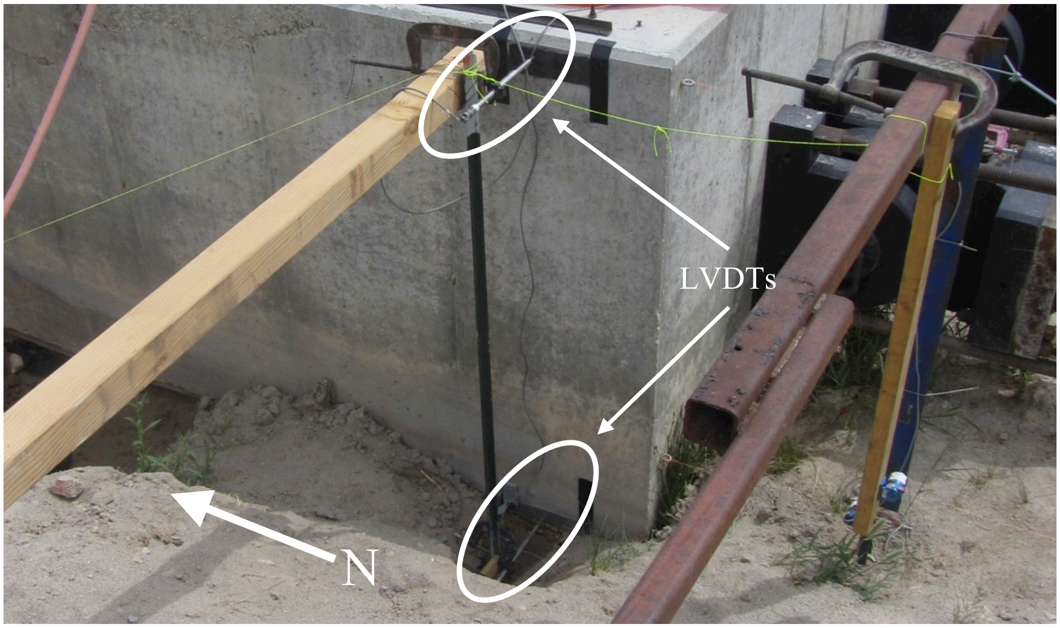

Figure 3-16: LVDTs for measuring transverse cap movement (south end)

Inclinometers and shape accelerometer arrays (SAA) were both used to detect pile cap movement in the longitudinal and transverse directions. Recordings were taken within protection tubes that were installed side-by-side in the center pile of each row of the pile cap.

Inclinometer tubes were installed to a depth of about 43 ft (13.1 m). These slotted tubes had an outside diameter of 2.75 inches (70 mm) and an inside diameter of 2.32 in (60 mm). Inclinometer readings were obtained at 2-ft (0.61-m) intervals using a Digitilt inclinometer probe (manufactured by Slope Indicator) and a DataMate portable data acquisition unit. Previous studies performed at this site used this same instrumentation (Rollins et al., 2009). Measurements were taken using the standard procedure of two, bottom-up passes to reduce error. A standard pulley assembly attached to the top of the casing was also used to provide a reliable measurement datum. Readings required approximately 15 minutes to complete. Unfortunately, to avoid creep, the actuators could only hold intermediate displacements for a couple of minutes. This restricted inclinometer readings to once just prior to the start of each test and again once the pile cap reached maximum displacement.

The shape accelerometer arrays (Danisch et al., 2005) were inserted into 1.1 in (27 mm) inside diameter schedule 40 PVC electrical conduits. The PVC pipe was originally installed to a depth of 50.2 ft (15.3 m) below the top of the pile cap, but recording depths for the north and south arrays only reached 38.75 ft and 23.08 ft (11.81 m and 7.03 m) because of array length restrictions and difficulty with installation.

Each array contained MEMS (Micromachined Electro-Mechanical System) accelerometers with a range of ± 2 g and a noise figure limited to 2 mG RMS by internal filtering. Data was recorded at 1-ft (0.30-m) increments and sent digitally through cables to a computer at approximately 5 samples/second averaged in 30-sample increments. Instantaneous readings were taken at each displacement interval throughout the tests. For this test series, a 24-ft (7.32-m) array was installed on the south end and a 48-ft (14.63-m) array on the north end.

The technological capabilities of SAAs relative to inclinometers and string pots made them extremely advantageous. However, SAAs can easily be misaligned and require corrective actions to obtain proper readings. For this study, the north direction was assigned as the primary y-axis. Inclinometer readings were already oriented in this direction but the arrays were not. Figure 3-17 shows the directions in which they appeared to be moving with increased pile cap displacement. The north array seemed to be slightly more than 180° off from the north direction while the south array was installed at approximately 140° off in the counterclockwise direction. Correction procedures for realigning the y-axis of the arrays with the north direction were performed using vector analysis and can be found in Appendix A of Marsh (2013).

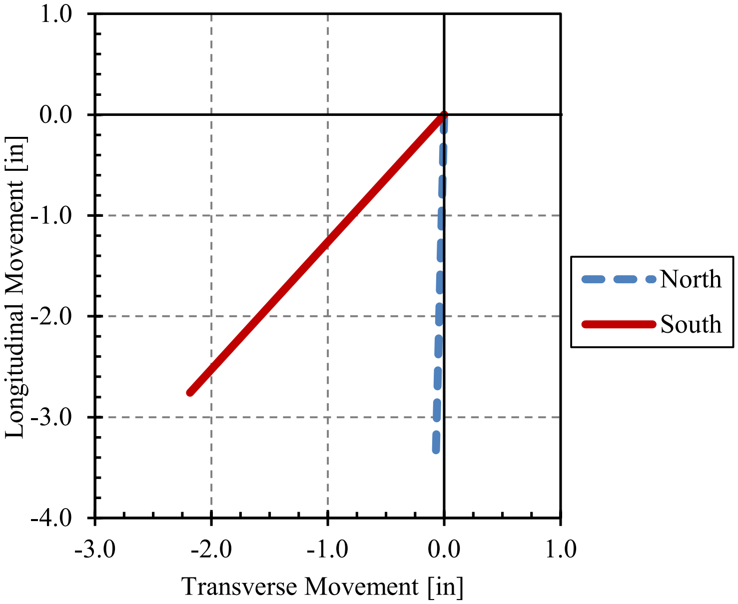

Figure 3-17: North and south shape array movement results relative to the north direction (Marsh, 2013)

Lateral pressure shifts within the backfill were monitored by six pressure plates installed horizontally on the face of the 30° wedge at a height of 22 in (0.559 m) from the base of the pile cap. These “Fat Back” pressure cells manufactured by Geokon were installed flush with the concrete surface and spaced at 21.5 in (0.546 m) center to center along a horizontal line, with the first plate 17.75 in (0.451 m) in from the west edge. This pressure plate configuration is shown in Figure 3-18 and Figure 3-19. The three eastern pressure plates were “Geokon Model 3510-2-600” 600 kPA pressure plates, and the three west plates were “Geokon Model 3510-2-1” 1 MPa pressure plates. These were hydraulic type pressure plates with a semiconductor pressure transducer that is capable of measuring dynamic pressures (Marsh, 2013).

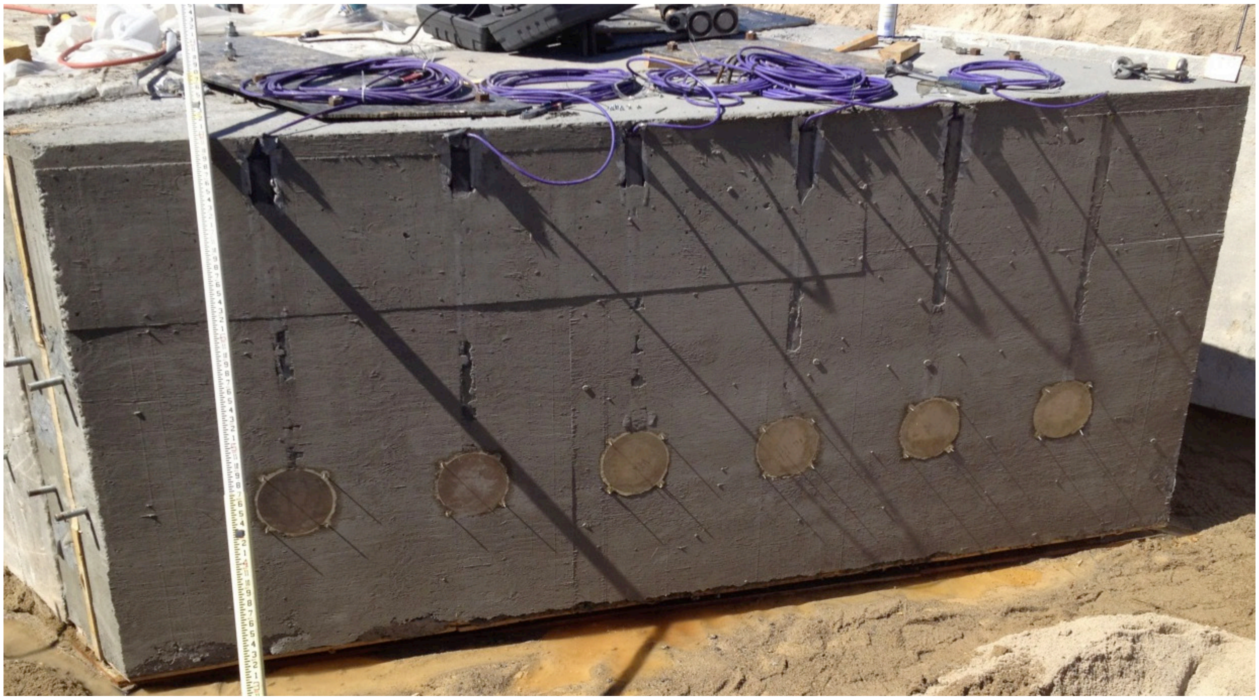

Figure 3-18: Photograph of embedded pressure plates in 30° wedge face (Marsh, 2013)

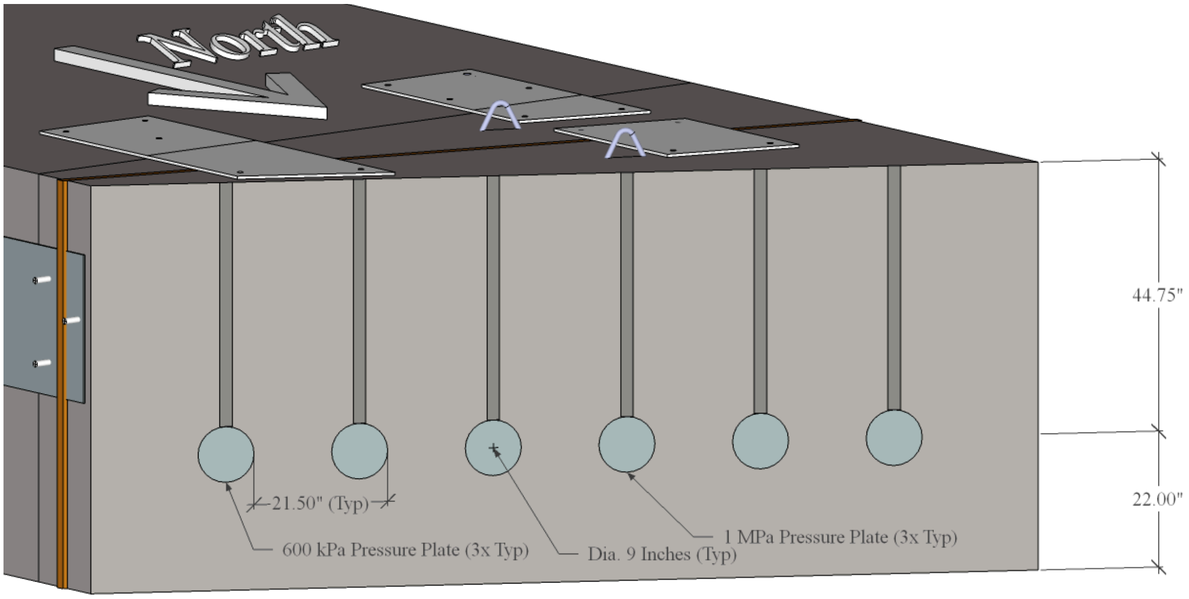

Figure 3-19: Drawing of embedded pressure plates in 30° wedge face (Marsh, 2013)

Backfill movement was also recorded manually in three separate ways: first, heave was detected by painting a 2 x 2 ft (0.61 x 0 61 m) grid and measuring the relative elevation of each grid intersection point before and after testing using a survey level; second, surface cracks were mapped out at the completion of each test using the painted grids as reference points; and third, red sand columns were inserted into the backfill longitudinally away from the pile cap and shear failure locations were detected at the completion of each test. All three of these procedures will be described in greater detail in Section 3.5 and can be seen Figure 3-35 of that section.

3.4 **Backfill Properties**

3.4.1 Soil Classifications

This study contained approximately 250 tons (227 metric tons) of poorly graded sand classified as SP soil type according to the Unified Soil Classification System or an A-1-b type soil according to the AASHTO Classification System. This soil was tested both before and after the study and results are shown in Figure 3-20. Slight differences between the two tests can be attributed to either natural variances in the backfill or to small exposures to clayey soils naturally present at the site. These values lie within the gradation limits of washed concrete sand (ASTM C33) except for a minor inconsistency in the fines content for the latter test. Soil gradation parameters including values for D_{10}, D_{30}, D_{50}, D_{60}, C_c, and C_u are provided in Table 3-1. These values can be used to assist in soil classification.

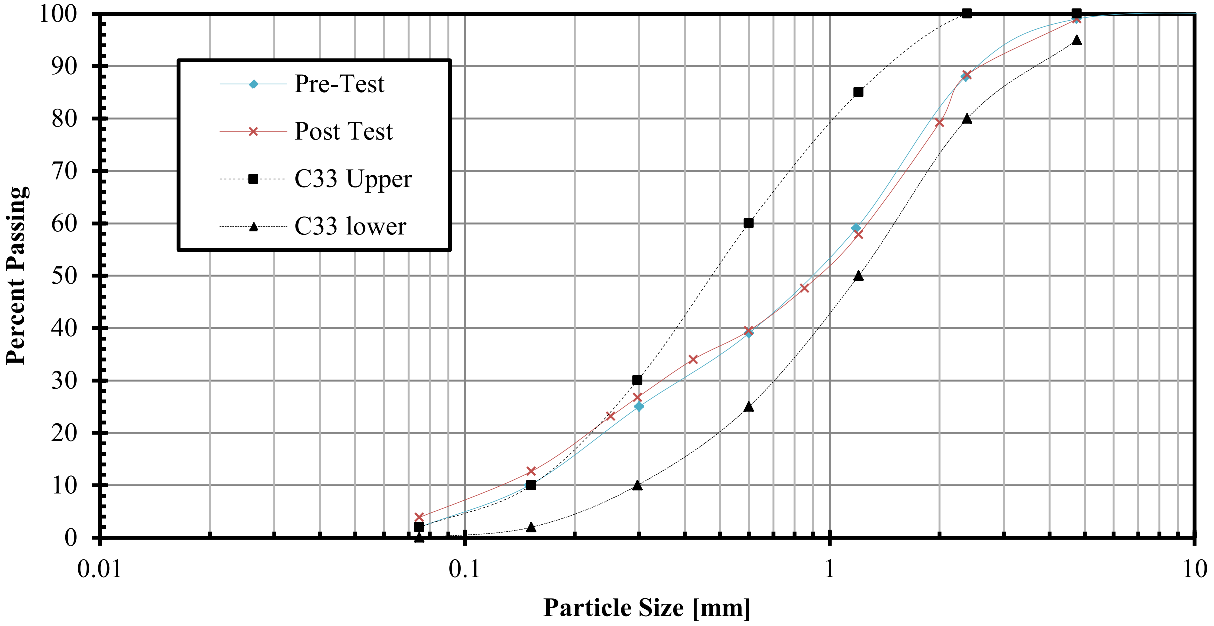

Figure 3-20: Particle size distribution of backfill soil pre- and post-test (Marsh, 2013)

Table 3-1: Soil Gradation Characteristics, Pre- and Post-Testing (Marsh, 2013)

	Sand	*Fines*	D_{60}		D_{50}		D_{30}		D_{10}		C_u	C_c
	%	%	in	(mm)	in	(mm)	in	(mm)	in	(mm)		
Pre-Test	98.0	2.0	1.22	(31.0)	0.9	(22.9)	0.4	(10.2)	0.16	(4.1)	7.6	0.8
Post-Test	96.1	3.9	1.26	(32.0)	0.92	(23.4)	0.34	(8.6)	0.13	(3.3)	9.7	0.7

Each backfill lift was tested with a nuclear density gage in two various locations of the backfill. This was done to ensure proper readings for moisture content, dry density, moist density, and relative compaction. This was also done to ensure that compaction values reached a minimum target value of 95% of the modified proctor maximum before proceeding with additional soil lifts. A modified proctor test (ASTM D1557) performed prior to testing showed the maximum dry density to be 111.5 pcf (17.52 kN/m^3) and an optimum moisture content of 7.1%. All readings presented by the nuclear density gage were recorded and compared to these values to assist in obtaining optimum values in the field.

Figure 3-21, Figure 3-22, Figure 3-23,and Figure 3-24 provide histograms showing the frequency of dry unit weight for each of the three tests and all three combined. A summary of measured and calculated field results for each test is also presented in Table 3-2.

Table 3-2: Summary of Backfill Dry Unit Weight Characteristics as Obtained from the Nuclear Density Tests

	0° Test		*15° Test*		*30° Test*	
	[pcf]	*[kN/m^3]*	*[pcf]*	*[kN/m^3]*	*[pcf]*	*[kN/m^3]*
Minimum Measured Dry Unit Weight	105.70	16.61	105.90	16.64	105.70	16.61
Maximum Measured Dry Unit Weight	110.10	17.30	110.10	17.30	109.70	17.23
Average Dry Unit Weight	107.03	16.81	108.06	16.98	107.50	16.89
Median Dry Unit Weight	106.80	16.78	107.70	16.92	107.10	16.83
Standard Deviation	0.80	0.13	0.36	0.06	1.14	0.18

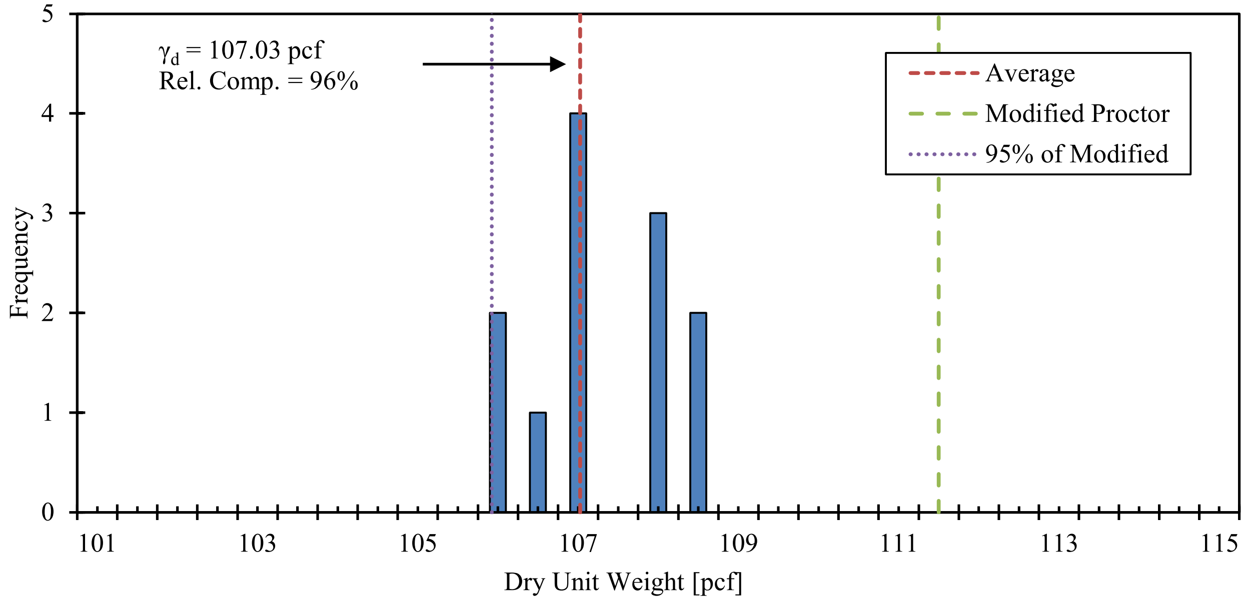

Figure 3-21: Backfill dry unit weight histogram for 0° skew test

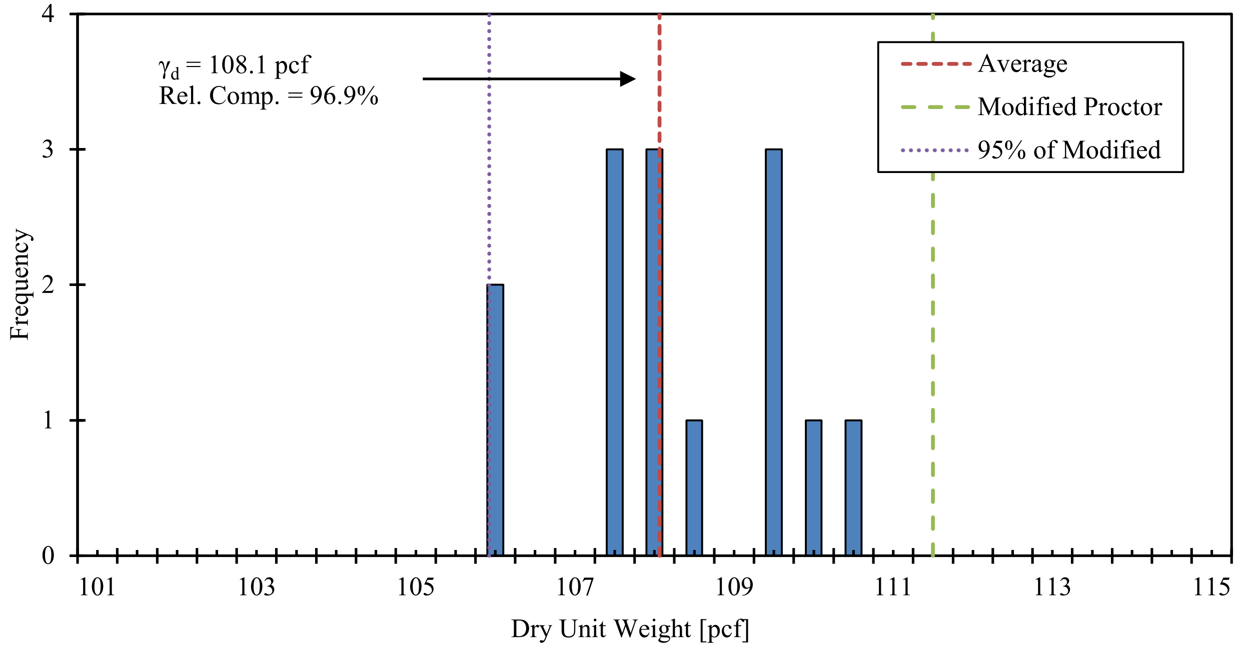

Figure 3-22: Backfill dry unit weight histogram for 15° skew test

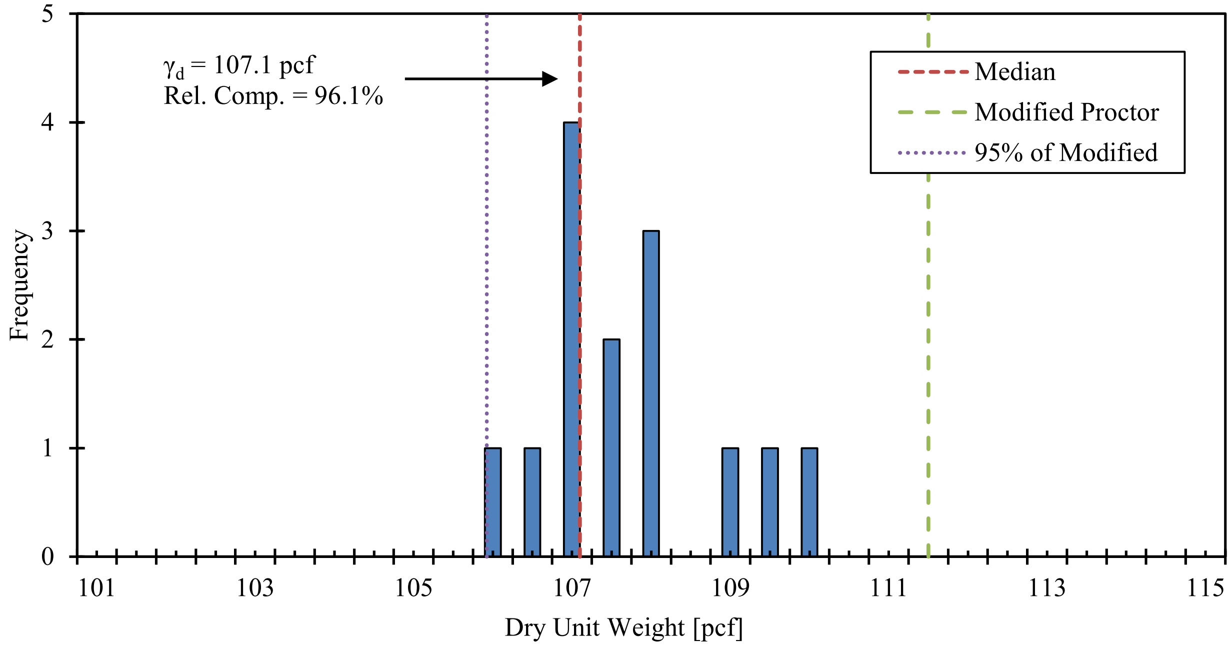

Figure 3-23: Backfill dry unit weight histogram for 30° skew test

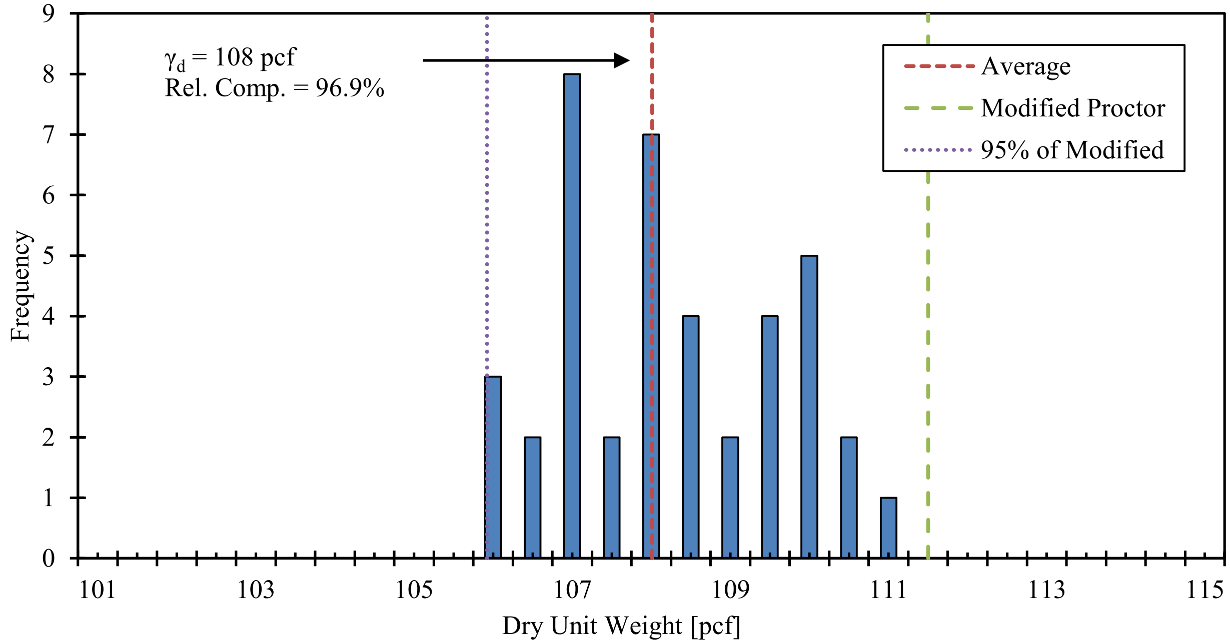

Figure 3-24: Backfill dry unit weight histogram for all tests

As can be seen above, the average dry unit weights for the 0°, 15°, and 30° tests are 107.03 pcf (16.81 kN/m^3), 108.06 pcf (16.98 kN/m^3), and 107.50 pcf (16.89 kN/m^3), with a total average of 108 pcf (16.97 kN/m^3) for all tests. These dry unit weights are within 1.03 pcf (0.16 kN/m^3) of one another and vary by an average of 3.5 pcf (0.55 kN/m^3) from the maximum dry density measured by the modified proctor test. This consistency suggests that the backfill soils are comparable to one another in all material respects.

Average relative compaction, R varied by an average of only 0.9% between tests. These relative compaction values can be seen with respect to elevation above the base of the pile cap in Figure 3-25. Relative density, D_r, for each fill was estimated using Equation (3-1), which correlates relative compaction with relative density, D_r in granular soils (Lee & Singh, 1971). The average relative density for each test equated to 81.3%, 84.6%, and 82.1% for the 0°, 15°, and 30° tests, respectively.

$$R = 80 + 0.2D_r \tag{3-1}$$

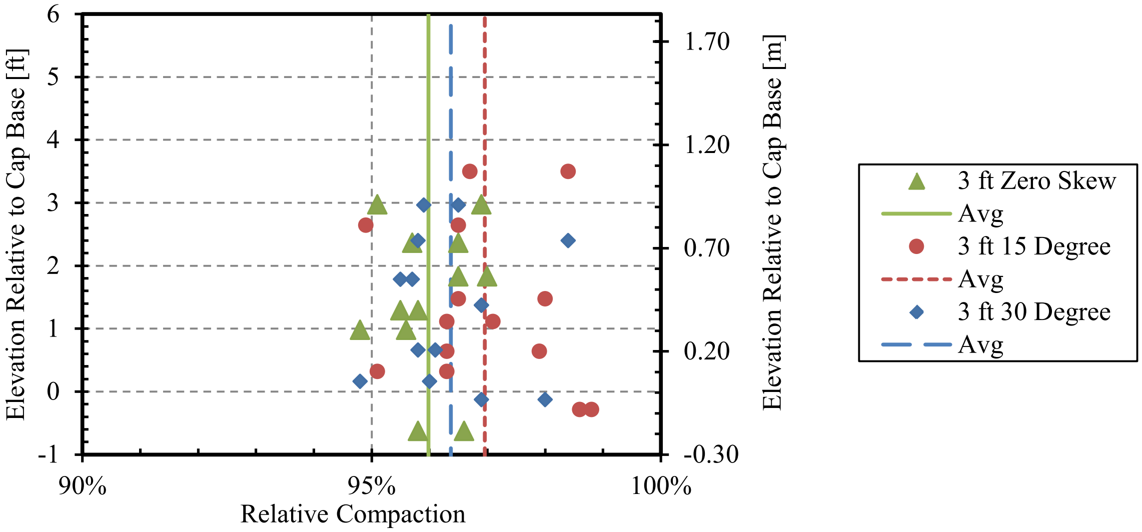

Figure 3-25: Relative compaction with respect to depth for all tests

Plots containing moisture content, dry unit weight, and moist unit weight can also be seen with respect to elevation above the base of the pile cap in Figure 3-26, Figure 3-27 and Figure 3-28 for all three tests. Depth appears to have little effect on these three parameters. Moisture content fell almost entirely within the range of 7% to 12%. Almost all of the dry unit weight values were within values of 105 and 110 pcf (16.5 to 17.3 kN/m^3) while moist unit weight values were within 115 and 120 pcf (18.1 to 18.9 kN/m^3) for most of the recordings.

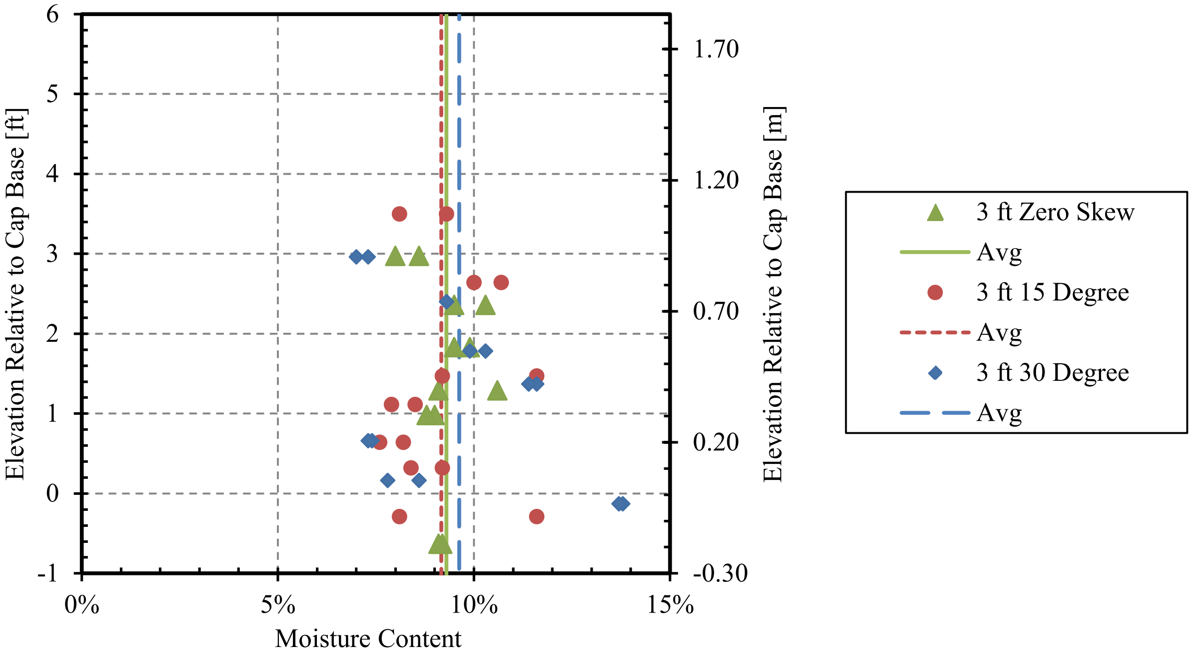

Figure 3-26: Moisture content with respect to depth for all tests

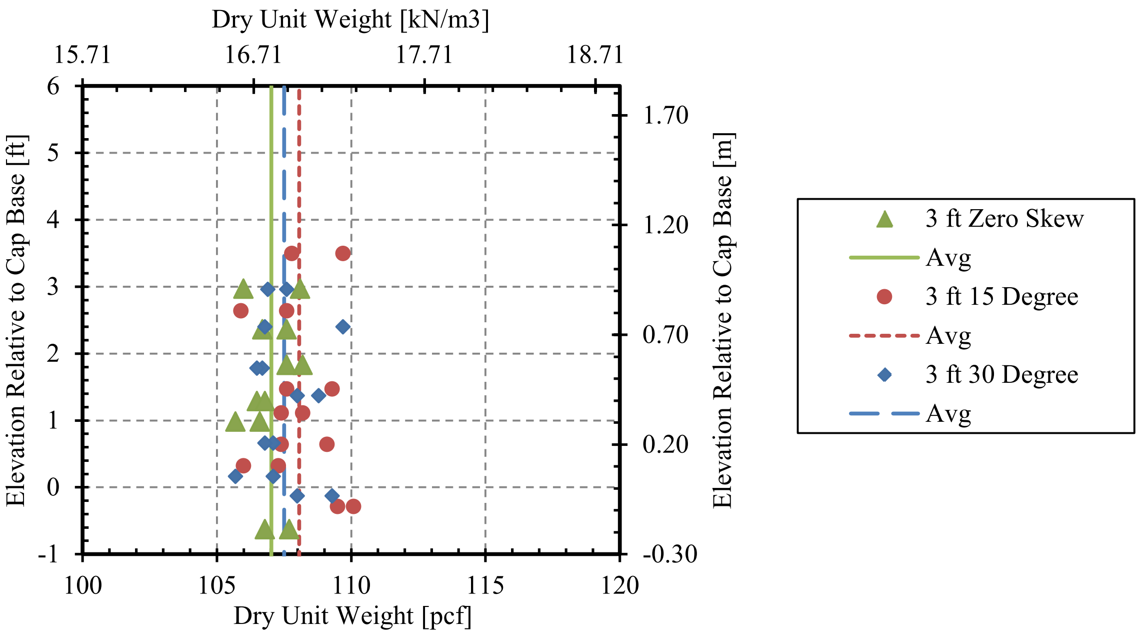

Figure 3-27: Dry unit weight with respect to depth for all tests

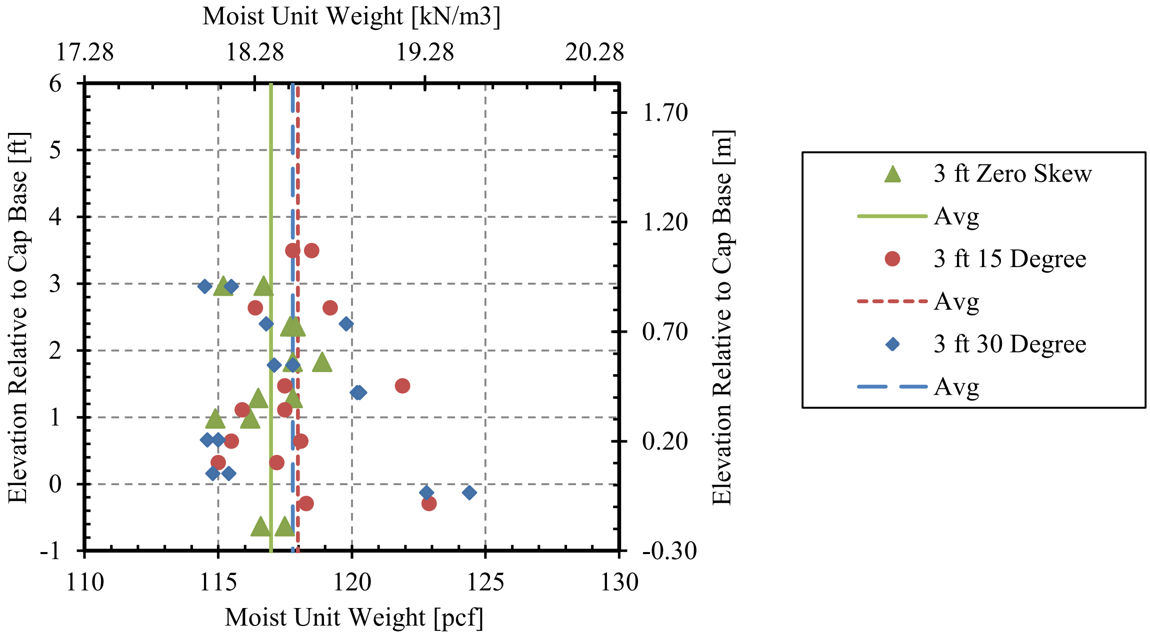

Figure 3-28: Moist unit weight with respect to depth for all tests

3.4.2 Backfill Shear Strength

The soil friction angle, ϕ and cohesion, c are two important backfill parameters that required direct shear tests to obtain their magnitudes. Tests were conducted in general accordance with ASTM D 3080 standards in the soils laboratory on the Brigham Young University campus. Normal stresses were selected based on possible vertical stresses the soil could experience during testing. These stresses included values of 4.1, 8.2, 16.3, and 24.5 psi (28.1, 56.3, 112.5, and 168.8 kPa).

Direct shear tests contained moisture contents typical of the field test results and were conducted in submerged and un-submerged conditions. Table 3-3 provides peak and ultimate friction angle and cohesion results for all direct shear tests conducted. Additionally, plots for the horizontal load versus deflection for the dry and submerged tests as well as normal stress versus shear stress for the dry and submerged tests can be seen in Figure 3-29, Figure 3-30, Figure 3-31, and Figure 3-32, respectively.

Table 3-3: Backfill Strength Parameters (Marsh, 2013)

Source of Test Result	*Peak*		*Ultimate*	
	ϕ (deg)	*c (psf)*	*ϕ (deg)*	*c (psf)*
Direct Shear (full range, dry)	46.7	161.6	40.4	113.8
Direct Shear (full range, dry, zero cohesion)	48.3	0	41.8	0
Direct Shear (full range, submerged)	42.7	92.9	41.4	78.8
Direct Shear (full range, submerged, zero cohesion)	43.8	0	42.3	0

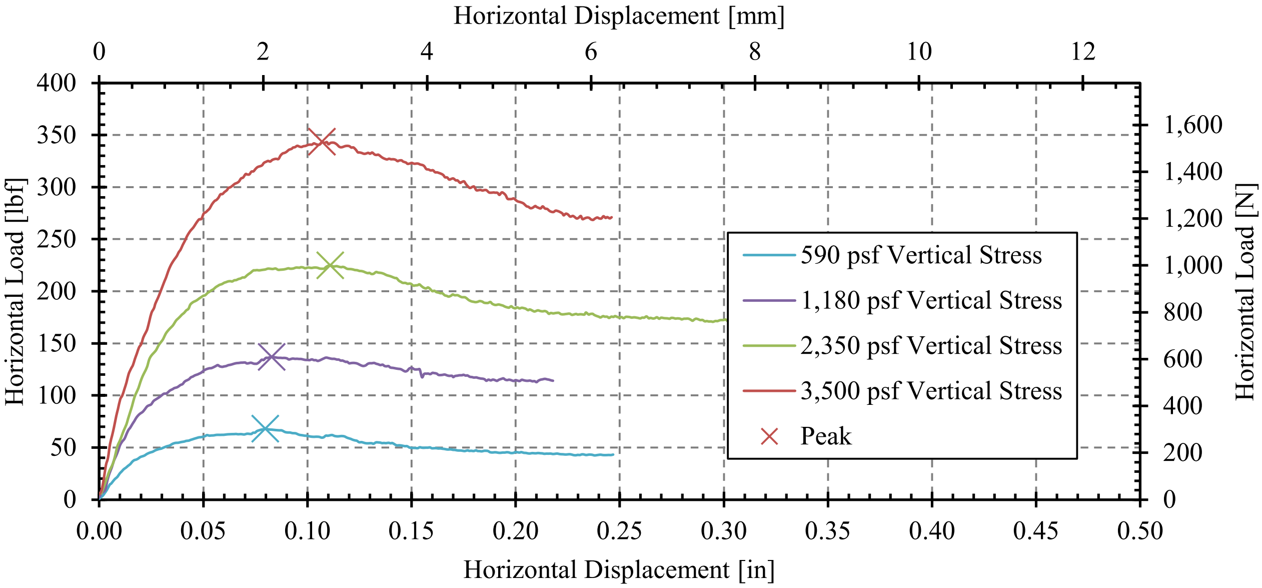

Figure 3-29: Horizontal load versus deflection plots for dry direct shear tests (Marsh, 2013)

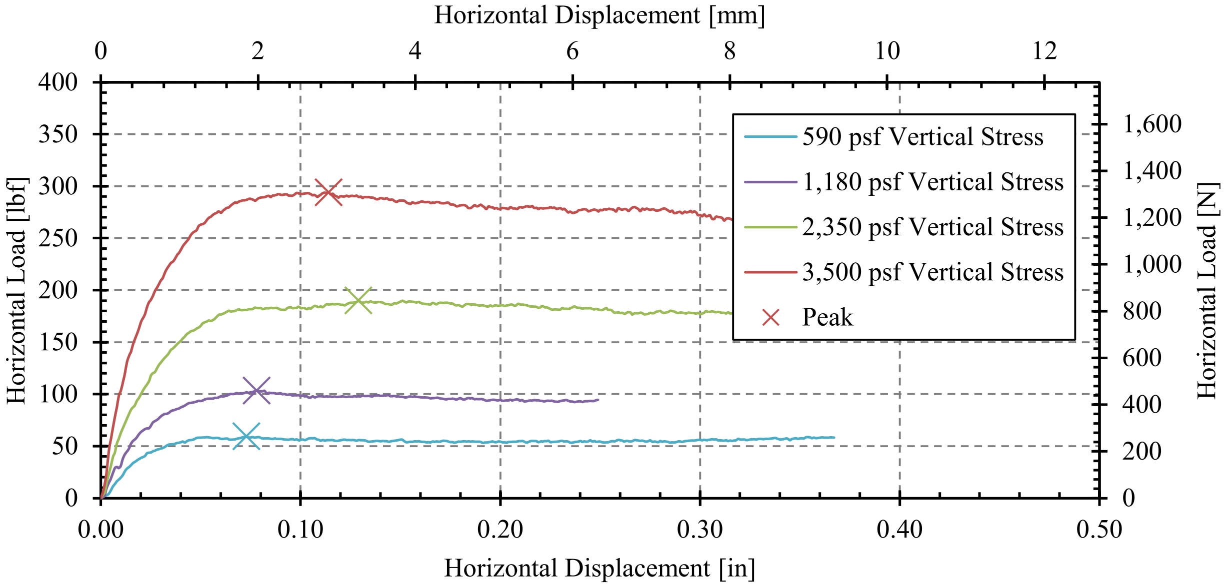

Figure 3-30: Horizontal load versus deflection plots for submerged direct shear tests (Marsh, 2013)

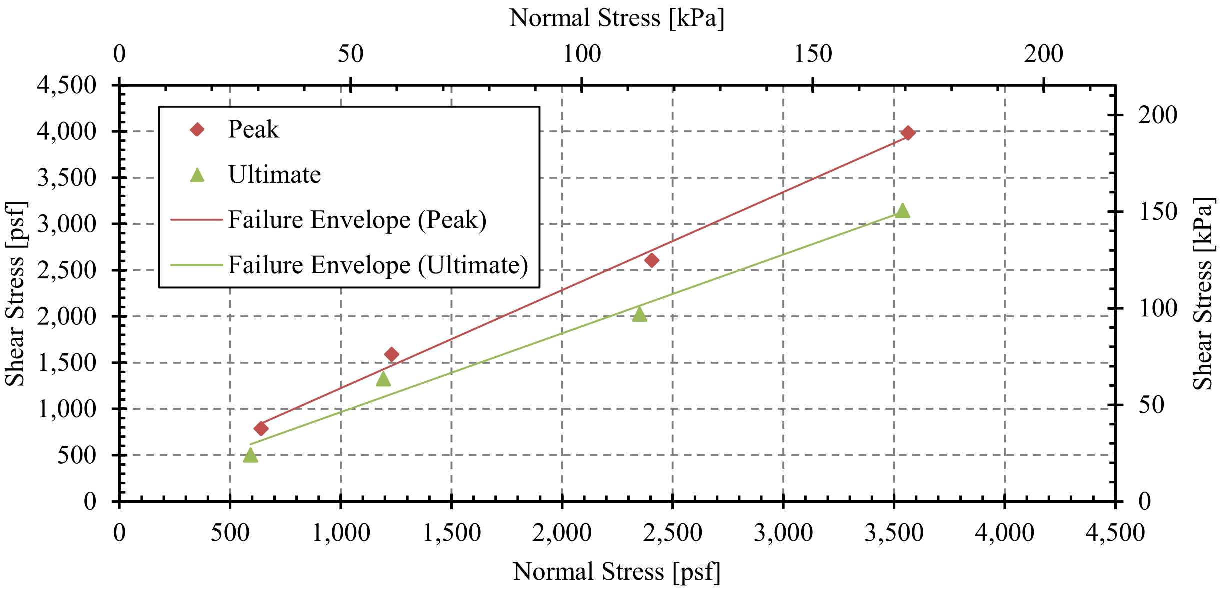

Figure 3-31: Normal stress versus shear stress plots for dry tests (Marsh, 2013)

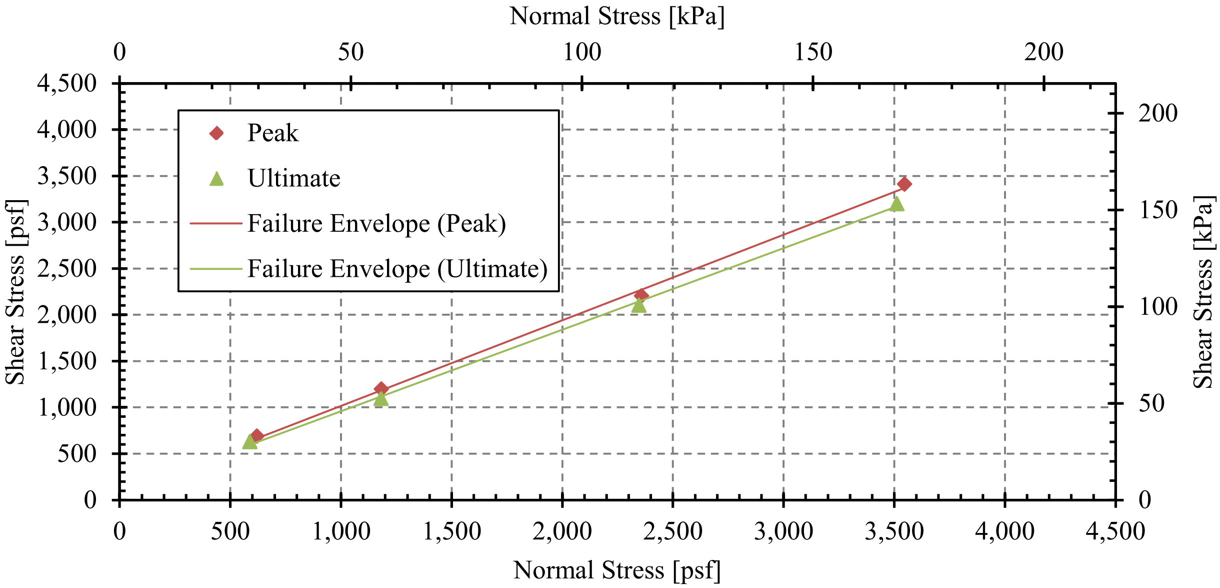

Figure 3-32: Normal stress versus shear stress plots for submerged tests (Marsh, 2013)

3.5 **General Test Procedure**

During the same time period when the 0°, 15°, and 30° skew 3-ft (0.91-m) unconfined backfill tests were performed, additional tests were also conducted for 5.5-ft (1.68-m) unconfined backfill and 5.5-ft (1.68-m) backfill MSE wall tests with the same skews. A summary of the testing order and their testing dates is given in Table 3-4. A total of 16 tests were conducted during this time period, ten backfill tests and six baseline tests. Two tests were performed for the 15° skew 3.0-ft (0.91-m) backfill test to confirm results that appeared to be uncertain. Since results were almost identical in the two tests, analysis of only the original 15° skew 3.0-ft (0.91-m) backfill test is presented in this thesis.

Table 3-4: 2012 Testing Summary

Test Number	*Test Date*	*Test Description*
1	4/25/2012	0° Baseline
2	4/25/2012	0° Baseline Retest
3	4/30/2012	0° 3.0 ft (0.91 m) Backfill
4	5/3/2012	0° 5.5 ft (1.68 m) Backfill
5	5/3/2012	0° Baseline Retest 3
6	5/8/2012	0° MSE, 5.5 ft (1.68 m) Backfill
7	5/14/2012	30° Baseline
8	5/15/2012	30° Baseline 2
9	5/18/2012	30° MSE, 5.5 ft (1.68 m) Backfill
10	5/24/2012	30° 5.5 ft (1.68 m) Backfill
11	5/30/2012	30° 3.0 ft (0.91 m) Backfill
12	5/31/2012	15° Baseline
13	6/4/2012	15° 5.5 ft (1.68 m) Backfill
14	6/6/2012	15° 3.0 ft (0.91 m) Backfill
15	6/8/2012	15° 3.0 ft Backfill Retest
16	6/13/2012	15° MSE, 5.5 ft (1.68 m) Backfill

At the beginning of each test setup, elevation readings were taken with reference to the top of the pile cap. Base level elevations varied from 6 to 9 in (15.2 to 22.9 cm) below the base of the pile cap and gradually sloped upward away from the pile cap. With each new lift, subsequent readings were taken to monitor the backfill depth. New lifts were added in approximately 6 in (15.2 cm) increments. Water was added when necessary to maintain optimum moisture in the backfill.

With each new lift, a hand compactor and a roller would repetitively pass over the soil until a minimum of at least 95% relative density was obtained, as is shown in Figure 3-33 (a) and (b). In place density and moisture measurements were taken using a nuclear density gage. Readings were always taken on both the east and west sides of the backfill to ensure that compaction was consistent throughout the soil (See Figure 3-33 (c)). In addition, the same rolling pattern was used through the entire fill area.


(a) (b) (c)

Figure 3-33 Backfill compaction including (a) vibratory plate compaction, (b) vibratory roller compaction, and (c) nuclear density gauge evaluation.

Once all lifts were complete and the proper depth of 3 ft (0.91 m) was obtained, an elongated piece of wood was used to create a smooth uniform surface on the backfill. A grid of 2 by 2 ft (0.61 by 0.61 m) squares was then marked as reference points on the surface using orange spray paint and initial elevation points were recorded using a survey level.

Similar to the gypsum columns used by Lemnitzer et al. (2009), four 2-in (5.1-cm) diameter columns were drilled into the compacted fill and replaced with compacted red sand (sand mixed with red chalk).. This produced red sand columns that were offset by the failure plane and identified the location of the shear failure plane within the soil. These columns were located at the center of the pile cap at distances of 2,4,6, and 8 ft (0.61, 1.22, 1.83, and 2.44 m) behind the soil-backwall interface. As discussed previously, to identify longitudinal displacement of the backfill surface, stakes were inserted at various locations and attached to string potentiometers. Initial readings for the inclinometer, SAA, and string pots were then recorded. An image of a fully prepared testing surface can be seen in Figure 3-34.

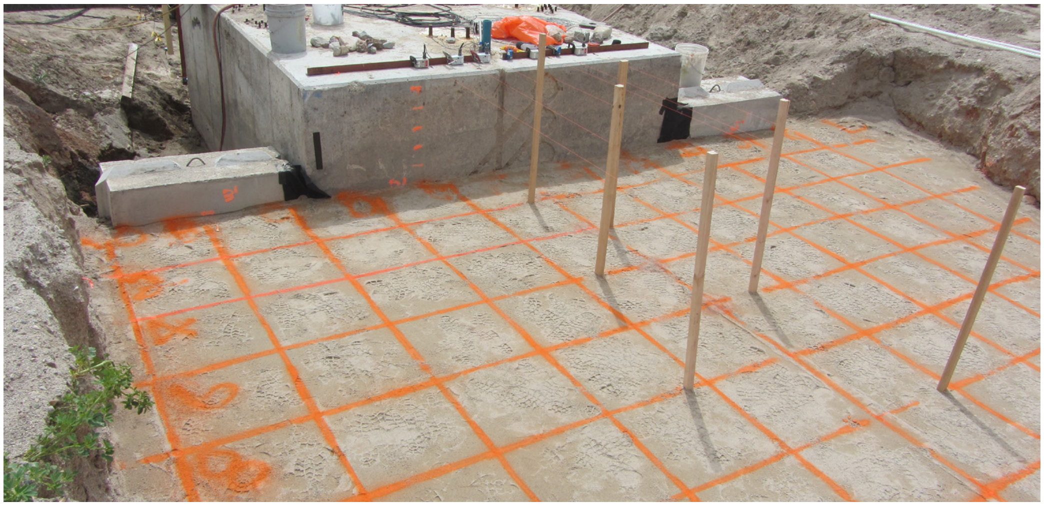

Figure 3-34: Backfill surface fully prepped for testing

Testing was performed in ¼ in (0.64 cm) movements. During this time, team members monitored the equipment, recorded testing values, and monitored the surface of the backfill. When cracks formed, spray paint was used to mark their paths.

Maximum displacements ranged between approximately 3.25 in to 3.75 inch (8.26 cm to 9.53 cm) for the various tests. Once the pile cap reached this final displacement, its positioning was held to allow for final measurements to be taken. These measurements included digital instrumentation readings as well as manual readings such as elevations of the backfill heave and drawings of developed soil cracks, as shown in Figure 3-35 (a) and (b). The actuator load was then released and locations of shear column failures were identified (see Figure 3-35 (c)).

(a) **(b)** **(c)**

Figure 3-35: Post-testing recordings including (a) backfill heave elevation, (b) mapping of developed soil cracks, and (c) shear failure locations within red sand columns

4 LOAD VERSUS DISPLACEMENT RESULTS

4.1 Baseline Test Results

A total of six baseline tests were performed during this study. These tests provided a way to eliminate forces not directly provided by the compacted backfill resistance in question including factors such as group pile resistance, the weight of the pile cap, and friction between the pile cap and the underlying soil. Results from the most applicable baseline test of each skew and their corresponding recording dates are shown in Figure 4-1.

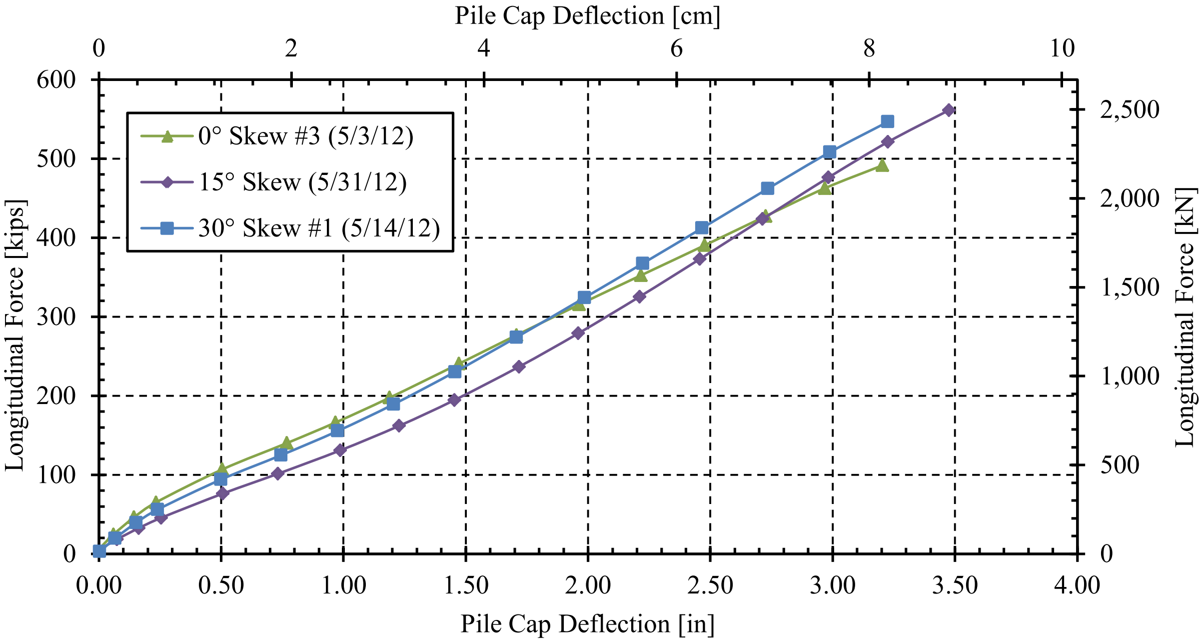

Figure 4-1: Best fitting baseline tests conducted for skews of 0°, 15°, and 30°

For the 0° skew baseline, three tests were performed—two being prior to testing and the third being conducted after the final 0° skew backfill test was completed. Both the first and second baseline tests were considered to produce unrealistic results since the first test loosened up the initial compacted soil and the second test was not given enough time to allow the soil behind the piles to fill the voids caused by pile movement. The third test produced results with additional stiffness caused by excavating the final 0° skew backfill test in a different manner than in other tests. This method forced soil into the gap beneath the base of the pile cap and into the voids behind the piles, thus resulting in significantly high readings. The third test results also proved to be unreasonable as will be described in Section 4.2.

The 15° baseline test was performed one day after completing the 30° skew 3-ft (0.91-m) backfill test. Both the resistance and stiffness were within the predicted range of values, deeming the need for any additional tests unnecessary.

Two baseline tests were performed for the 30° skew baseline. The first test was conducted six days after completion of the 0° 5.5-ft (1.68-m) MSE wall test and the second test was performed the following day. The first 30° baseline was selected for use in this study since the 3-ft (0.91-m) backfill test also experienced a six-day waiting period before test conduction.

4.2 **Passive Force-Deflection Curves**

Data presented by load-displacement curves is extremely valuable for tests that investigate passive pressure behavior. Load-displacement curves provide an understanding regarding the soil stiffness, the magnitude of the maximum passive pressure, the deflection needed to obtain maximum passive pressures, residual strength, and the all-around behavior of the backfill.

Passive force deflection curves were obtained in this study by subtracting the baseline resistance from the total load as shown in Figure 4-2. Since baseline tests were performed separately from total load tests, deflections of the two tests were somewhat misaligned. To avoid interpolation errors a sixth-order polynomial regression equation was developed to define the baseline resistance curve. This allowed the baseline force to be specified continuously as a function of displacement and align properly with the total load curve. Linear extrapolation was also used for the tail portion of the baseline curve in situations where the final total load displacement value extended further than the final baseline resistance.

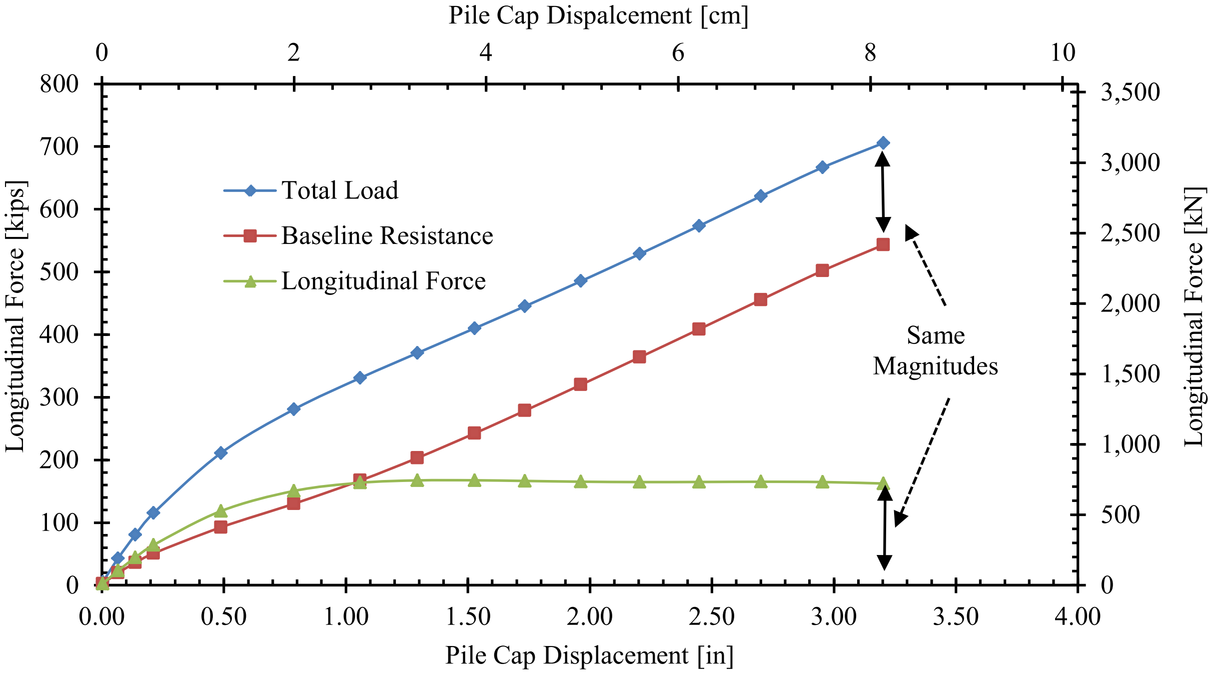

Figure 4-2: Relationship of total load and baseline resistance to backfill resistance for the 0° skew test

As shown in Figure 4-2, the shape of the load-displacement curves agreed well with previous large scale tests in that they were hyperbolic in nature (Rollins & Cole, 2006;

Shamsabadi et al., 2006). In theory, once maximum passive pressures were obtained the soil sheared and the resistance declined. The maximum passive force was used to provide a correlation between skew angle and strength reduction as was done in Equation (1-1). These ratios were then plotted against values presented by Rollins and Jessee (2012) in Figure 2-18. Although residual strengths typically aren't accounted for in current load-displacement models, these values were also analyzed due to their benefit in situations where failure occurs but the backfill still must continue to support the bridge structure.

Typically, a baseline recorded for a specific skew angle would be used for that backfill test. However, this was not the case for the 0° skew test. Unfortunately, a storm passed through the testing site before the 3-ft (0.91-m) unconfined backfill test was performed. As explained in Section 4.1, pile cap retraction after forward movement typically creates a void between the supporting piles and adjacent soil. The storm altered this behavior by washing sand beneath the pile cap, thus filling the voids with sand and water. The resulting test had stiffer resistance values than anticipated which were not accounted for in the 0° baseline tests.

Extensive consideration was given to all six baselines in seeking to find one that best matched the post-storm conditions presented in the 0° skew test. Figure 4-3 shows force-deflection curves for the two most appropriate baselines found—the third 0° baseline and the first 30° baseline. After careful consideration, the first 30° baseline test was selected for several reasons: this curve had extremely similar initial stiffness and maximum longitudinal force values compared to that of the best 0° skew baseline; field conditions of the 30° baseline test were capable of simulating additional restraint caused by the storm runoff; and the feasibility of the 30° curve compared to that of the other baselines was the most intuitive.

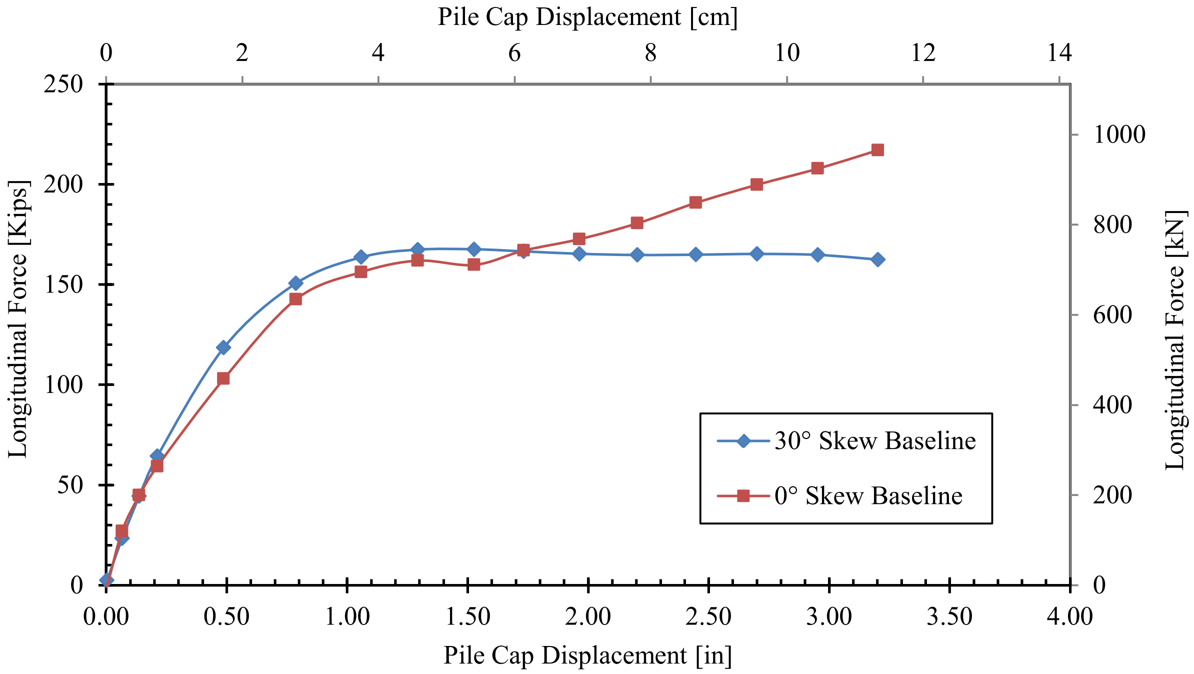

Figure 4-3: 0° skew passive force-deflection curve using 0° and 30° skew baselines

As can be seen in Figure 4-3, the 0° baseline passive force-deflection curve was acceptable through the initial peak, but the subsequent portion behaved in a questionable manner. Typical passive-force deflection curves show a gradual decrease in strength once the slope of the line reduces to zero, but use of the 0° baseline curve caused the passive force curve to gain strength after the initial peak occurred. Signs of internal shear failure provided by Figure 6-5 are likely to have caused the soil to lose strength, not increase as it did with the 0° baseline.

The addition of both the 15° and 30° concrete wedges to the 30° baseline test provided added force resistance and forward rotation restriction to account for the stiffness from the storm-wash sand. Fortunately, initial stiffness values for both baselines differ by only 23.7 kip/in (4.15 kN/mm) and the peak passive pressures vary by 5.7 kip (25.3 kN). This is an 8.5% increase in stiffness and a 4.3% increase in passive pressures. The differences are extremely small compared to the overall variations between the 0°, 15° and 30° skews and final results still produced ratios comparable to those of Rollins and Jessee (2012). A comparison between passive force-deflection curves produced by both baselines is provided in Table 4-1.

Table 4-1: Passive Force-Deflection Curve Variations between the 0° Skew and 30° Skew Baseline Tests

	Peak Passive Force [kip] (kN)	*Deflection [in] (mm)*	*Stiffness [kip/in] (kN/mm)*
0° skew	161.9 (720.2)	1.29 (32.8)	279.9 (49.0)
30° skew	167.6 (745.5)	1.53 (38.8)	303.5 (53.2)
Difference	5.7 (25.3)	0.23 (6.0)	23.7 (4.15)

Figure 4-4 provides the longitudinal force-deflection curves for the 3-ft (0.91-m) unconfined backfill tests with the appropriate baseline selections for skews of 0°, 15°, and 30°. The maximum longitudinal resistances for the for skews of 0°, 15°, and 30° skews were reached at approximately 167.6 kips (745.5 kN), 123.7 kip (550.2 kN), and 86.1 kip (383.0 kN), as shown in Figure 4-4. According to Equation (2-1), the maximum passive forces were obtained by multiplying the longitudinal force by the cosine of their respective skew angles. The remainder of the longitudinal force can be accredited to shear resistance in the direction parallel to the skewed wedge interfaces. Since there was no skew in the 0° skew test, the passive force was equal to the longitudinal force. The resulting peak passive forces were 167.6 kips (745.5 kN), 119.5 kip (531.6 kN), and 74.5 kip (331.4 kN) for skews of 0°, 15°, and 30°, as shown in Figure 4-5. For reference purposes, Figure 4-6 is also included to show the passive force in relation to the deflection perpendicular to the skew angle. Maximum forces occurred at longitudinal displacements of 1.53 in (3.89 cm), 1.23 in (3.12 cm), and 1.02 in (2.59 cm) for the 0°, 15°, and 30° skew tests and equate to 0.043H, 0.034H, and 0.028H where H is the height of the backwall. These results suggest that the displacement required to develop full passive resistance decreases somewhat with skew angle. Nevertheless, all three normalized displacement values fall within the range of 0.03H to 0.05H, which has been observed in previous full-scale tests (Rollins & Cole, 2006).

The initial stiffness values obtained for all three skew tests are extremely similar until the failure force is approached. These field test results agree with laboratory test results from Rollins and Jessee (2012) found in Figure 2-17 wherein they noticed that skew had very little effect on the initial stiffness. Instead, differences in stiffness came with increased pile cap deflection. For the 30° skew test, this displacement occurred within 0.1 in (0.25 cm) while decreased stiffness didn't occur until deflections of approximately 0.2 in (0.51 cm) for the 15° skew test and 0.3 in (0.76 cm) for the 0° skew test.

Figure 4-7 presents the normalized passive force versus the normalized wedge displacement for the 0°, 15°, and 30° skew tests while Figure 4-8 includes the normalized passive force versus the wedge displacement perpendicular to the skew interface. Regarding stiffness, the 0° skew test produced the softest response. This is caused by the additional deflection needed to develop a higher passive resistance for non-skewed abutments.

Densely compacted granular backfill might be expected to exhibit a peak strength followed by a reduction in strength to an ultimate or residual value. When dense sand shears, it initially densifies, leading to a peak in strength, but with continued shearing it tends to dilate or expand. As the soil dilates and becomes looser, the strength tends to decrease. Once maximum peak passive resistance was achieved for the 0° skew tests, passive resistance remained relatively constant with a minimum residual strength of 0.97P, where P is the maximum passive pressure.

As for the 15° and 30° skew residual strengths, their magnitudes dropped to as low as 0.79P and 0.84P, where P is again their maximum passive pressures. These test results suggest that the backfill soil for the 15° and 30° skew tests was somewhat denser than that for the 0° skew test. While there is some evidence to the effect in the nuclear density test results, the differences are quite small. Nevertheless, small differences in relative compaction can lead to substantial differences in both strength and load-displacement behavior.

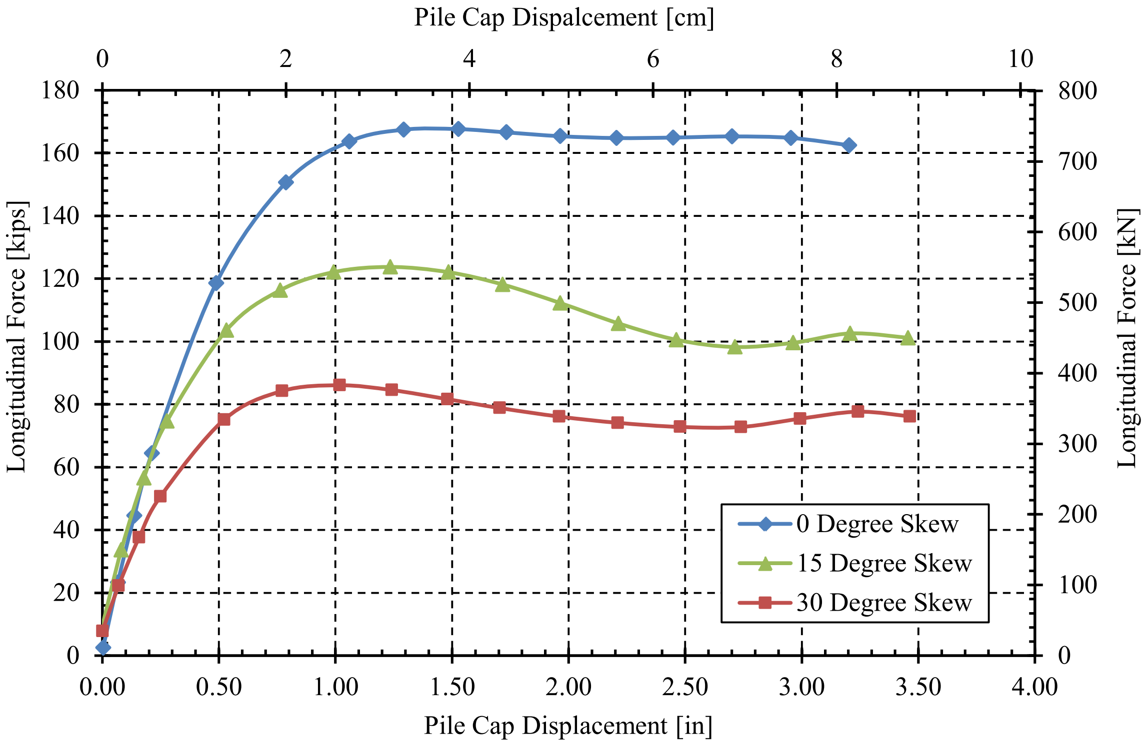

Figure 4-4: Longitudinal force-deflection curves for skews of 0°, 15°, and 30°

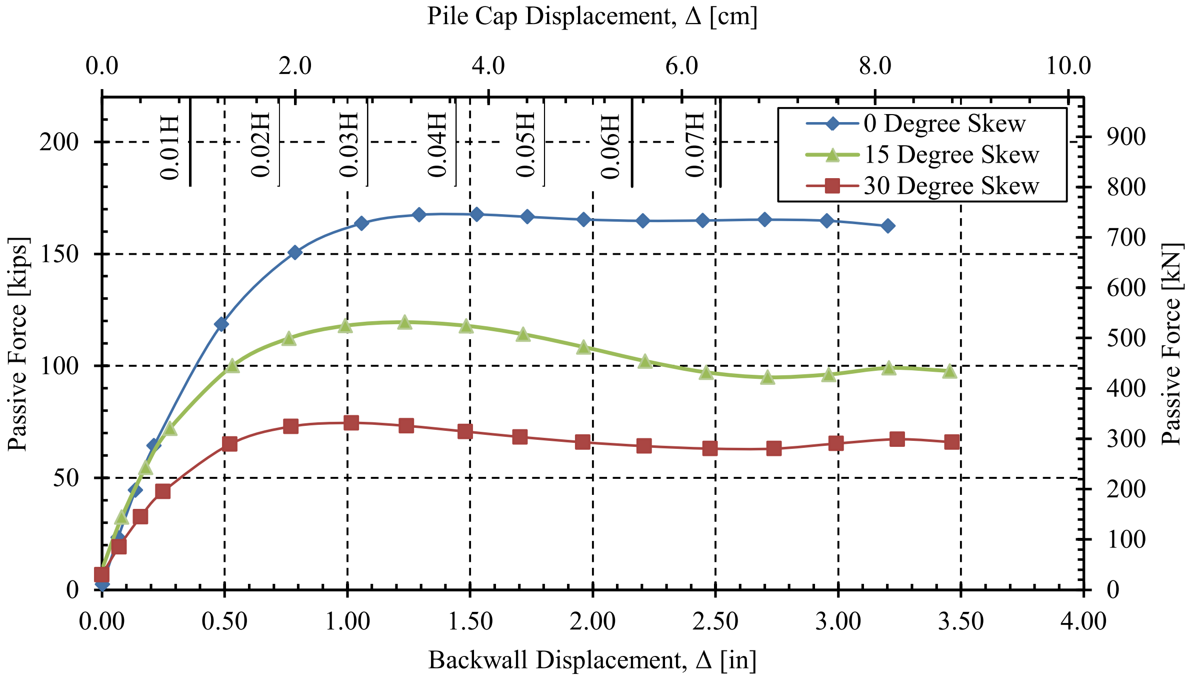

Figure 4-5: Passive force-deflection curves for skews of 0°, 15°, and 30°

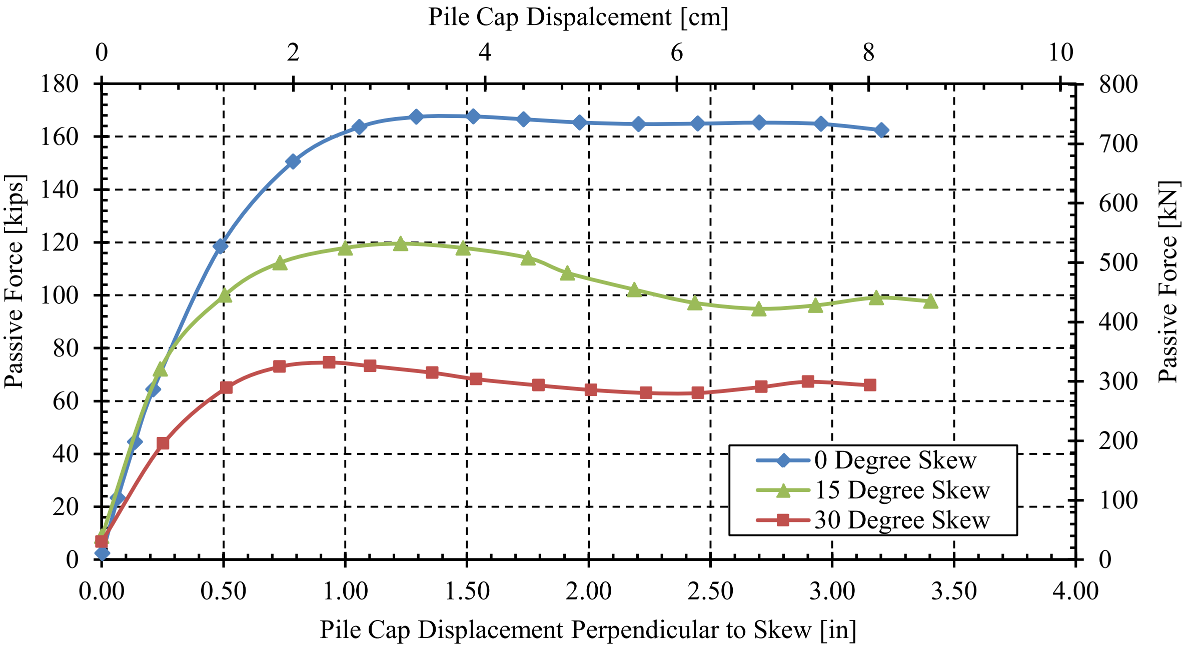

Figure 4-6: Passive force vs. deflection perpendicular to skew interface for 0°, 15°, and 30° skews

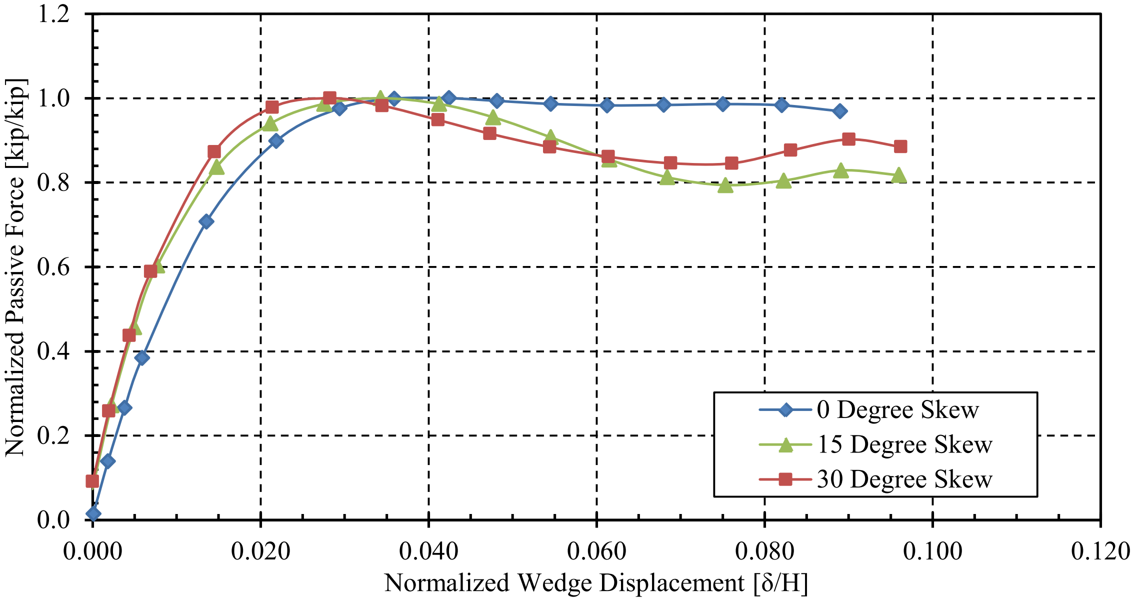

Figure 4-7: Normalized passive force vs. normalized pile cap displacement

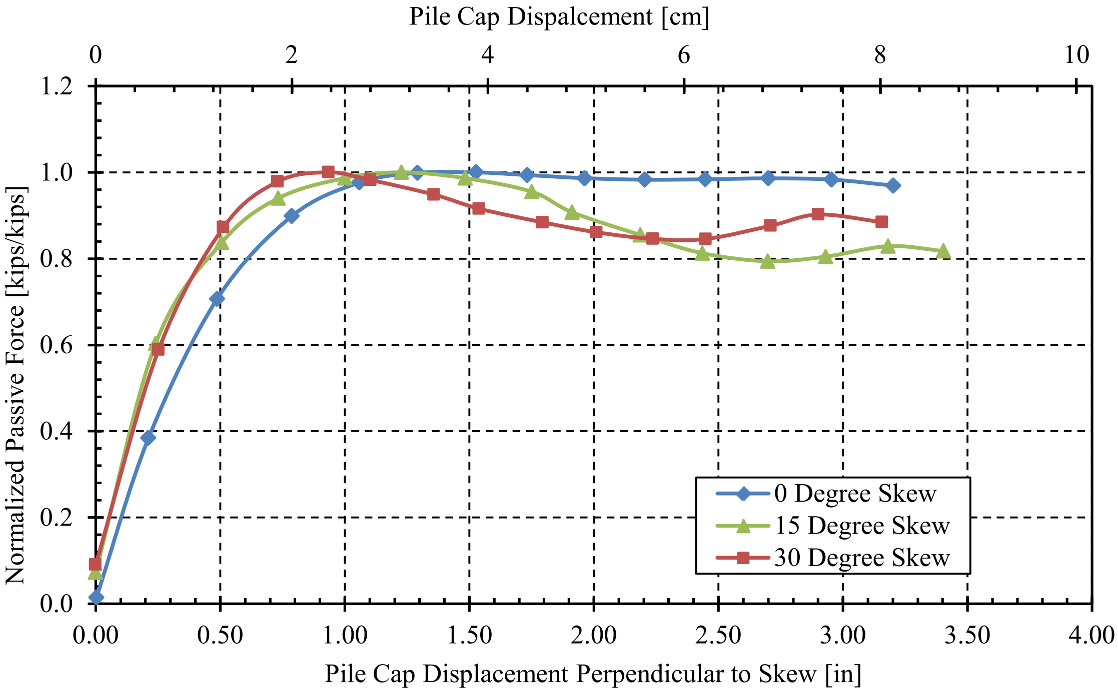

Figure 4-8: Normalized passive force vs. deflection perpendicular to skew

4.3 Reduction Factor for Skewed Abutments

The main objective of this study was to define a correlation between skew angle and passive resistance reduction to apply to bridge design. To obtain this ratio, skewed backwall test values were normalized by the passive force for the 0° skew test. Results for this study are summarized in Table 4-2 below.

Table 4-2: Passive Force-Skew Angle Relationship, Deflection of Peak Passive Forces, and Ratio of Peak Force Deflection to Wall Height

Skew	*Peak Passive Force [kip] (kN)*	*Strength Reduction with Skew [%]*	*Deflection at Peak Passive Force [in] (cm)*	*Deflection Relative to Wall Height Δ/H [%]*
0°	167.6 (745.5)	100	1.53 (3.89)	4.3
15°	119.5 (531.6)	71.3	1.23 (3.12)	3.4
30°	74.52 (331.4)	44.5	1.02 (2.59)	2.8

As can be seen, significant strength reductions were shown as the skew angle increased. For this study, the 15° skew produced results that were 71.3% of the 0° skew strength, a difference of 28.7%. The 30° skew resisted 44.5% of the passive force resisted by the 0° skew, a decrease of 55.5%. Oftentimes, bridge damage is accredited to bridge deck rotation. However, these results make it apparent that underestimating the passive force would likely exacerbate the bridge damage.

The reduction in passive strength with increased skew angle can be explained by force distribution. As stated previously, both shear resistance and passive resistance counteract the longitudinal force acting on a bridge. When an abutment is positioned normal to the soil backfill, resistance is attributed entirely to the passive resistance. This would correspond to a reduction factor, R_{skew} of 1 in this study. As the angle increases, shear resistance withstands the horizontal component of the longitudinal force and must continue taking on larger components of this force until the skew reaches a maximum of 90°. By this point, the resistance is considered to be entirely due to shear strength, which is weaker than passive strength. Since passive strength no longer exists, R_{skew} would be equal to a value of 0. These forces will be described in greater depth in Section 4.5.1.

By plotting the passive force ratios from this study along with the proposed reduction ratio equation of Rollins and Jessee (2012) presented in Figure 2-18, we obtain Figure 4-9. As can be seen, the ratios from this study are in good agreement with the predicted reduction factors produced by laboratory test results from Rollins and Jessee and numerical results presented by Shamsabadi et al. (2006). However, the higher width to height ratio of the backfill in this field study may have affected the reduction factor of the 30° skew test results as this value is somewhat lower than the predicted curve. Therefore, further testing at an angle of 45° is recommended to confirm this variance in force reduction.

The second order polynomial regression curves for the field test data, laboratory test data (Rollins & Jessee, 2012), and numerical analysis results (Shamsabadi et al., 2006) are presented in Figure 4-10. Each curve produced a slightly different equation, but when test results from all three tests were combined, the regression curve was almost identical to the one proposed by Rollins and Jessee. Equation (4-1) gives the reduction factor, R_{skew} corresponding to each of the regression lines in Figure 4-10.

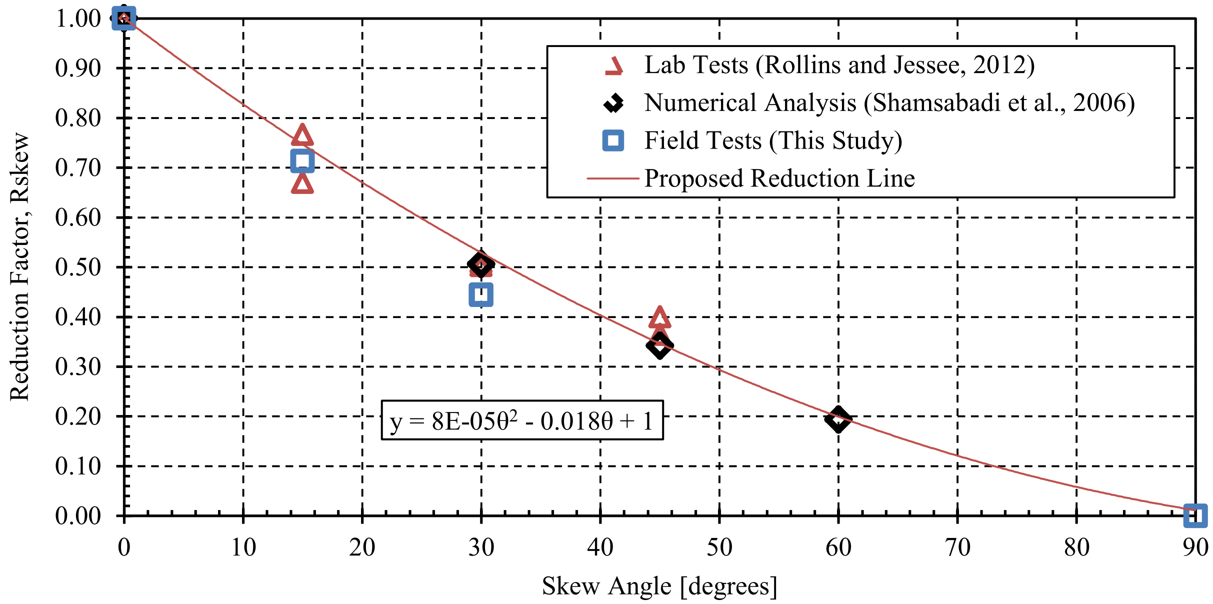

Figure 4-9: Reduction factor, R_{skew} plotted versus skew angle based on lab tests (Rollins & Jessee, 2012), numerical analyses (Shamsabadi et al., 2006), and field tests in this study

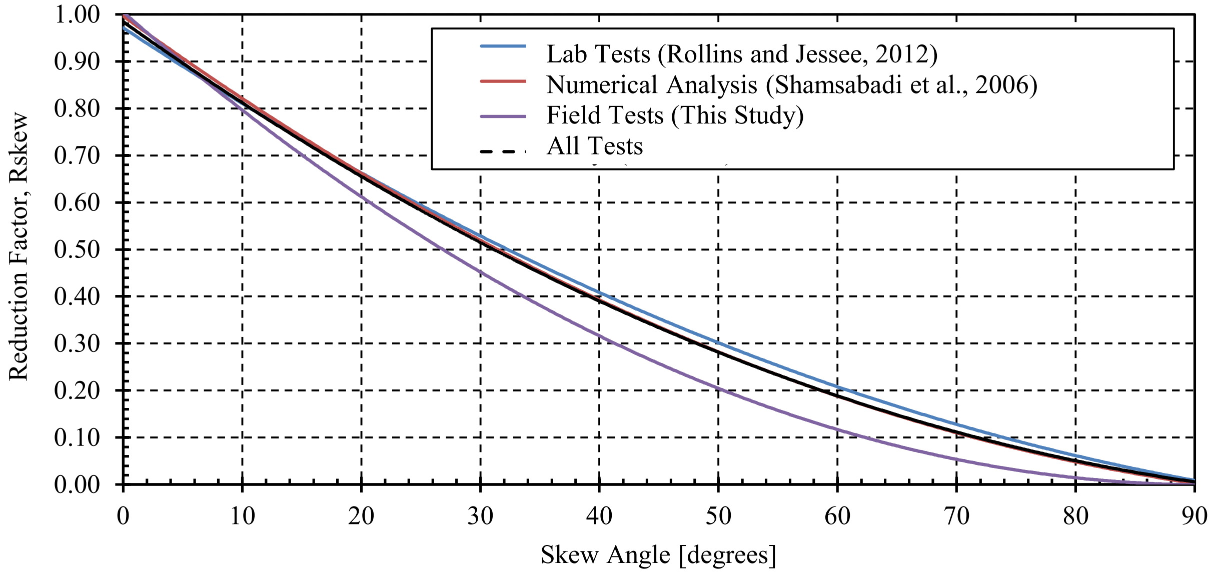

Figure 4-10: Reduction factor trend lines plotted versus skew angle for lab tests (Rollins & Jessee, 2012), numerical analyses (Shamsabadi et al., 2006), and field tests in this study

$$R_{skew} = 1 * 10^{-4}\theta^2 - 0.0221\theta + 1.0\ (field\ tests) \tag{4-1}$$

$$R_{skew} = 7 * 10^{-5}\theta^2 - 0.0168\theta + 1.0\ (lab\ tests) \tag{4-2}$$

$$R_{skew} = 8 * 10^{-5}\theta^2 - 0.0183\theta + 1.0\ (numerical\ analysis) \tag{4-3}$$

$$R_{skew} = 8 * 10^{-5}\theta^2 - 0.018\theta + 0.98\ (all\ data\ points) \tag{4-4}$$

where

$$R_{skew} = \frac{P_{P-skew}}{P_{P-no\ skew}} \tag{1-1}$$

Each of the regression curves appropriately assumes that R_{skew} is 1 at 0° and 0 at 90°. Considering the relatively good agreement between the various curves, at this point is seems appropriate to recommend the use of the equation proposed by Rollins and Jessee (2012). Passive force estimations for bridges with skewed abutments can be obtained by estimating the passive force for a non-skewed bridge abutment using proper methods and then multiplying this value by the appropriate reduction value, R_{skew} obtained in Figure 4-10 or Equation (4-1).

4.4 Actuator Load Variation

Both the east and west actuator loads combined to produce the total load exerted on the pile cap during testing. Due to damage concerns from over-rotation and lateral deflection, efforts were made to minimize these movements by applying uneven loads with the actuators so that the pile cap moved longitudinally into the backfill soil.

Unique to the 0° skew test, Figure 4-11 presents certain points in the test where the actuators experienced a greater force on the east side than on the west. This was to be expected for a non-skewed interface where the pile cap did not have passive resistance forcing it to one side or the other and could therefore move in both transverse directions. The initial increase in east actuator forces prevented movement to the east, but this additional force then had to be compensated by the west actuator to prevent over-rotation to the west. These actuator forces can be viewed by their respective contributions toward the total applied load in Figure 4-12.

On average, the east actuator contributed approximately 49% of the passive force while the west actuator contributed 51%. The west actuator force exceeded the east side at a displacement of approximately 1.6 in (4.06 cm). This is at relatively close to the displacement for which the total peak passive pressure was achieved. After this point, the west actuator continued to increase while the east actuator gradually decreased. At the completion of the test, the west actuator extended 0.04 in (0.10 cm) further than the east actuator, resulting in a small clockwise rotation of the pile cap.

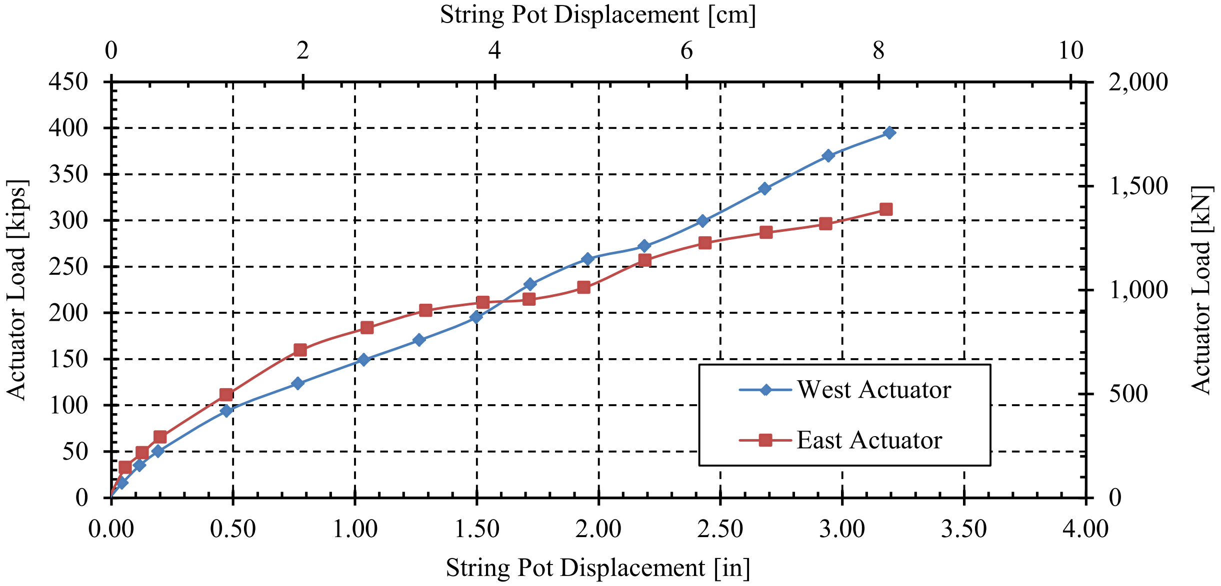

Figure 4-11: Individual actuator contribution to the load vs. displacement curve for the 0° skew test

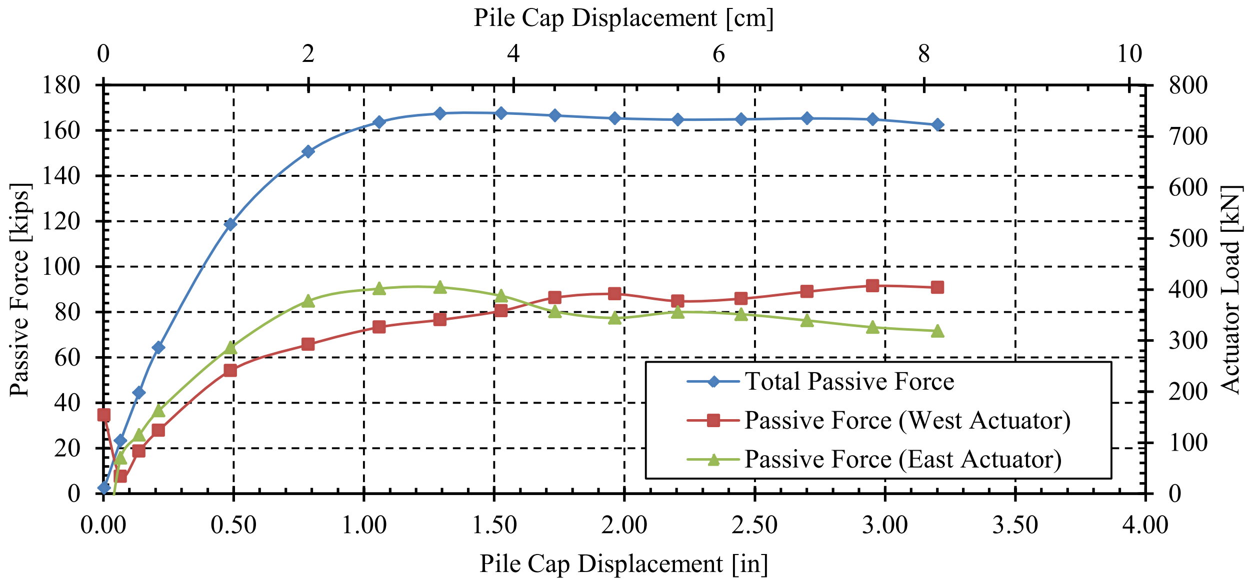

Figure 4-12: Total and individual actuator contribution to the passive force-displacement curve for the 0° test

Actuator load results for the 15° skew test are shown in Figure 4-13. For this test, both actuators steadily increased at approximately the same rate with the west actuator being continually higher by an average of 10.4 kips (46.3 kN). The higher force contribution of the west side enabled the pile cap to withstand some of the lateral resistance provided by the passive force, thus maintaining movement in the longitudinal direction.

The east actuator for the 15° skew test contributed approximately 47% of the passive force while the west actuator contributed 53%. At the completion of the test, the west actuator extended 0.015 in (0.04 cm) further than the east actuator, resulting again in a clockwise rotation of the pile cap that was actually smaller than in the 0° skew test.

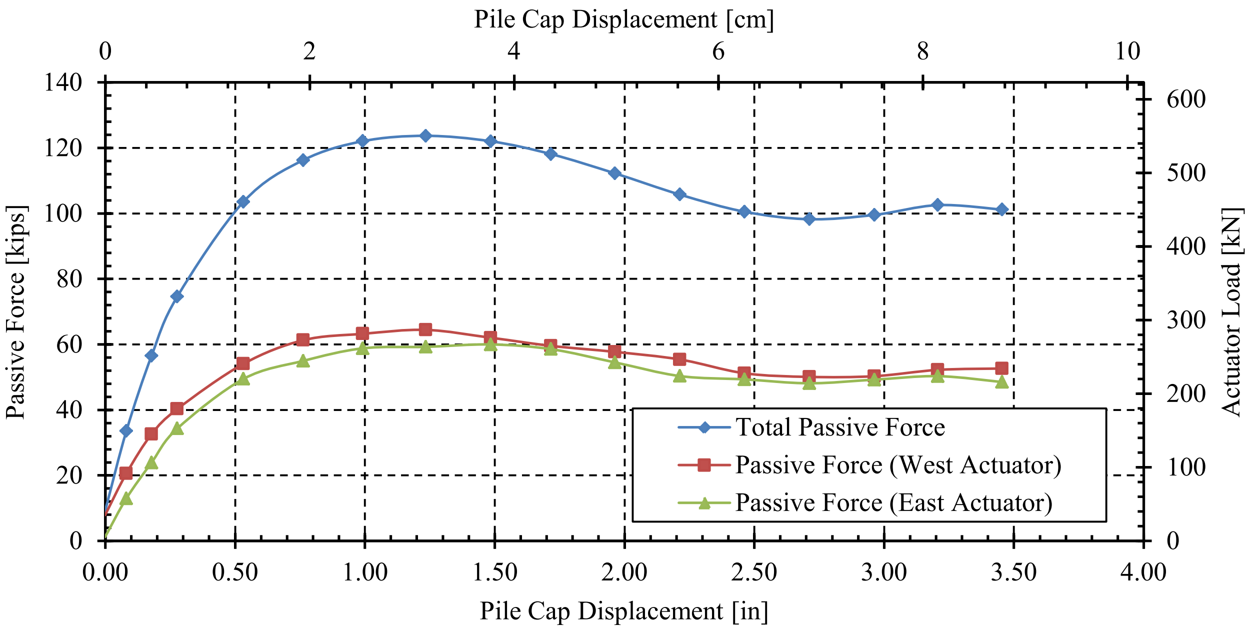

Figure 4-13: Total and individual actuator contribution to the passive force-displacement curve for the 15° test

The 30° skew test had similar results to those of the 15° skew test except more dramatic. As can be seen in Figure 4-14, the west actuator contributed a significantly greater force than that of the east actuator with an average contribution of 59% from the west side and 41% from the east. The greatest difference was seen at a displacement of 1.02 in (2.59 cm), the location of the peak passive force. The final longitudinal displacements of both actuators were virtually identical.

Actuator load contribution percentages for both the east and west side of the 15° and 30° skew tests are shown in Figure 4-15. As can be seen, actuator load percentages for the 15° skew test leveled out at approximately 0.53 in (1.35 cm) while 30° skew actuators did not become steady until approximately 1.7 in (4.32 cm). The load deviation is also much more apparent for the 30° skew test. This variance is expected to continue increasing with skew angle.

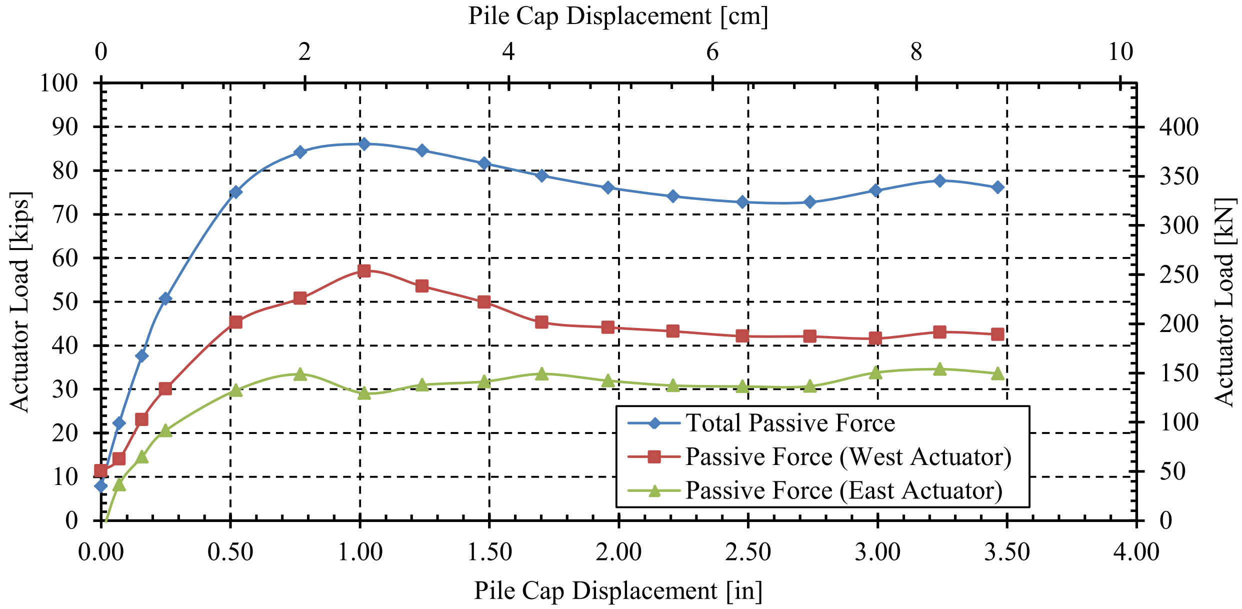

Figure 4-14: Total and individual actuator contribution to the passive force-displacement curve for the 30° test

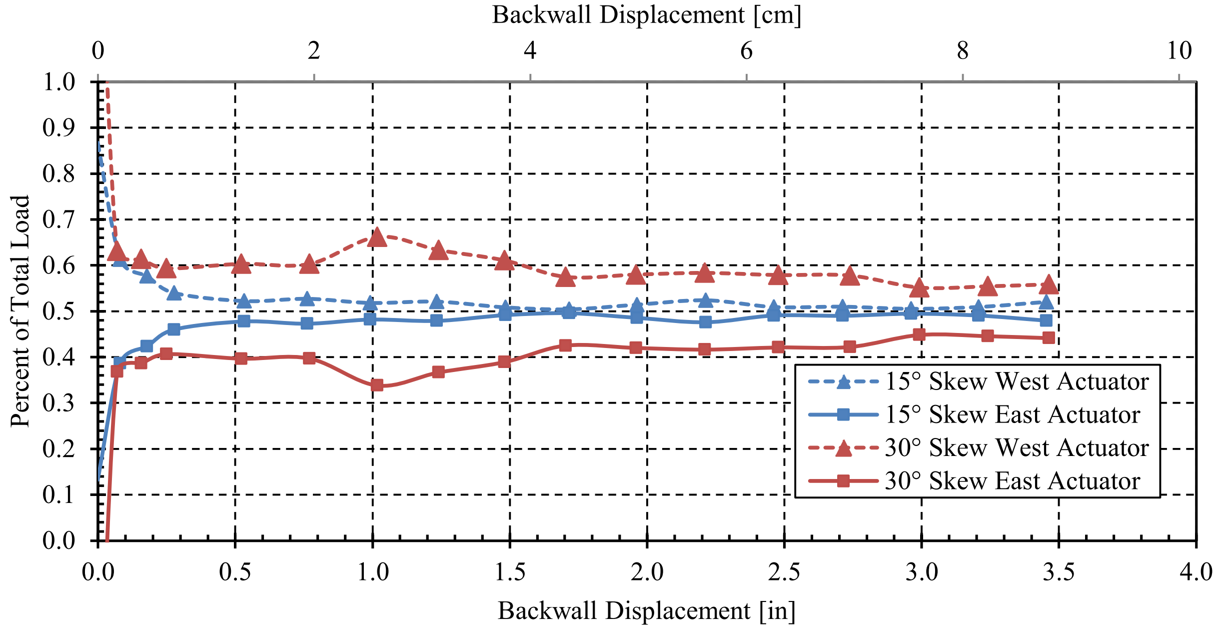

Figure 4-15: Percentage of total load resisted by west and east actuators for skewed tests

Variations between the two actuators caused moments to be applied to the pile cap. These moments can be seen in Figure 4-16 below with the counterclockwise direction referring to positive moments. For the 0° skew test, a maximum moment of 48.0 kip-ft (65.1 kN-m) was experienced at a deflection of 0.79 in (2.01 cm), and the final moment was a clockwise magnitude of 47.8 kip-ft (64.8 kN-m). Maximum applied moments for the 15° and 30° skew tests were 21.4 kip-ft (29.0 kN-m) and 69.7 kip-ft (94.5 kN-m) respectively. Both tests experienced clockwise rotations for their entire durations. This was done to restrain the pile cap from the rotation that was being induced by the passive soil pressure.

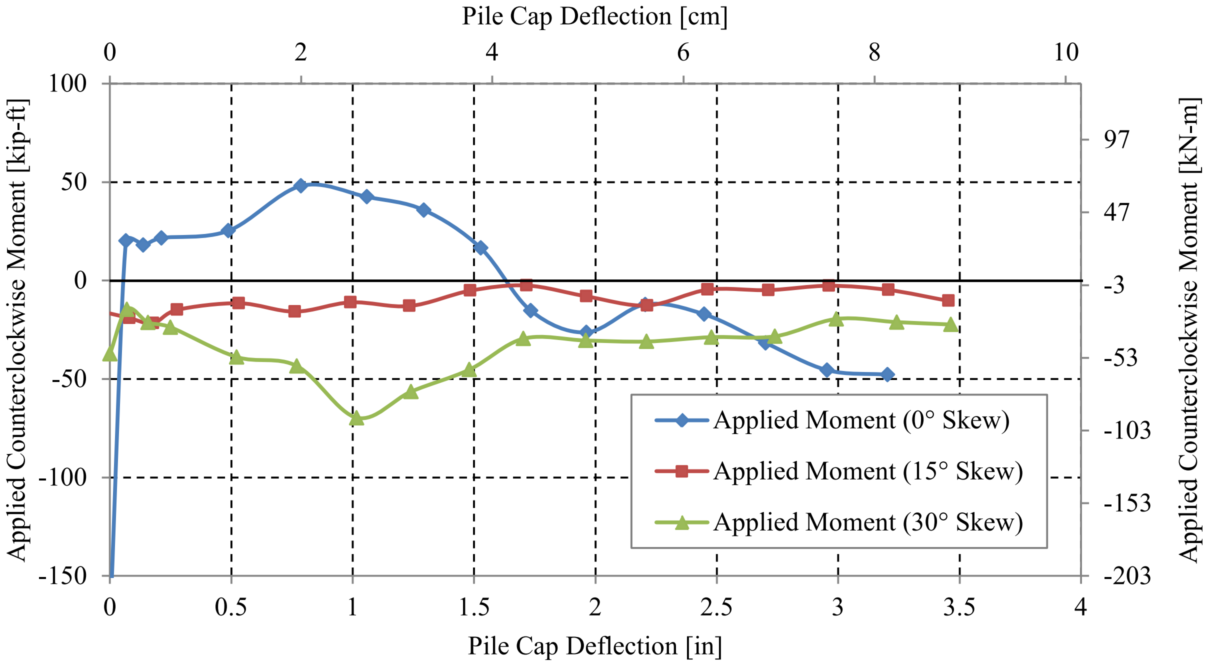

Figure 4-16: Actuator applied counterclockwise moment for the 0°, 15°, and 30° tests

4.5 Variations of Forces with Skew Angle

This section describes the forces acting on two regions of the testing apparatus including the soil-backwall interface and the entire pile cap. The first analysis specifically addresses shear resistance while the purpose of the latter analysis is to use these shear resistance values to estimate the contribution of the pile groups to lateral resistance of the pile cap.

4.5.1 Forces on the Soil-Backwall Interface

As explained in Section 2.2, four main forces act on the soil-wedge interface between the abutment and backfill including the longitudinal force, passive resistance, shear resistance, and applied shear force. Learning the balance between these forces can improve understanding of soil behavior. A comparison of these forces for the 0°,15°, and 30° skew tests and can be seen in Figure 4-17 below. Values were developed using Equations (2-1), (2-2), and (2-3) for forces due to skewed bridges based on force equilibrium principles. Shear resistance with an assumed friction angle, $\phi°$ of 42 and a cohesion, *c* of 100 lbf/ft^2 (4.79 kN/m^2). These values were selected based on a comparison with the measured passive force using computer optimization the log-spiral approach which will be discussed in more detail in Section 7.2.

For the 0° skew 3-ft (0.91-m) unconfined backfill test, the longitudinal force did not produce a component in the transverse direction. Thus, the passive force accounted for the entire longitudinal force and the pile cap was assumed to induce no shear force. Despite this lack of shear force, shear resistance was still present from the soil cohesion and the wall friction.

For the 15° skew test, the shear resistance exceeded the applied shear force as shown in Figure 4-17 and the factor of safety against shearing was approximately 2.2. This result tells us that the soil most likely did not shear along the interface of the pile cap. Similar findings were obtained by Rollins and Jessee (2012) in their laboratory-scale test. For the 30° skew test, the applied shear force was almost exactly equivalent to the shear resistance at an average factor of safety of 1.05. With such a low factor of safety, it is likely that shear failure occurred between the backwall and soil backfill, thus compromising the lateral stability of the pile cap and allowing increased lateral displacement.

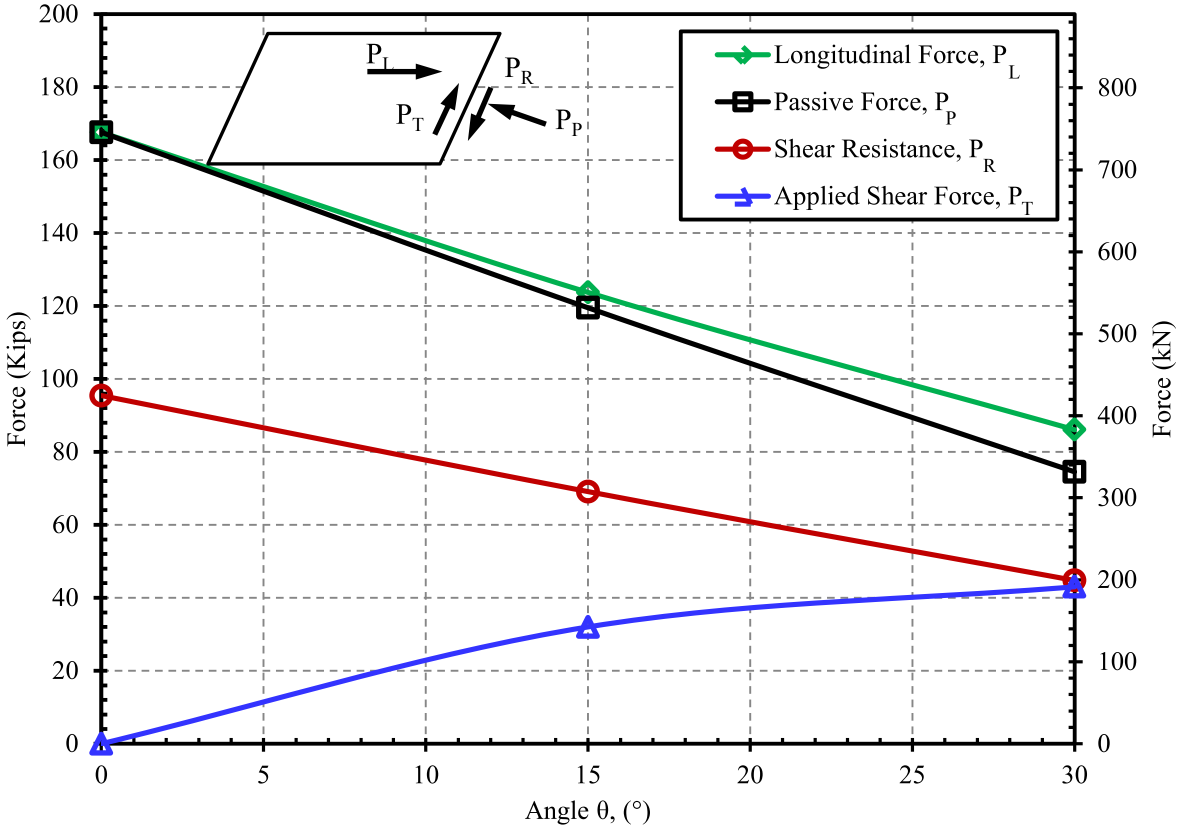

Figure 4-17: Plot of longitudinal force (P_L), passive force (P_p), transverse shear resistance (P_R) and applied shear force (P_T) as a function of skew angle

From these findings, it is important to note that as the skew angle increased, the shear resistance decreased and the applied shear force increased despite the fact that the passive force was decreasing. The skew at which they were relatively equal occurred at 30°. It can be predicted that any skew greater than this magnitude would cause the backfill to fail via shear failure at the interface of the backwall. This shear failure would allow the pile cap to move more freely in the transverse direction and could also possibly alter the behavior of the failure plane of the backfill failure wedge.

The relationship between applied shear force and transverse displacement can be seen in Figure 4-18 (a) below. Figure 4-18 (b) presents the normalized applied shear force versus transverse displacement to facilitate comparisons. Displacement values are based on shape array measurements taken during testing which are discussed in more detail in Chapter 5.

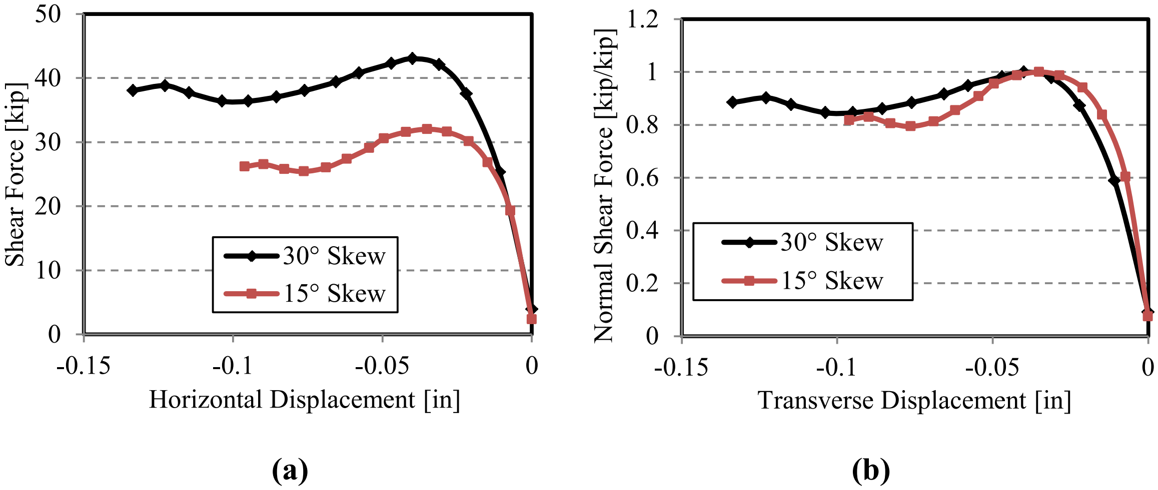

Figure 4-18: (a) Transverse shear force vs. transverse displacement (b) normalized transverse shear force vs. transverse displacement

As explained previously, the sharper angle of the 30° skew caused the shear force to be greater for the 30° skew test than for the 15° skew test. This also resulted in greater ultimate transverse movements toward the acute side of the pile cap as portrayed in Figure 4-18 (a). Theoretically, the maximum shear force of the soil adjacent to the skewed abutments occurred when the applied shear force equaled the shear resistance of the soil. At this point, friction reached its maximum capacity and the soil sheared along the face of the backwall. In this study, the maximum shear force for the 30° skew test occurred at almost the same displacement as that of the 15° skew test [0.035 to 0.04 in (0.09 to 1.02 cm)], as can be seen in Figure 4-18 (b). Once the shear force overcame the shear resistance, transverse movement occurred more freely, resulting in the flatter portions of the curves seen in Figure 4-18 (a) and (b) above. According to Duncan and Mokwa (2001b) the amount of movement typically required to mobilize skin friction on an interface ranges from 0.1 to 0.25 in (2.54 to 6.35 mm). Our findings of 0.035 and 0.04 in (0.89 and 1.0 mm) for the 15° and 30° skew tests, respectively are below this range of values. However, the shear force in relation to movement parallel to the pile cap (Figure 4-19) was greatest at displacements of 0.29 in and 0.49 in (7.4 and 12.4 mm), which is slightly higher than the predicted range.

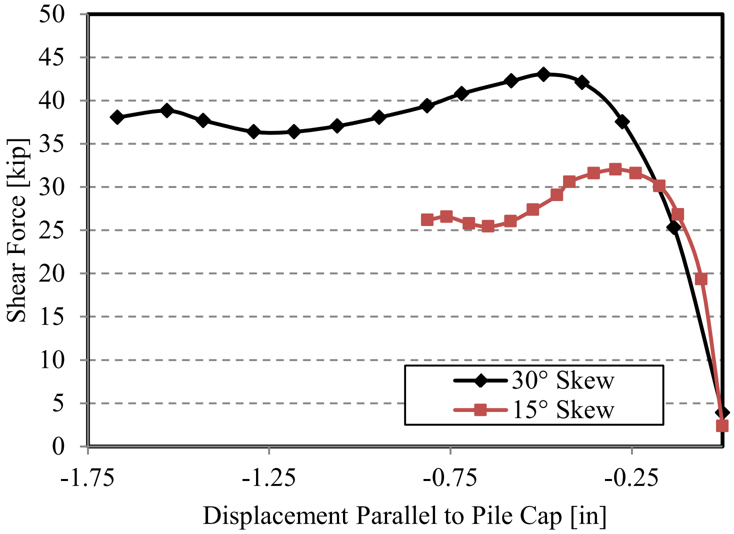

Figure 4-19: Transverse shear force vs. displacement parallel to skewed pile cap interface

4.5.2 External Forces Acting on the Entire Testing Apparatus

Although the pile cap experienced lateral deflection during the 3-ft (.91-m) backfill tests, none of the baseline tests simulated this movement. Therefore, the following calculations were performed to investigate possible concerns regarding the influence of the piles on transverse forces that could have been unaccounted for.

Referring to Figure 4-20, six main forces acted on the pile cap that had an effect on either the moment equilibrium or lateral movement. These forces included the north pile group, F_{pn}, south pile group, F_{ps}, the horizontal component of the backfill shear resistance, $F_{shear\ (h)}$, the horizontal component of the backfill passive resistance, $F_{passive\ (h)}$, and the forces applied by the east and west actuators, F_{ae} and F_{aw}. Passive and shear resistance forces were taken from calculations obtained in Section 4.5.1.

For these calculations, the north and south pile groups were assumed to act as a force couple with equal magnitudes. Moment equilibrium calculations for the 30° skew 3-ft (0.91-m) backfill test revealed that while the passive force and shear resistance had magnitudes of 435.1 kip-ft (589.9 kN-m) and 430.8 kip-ft (584.1 kN-m), the coupling moment provided by north and south pile groups had a combined magnitude of 58.5 kip-ft (79.3 kN-m), 13.4% compared to that of the moment provided by the passive resistance. This percentage was lower for the 15° skew test where smaller rotations and transverse displacements were detected.

Using the pile group loads obtained in the moment equilibrium results above, equilibrium was also measured in the horizontal direction. Four main components were included in these calculations: the north pile group, south pile group, horizontal component of the backfill shear resistance, and the horizontal component of the backfill passive resistance. This horizontal force summation resulted in an imbalance of 0.36 kip (1.60 kN) to the west, a magnitude of only 1.0% compared to that of the passive resistance. A value this small can easily be attributed to minor errors in force predictions, friction at the base of the pile cap, or the force imbalance pushing the pile cap to the west.

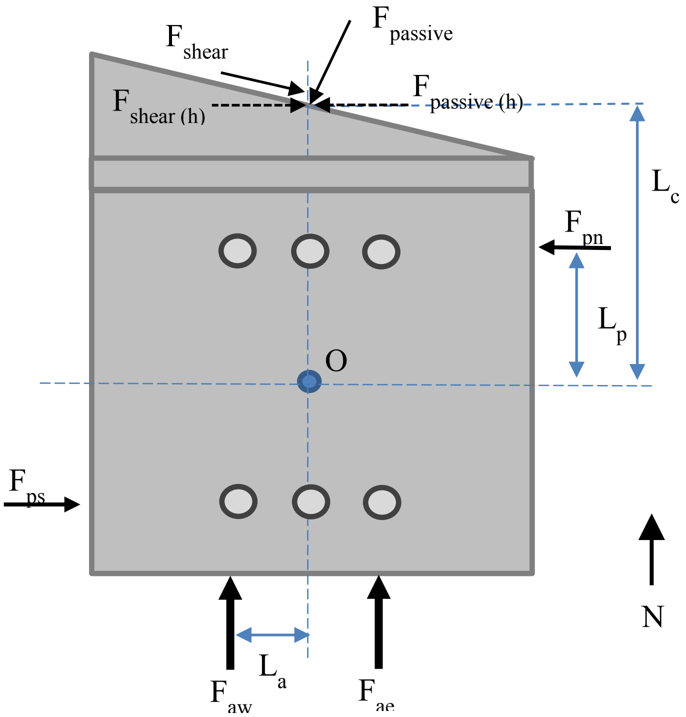

Figure 4-20: External forces causing moments about the center of the pile cap

A comparison of the force equilibrium magnitudes in the x-, y-, and rotational directions can be seen in Table 4-3. The pile groups contributed 4.87 kips (21.7 kN) each in opposite horizontal directions, a magnitude of 13.1% of the magnitude produced by the passive force. Based on this analysis, the force on the pile groups likely had very little influence on the overall relationship between the pile cap and adjacent backfill in the transverse direction.

Table 4-3: Force Equilibrium of the Pile Cap in the x-, y-, and Rotational Directions

	Force Equilibrium	*Units*
x-Direction	-0.36 (-1.60)	kip (kN)
y-Direction	-9.95 (-745.5)	kip (kN)
Rotation	Equal	kip-ft (kN-m)

Note: North= Positive y-direction

5 PILE CAP DEFLECTION

The purpose of this chapter is to address the behavior of the abutments, piles, and the adjacent backfill with longitudinal movement through test data analysis. This study recorded pile cap movements using shape arrays, inclinometers, string pots, and LVDTs for the 0°, 15°, and 30° 3-ft (0.91-m) unconfined backfill tests. Data is provided for movement in the longitudinal and transversal directions as well as rotation about the longitudinal and transverse axes. Accuracy of the different types of instrumentation is also assessed in this chapter.

5.1 **Longitudinal Pile Cap Movement**

The inclinometers and shape arrays provided displacement vs. depth profiles within the piles and pile cap for both the longitudinal and transverse directions. Inclinometer readings were recorded in 2-ft (0.61-m) increments whereas shape array recordings were taken once every foot (0.30 m). On the north end of the cap, both inclinometer and shape array readings were measured to a depth of approximately 39 ft (11.9 m) below the top of the cap, making this the reference point for the inclinometer. For the south end, the inclinometer extended to a depth of 41 ft (12.5 m), but the shape array was limited to a depth of 23 ft (7.0 m) below the cap owing to the shorter length of the available array. String pots were attached to the back of the pile cap at depths of 0.25 ft (0.08 m) and 4.25 ft (1.30 m) below the top of the pile cap.

Figure 5-1, Figure 5-2, and Figure 5-3 provide plots of the longitudinal displacement versus depth results provided by the string pots, shape arrays and inclinometers for the 0°, 15°, and 30° tests, respectively. These figures show the final displacements for each test. The displacement profile typically shows a steep linear slope within the pile cap and a curvilinear shape within the piles below the cap as would be expected. Despite the thickness of the pile cap being 5.81 ft (1.77 m), the slope to the displacement vs. depth profile within the cap indicates that the cap is not completely fixed against forward rotation, although the rotation is quite small.

A review of the results in these figures indicates that the various forms of instrumentation were generally in very good agreement for the 0°, 15°, and 30° tests. According to Rollins et al. (2009), the limit of precision for shape arrays and inclinometers is ± 0.059 in (1.5 mm) and ± 0.049 in (1.24 mm) per 98.4 ft (30 m), respectively. Extensive calculations were later performed that incorporated all three studies from the summer of 2012 (Franke, 2013; Marsh, 2013). These results concluded that both the inclinometers and shape arrays produced measurements within their given ranges of instrumentation error for the longitudinal direction. Moreover, the majority of shape array readings were found to be within 0.03 in (0.8 mm) of the string potentiometers. This is well within their given range of error. These results generally confirm the experience of Rollins et al. (2009) regarding the accuracy and reliability of shape arrays relative to inclinometers. Rollins et al. (2009) Rollins et al. (2009) Rollins et al. (2009) Rollins et al. (2009) Discrepancies between the north and south ends are possibly due to human error while taking measurements or to lateral movement that caused the north end to move more towards the west than the south end did.

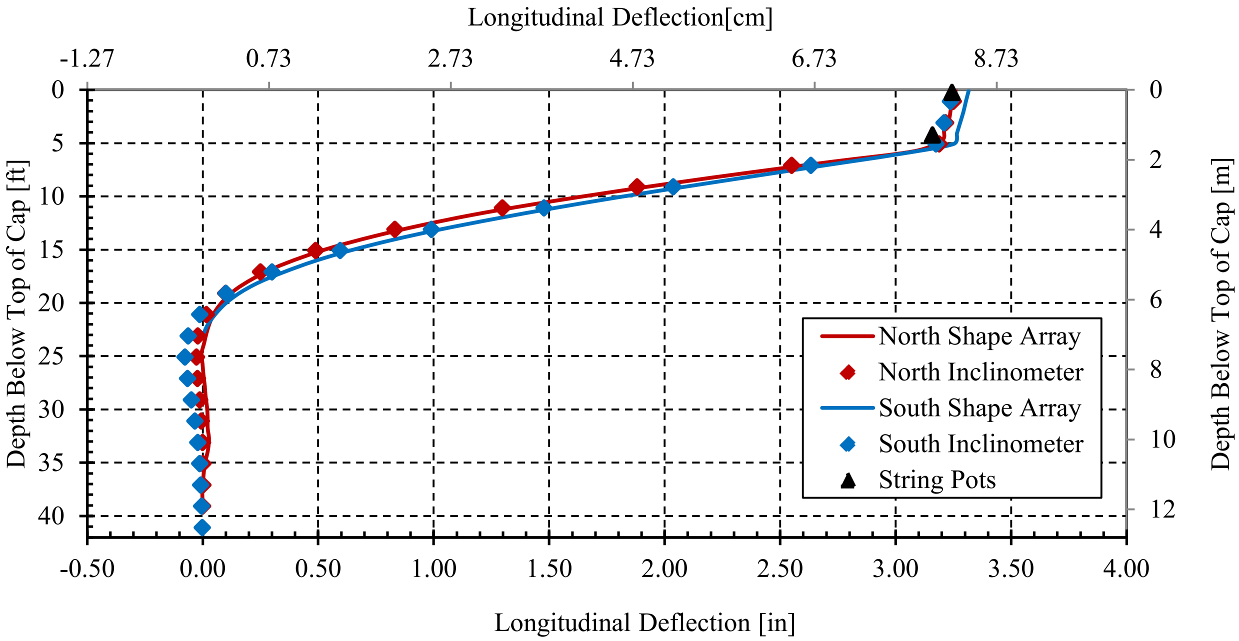

Figure 5-1: Longitudinal pile deflection as measured by the north and south shape arrays, inclinometers, and string pots for the 0° test

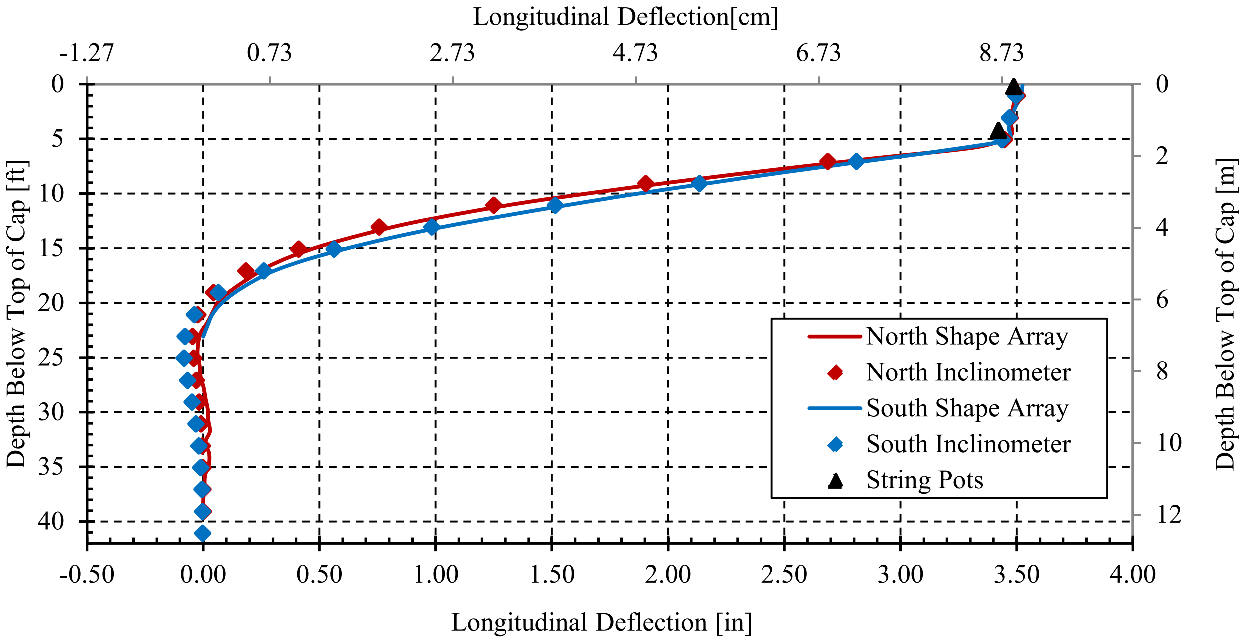

Figure 5-2: Longitudinal pile deflection as measured by the north and south shape arrays, inclinometers, and string pots for the 15° test

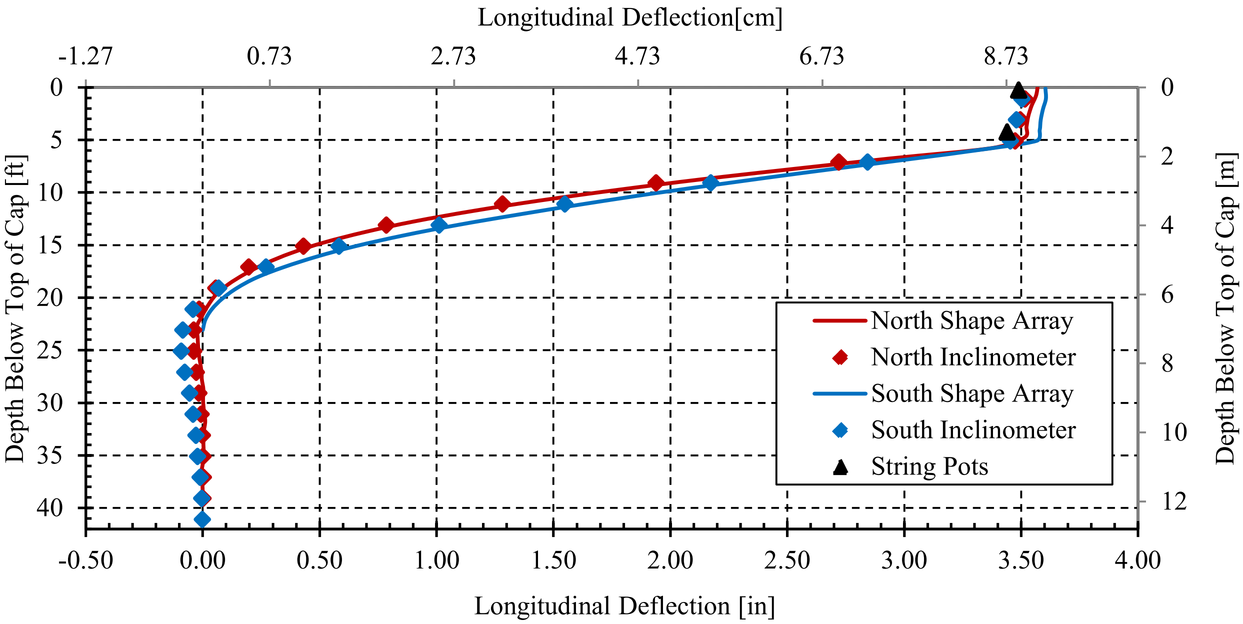

Figure 5-3: Longitudinal pile deflection as measured by the north and south shape arrays, inclinometers, and string pots for the 30° test

The extended amount of time required to take a reading with the inclinometer (15 to 20 minutes) restricted the number of readings to once at the beginning of each test and once at the end. However, the instantaneous recording capabilities of the shape arrays enabled measurements to be taken at every displacement increment throughout the test, as is shown in Figure 5-4, Figure 5-5, and

Figure 5-6. Referring to these three figures, pile cap displacement had very little effect on the piles for depths greater than about 22 ft (6.7 m) below the top of the pile cap. Beneath this point, the piles remained in a relatively fixed position, with a displacement of less than 1% of the maximum displacement. Unfortunately, this minor displacement still affected the south shape array, which used its lowest depth as an absolute zero reference point.

These figures also show the progression of forward pile cap rotation with increased displacement. This rotation will be discussed in greater depth in Section 5.4. Discrepancies between the north and south arrays can be attributed to movement below the zero reference for the south array, human errors, and to unequal lateral movement.

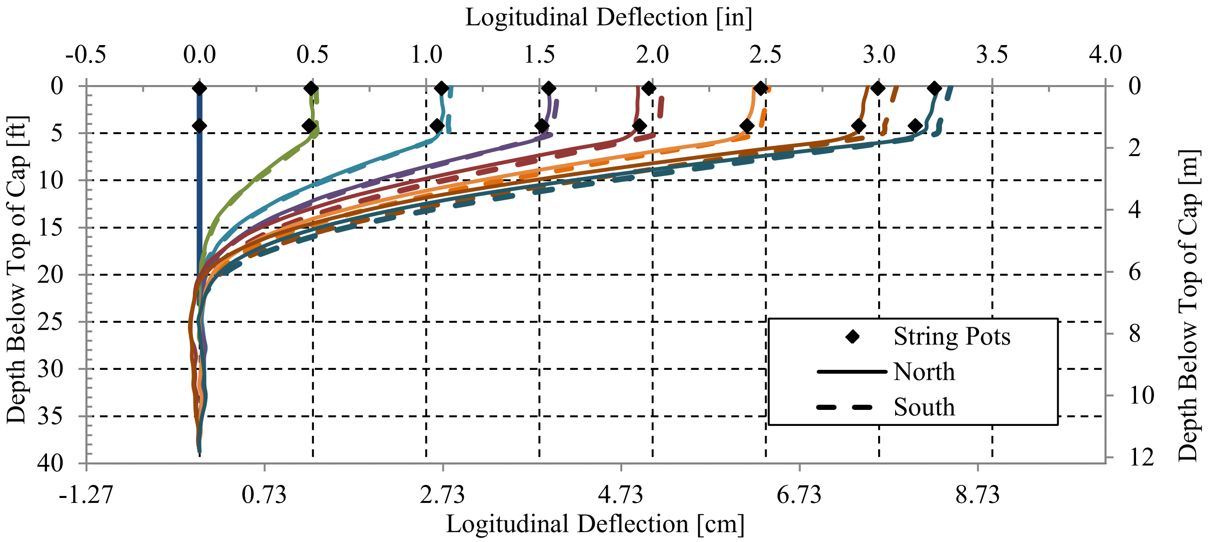

Figure 5-4: Longitudinal pile deflection at selected pile cap displacement intervals as measured by the north and south shape arrays for the 0° test

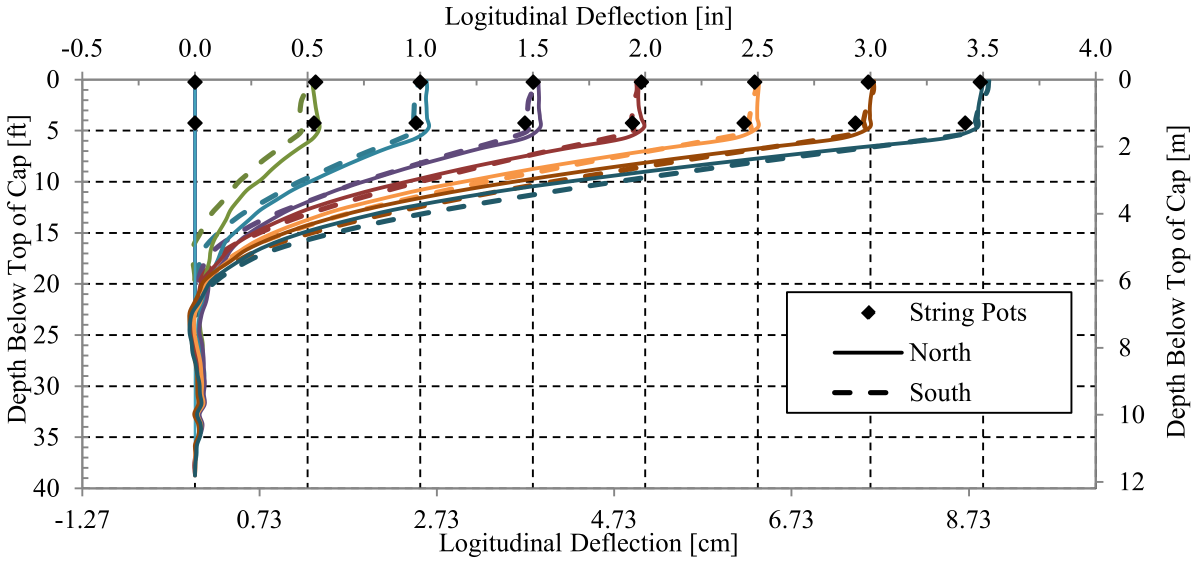

Figure 5-5: Longitudinal pile deflection at selected pile cap displacement intervals as measured by the north and south shape arrays for the 15° test

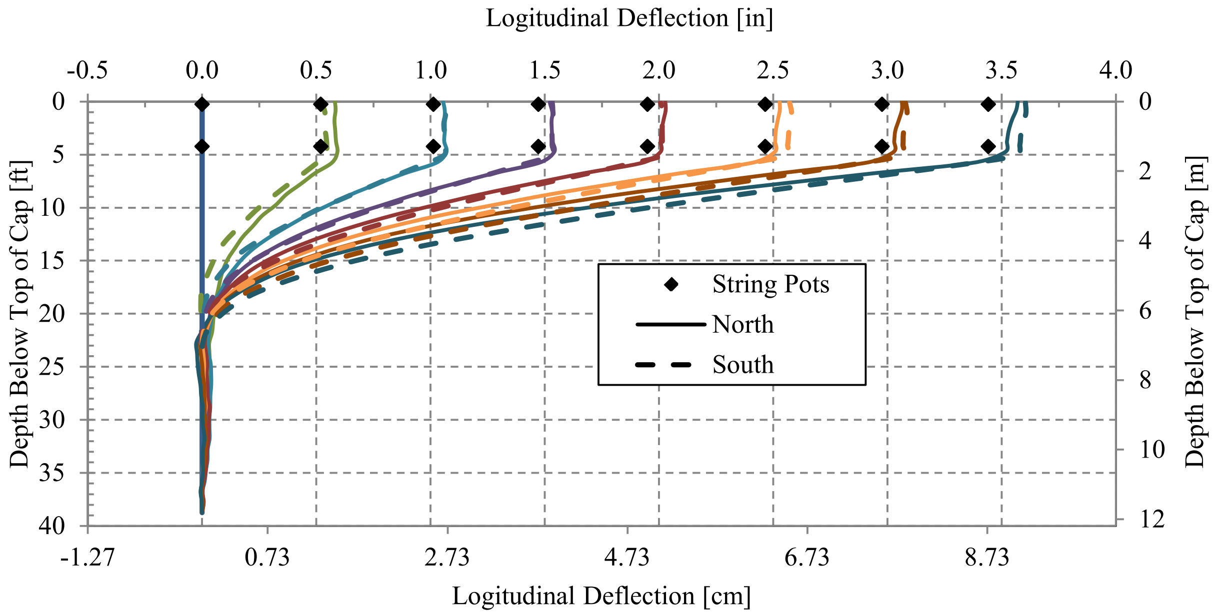

Figure 5-6: Longitudinal pile deflection at selected pile cap displacement intervals as measured by the north and south shape arrays for the 30° test

5.2 Transverse Pile Cap Movement

The pile cap was pushed in the longitudinal direction by keeping the deflection of the east and west sides of the pile cap equal. However, transverse displacements of the pile cap were still observed that can be used to understand the general behavior of the pile cap and adjacent backfill. Figure 5-7, Figure 5-8, and Figure 5-9 show the transverse pile deflection for the 0°, 15°, and 30° tests, respectively at test completion as measured by the shape arrays and inclinometers. LVDTs were also installed for the 15°, and 30° tests but data from this instrumentation proved to be unreliable and was therefore omitted from this analysis.

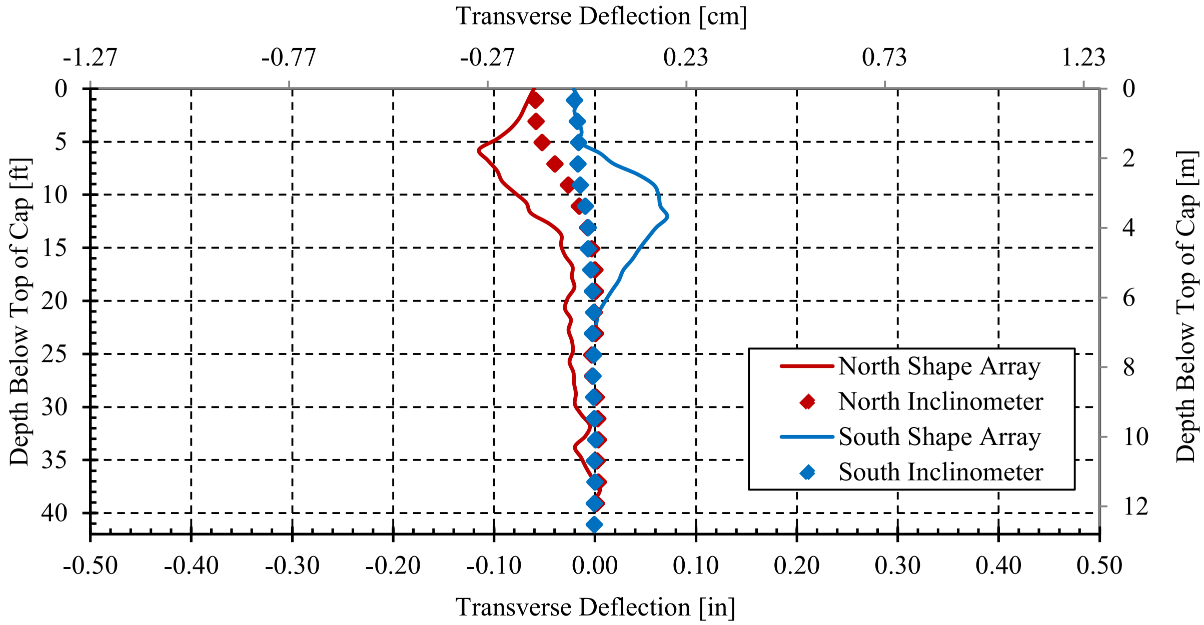

Figure 5-7: Transverse pile deflection as measured by the shape arrays and inclinometers for the 0° test

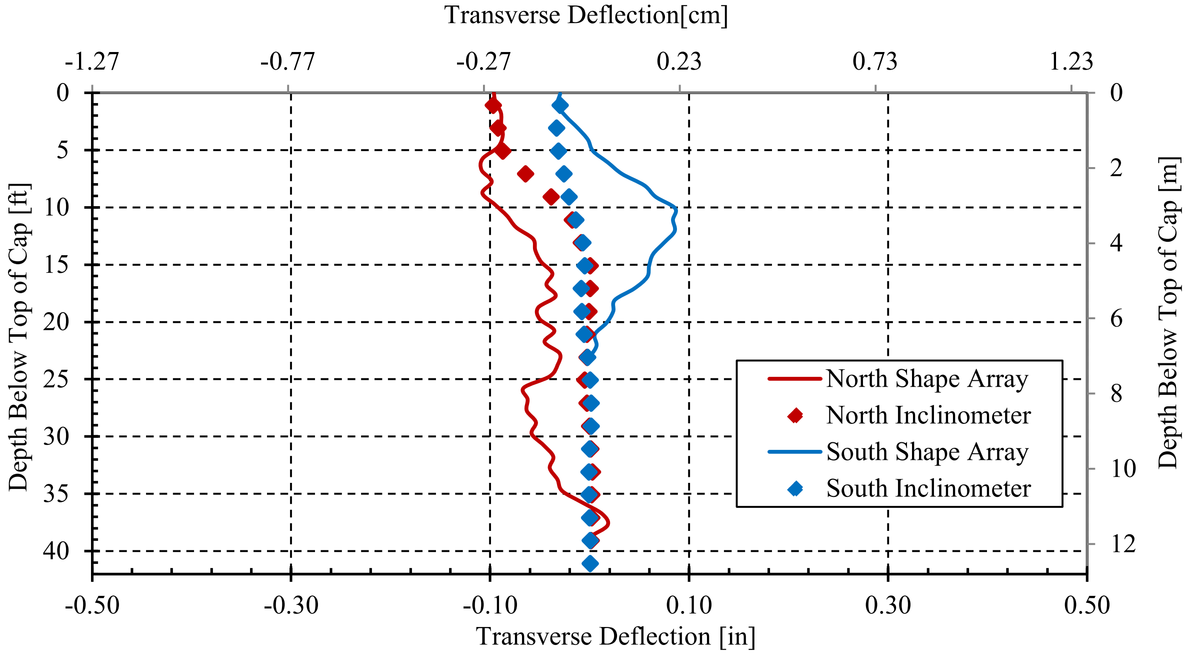

Figure 5-8: Transverse pile deflection as measured by the shape arrays and inclinometers for the 15° test

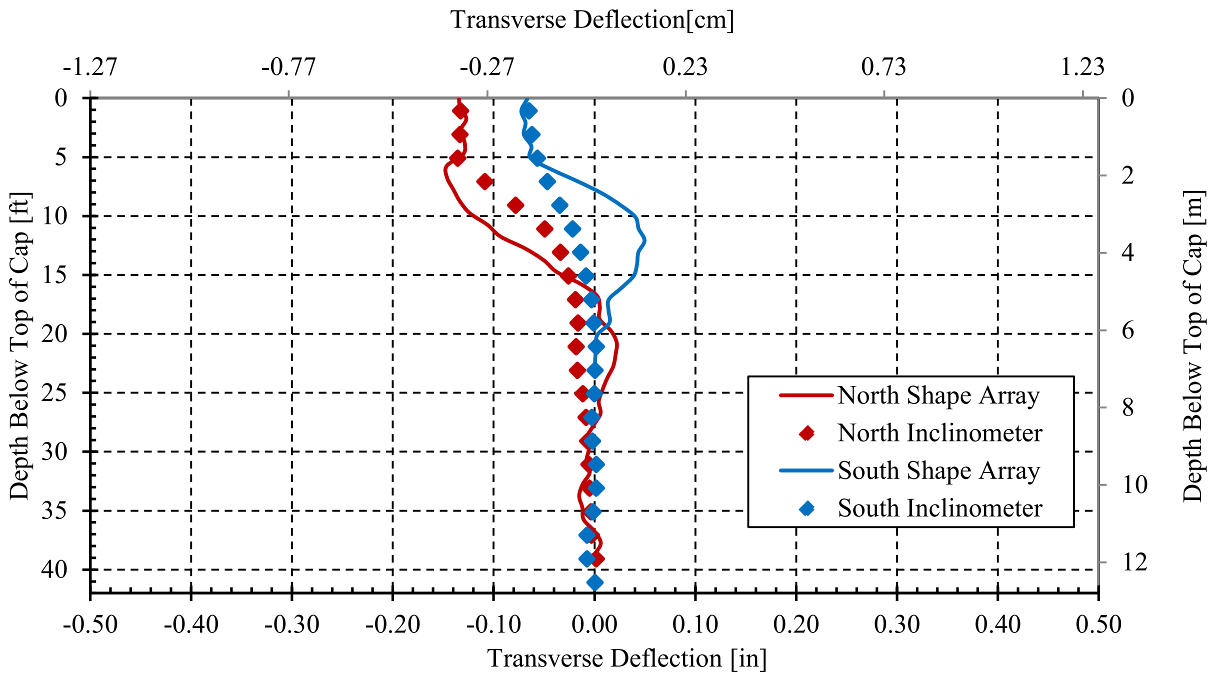

Figure 5-9: Transverse pile deflection as measured by the shape arrays and inclinometers for the 30° test

All three curves show a final lateral deflection in the westward direction with the north end having a greater magnitude than the south end. These transverse deflections increase as the skew angle increases. This behavior can be expected since the backfill applied passive resistance to the pile cap interface in a westward direction perpendicular to the skewed abutment face.

The final lateral deflections with respect to the top of the pile cap were -0.059 in, -0.097 in, and -0.133 in (-0.15 cm, -0.25 cm, and -0.34 cm) for the 0°, 15° and 30° tests, respectively. The south end experienced smaller deflections of -0.020 in, -0.029 in, -0.065 in (-0.05 cm, -0.07 cm, -0.17 cm) for the 0°, 15° and 30° tests, respectively. These values will later be used in Section 5.3 to examine the rotation about the longitudinal axis.

The three figures above show that discrepancies between the inclinometers and shape arrays were very apparent in the transverse direction. In this case, the shape arrays were considered to be accurate at the top and bottom of the arrays but not in the region between these two points. As indicated by Rollins et al (2009), shape array deflections are not particularly accurate at the small deflection levels typical of the transverse deflections. For the majority of the points within the depth profiles, these results are within the range of error provided by the manufacturers. Fortunately, this error has little effect on results for the longitudinal movement where the magnitude of displacement is much larger. To improve accuracy at smaller displacements, it is recommended that the number of samples being averaged be at least a minimum of 1000 samples—unlike the value of 30 samples that was used in this study (Levesque, 2012). Although other means of error would still have been present, increasing the number of samples being averaged would likely have improved accuracy to at least some degree. Given the sporadic results in the transverse direction but the accurate results in the longitudinal direction, shape arrays may not be the optimum form of instrumentation for small deflections; however, they still have good potential and benefits in other geotechnical applications where larger deflections occur.

5.3 Pile Cap Rotation about the Longitudinal Axis

Imbalanced forces about the centroid of the pile cap caused it to rotate slightly during testing. This rotation occurred about both the vertical and transverse axes. As with transverse movement, rotation about the vertical axis was also restricted by the actuators due to safety precautions. Both shape arrays and inclinometers were used to measure rotation in this direction by recording the total magnitude of transverse movement at the south and north ends of the pile cap and using simple trigonometry to calculate the degree of rotation. These north and south locations were installed in line with the longitudinal axis and were spaced 12 ft (3.66 m) apart.

Maximum rotation data recorded by both the shape arrays and inclinometers for the 0°, 15° and 30° tests is shown in Figure 5-10.

As predicted by previous studies, pile cap rotation occurred in the direction opposite to the skew angle, which in this case resulted in a counterclockwise rotation (FHWA, 2011). The maximum rotations increased with skew angle as shown in Figure 5-10 and had magnitudes of 0.015°, 0.026°, and 0.027° for the 0°, 15° and 30° tests, respectively. With such small rotation values, it can be concluded that the pile cap underwent very little rotation during testing. Rotation magnitudes can be expected to increase for actual skewed bridge decks where this movement is not properly restricted.

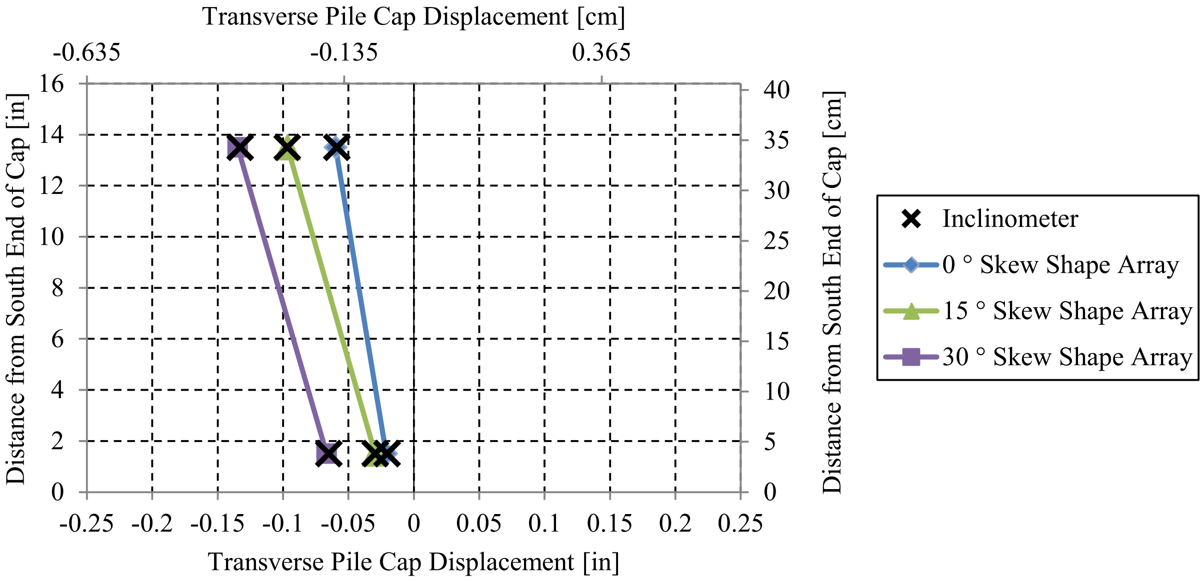

Figure 5-10: Transverse movement of the pile cap at final displacements for the 0°, 15° and 30° test as measured by the shape arrays and inclinometer

5.4 Pile Cap Rotation about the Transverse Axis

Shape arrays, inclinometers, and string pots all detected forward rotation of the pile cap about the transverse axis. This rotation is shown by the forward slant at the tail end of Figure 5-11.

Figure 5-12 provides forward rotation measurements for all three tests as recorded specifically by the string pots. According to these findings, all three tests the pile cap experienced forward rotation to some degree or another. This rotation was caused by a coupling force from the actuators and the piles—as the actuators applied a longitudinal force to the center of the pile cap the piles resisted this force on the bottom of the pile cap in the backward direction.

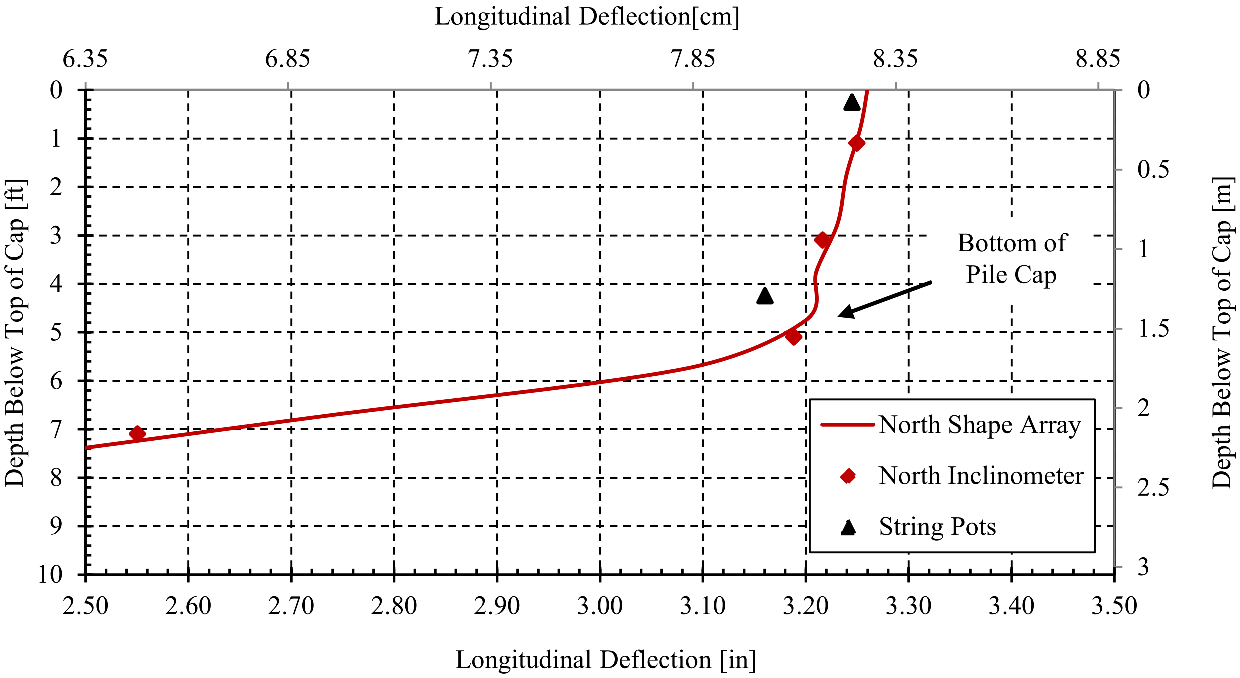

Figure 5-11: Pile cap rotation about the transverse axis as shown by the shape array, string pots, and inclinometer for the 0° test

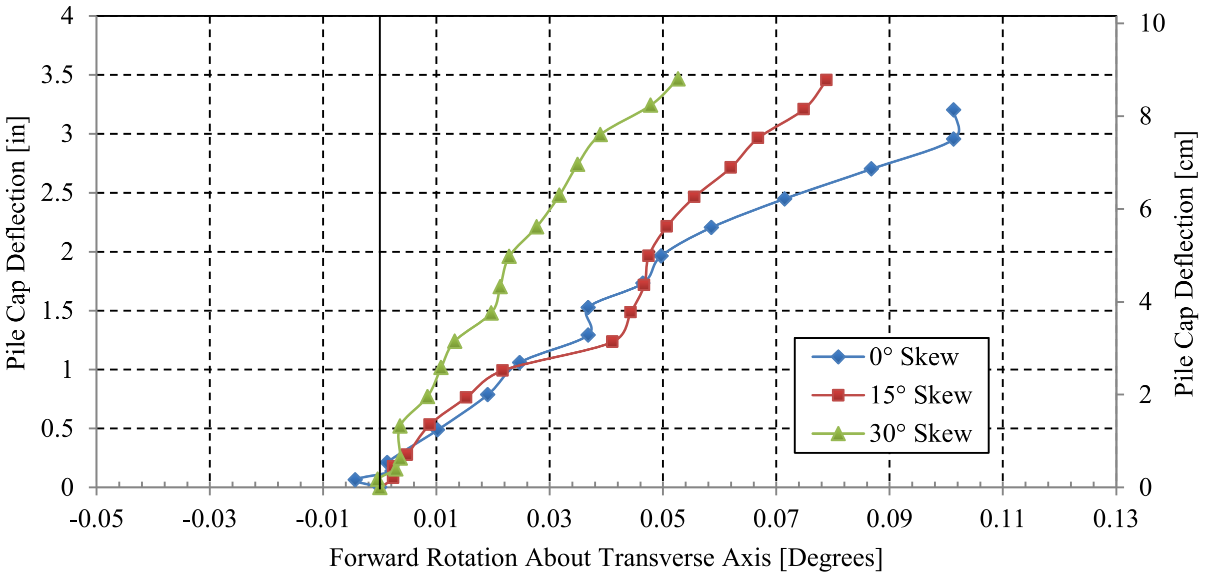

Figure 5-12: Forward rotation of the pile cap about the transverse axis as measured by the string pots for the 0°, 15° and 30° test

As can be seen in the figure above, rotation increased as the longitudinal displacement increased, resulting in maximum forward rotations at the greatest longitudinal displacement magnitudes. These maximum rotations had magnitudes of 0.10°, 0.075°, and 0.048° for the 0°, 15° and 30° tests, respectively. Although these magnitudes are small, they reveal that forward rotation decreased with increased skew. This behavior is caused by the concrete wedges attached to the front of the pile cap resisting downward movement as the pile cap rotated forward. Maximum displacement variations between the base of the 3-ft (0.91-m) backfill and the top of the backfill never exceeded 0.07 in (0.18 cm). Displacement variations of this magnitude are too small to have a significant effect on the behavior of the backfill.

6 BACKFILL DISPLACEMENT, STRAIN, AND FAILURE

The shear failure wedge for all three tests was determined three-dimensionally by visually examining cracks in the surface, recording surface heave elevations in a grid-like manner across the entire backfill surface, and inserting red sand columns that detected the shear failure plane through the backfill, as described in Section 3.5. This chapter includes contour plots and shear failure plane plots constructed using these test results. Additionally, backfill displacement and strain results are included in this chapter as recorded by string potentiometers attached to stakes located in a longitudinal direction away from the backwall.

6.1 Backfill Heave and Surface Cracking

Contour maps showing the backfill heave and surface cracks for the 0°, 15°, and 30° tests are shown in Figure 6-1, Figure 6-2, and Figure 6-3, respectively. For the 0° test, the backfill heave reached a maximum of 2.4 in (6.10 cm) at a location oriented 1.75 ft (53.34 cm) inward from the west side of the pile cap; however roughly comparable heave concentrations occurred near each side of the cap. Heave was slightly lower on a line perpendicular to the center of the cap. Heave contours were relatively symmetric about the centerline with a slight shift to the right side. This imbalance was possibly caused by the uneven force distribution produced by the actuators to keep the pile cap moving relatively straight. Maximum heave was 6.7% of the backfill height. Surface cracks identify the locations where the failure surface daylights and locations where soil is deforming and shearing excessively. These cracks radiate outward from the corners of both sides of the cap at an angle of about 50 degrees relative to the face of the cap. These shear planes at the ends of the cap extend the effective width of the cap leading to greater passive resistance. A full failure surface crack developed at a distance of 10 ft (3.05 m) from the face of the pile cap which identifies the back edge of the failure surface. At greater cap displacements the surface cracks would be expected to connect and define the complete failure bulb boundary which would appear to roughly follow the 0.6 inch heave contour.

For the 15° test the highest heave occurred in the middle region at a maximum magnitude of 1.9 in (4.8 cm) and a distance between 3 and 6 ft (0.91 and 1.83 m) from the face of the pile cap. This heave is about 5% of the backfill height. Although this heave is somewhat lower than for the 0° skew test, the values are similar. Heave was greatest for the 30° test with a maximum value of 3.8 in (9.65 cm) being located at a small bulge near the obtuse corner of the pile cap. This behavior is likely caused by the greater rotation of the pile cap for the 30° test relative to the other tests along with the shear failure on the soil-wedge interface where the soil slid along the face of the wall but was then restrained by the adjacent soil beyond the edge of the backwall. The mechanism behind this shear failure is described in Section 4.5.1, which explains that the calculated factor of safety against shear failure for the 30° skew soil-wedge interface was approximately 1.05 and very possibly could have sheared along this surface. Unfortunately, no direct mathematical correlation could be drawn between heave and skew angle or total pile cap deflection for this study. However, the trends described in this portion can still be used to understand the soil behavior.

Overall, the most heave was produced on the acute side of the 15° skew wedge whereas greater heave was shown on the obtuse side for the 30° skew wedge. This can again be attributed to soil-wedge shear failure and greater rotation which would both push the heave to the obtuse end on the 30° skew test. Corresponding results for the 30° skew test are found in Chapter 6.5 relating the internal horizontal pressure distribution to soil wedge upheaval. However, the 30° skew 5.5-ft (1.68-m) unconfined backfill test performed by Marsh (2013) showed greatest heave occurring on the acute side. It is possible that the failure mechanism in that study was backfill shear failure instead of shear failure along the soil-backwall interface, producing different heaving behaviors.

When examining strictly the soil-wedge interface, all three tests portray greater heave near the edges than they do for the middle portion. Cummins (2009) observed similar heave patterns in their tests and stated that the highest passive pressures on the wall face for his study were likely concentrated at its edges.

All three failure surfaces extended perpendicular to their respective skewed backwalls as was predicted by Shamsabadi et al. (2006). The distance to the back edge of the failure surface was typically about 10 ft (3.05 m) normal to the face of the skewed wall. Therefore, in this case, skew appears to have had little effect on the total length of the failure wedge. In consideration of 3D end effects, the effective widths parallel to the skewed interfaces for the 0°, 15°, and 30° tests were approximately 17 ft (5.18 m) , 16 ft (4.88 m), and 17 ft (5.18 m). This corresponds to 1.54L, 1.41L, and 1.35L where L is their respective wedge interface lengths. This is a reduction of 19% between skews of 0° and 30°, indicating that the effective width decreased as skew angle increased. These effective widths also shifted towards the acute side as skew angle increased as can be seen by the contour maps of Figure 6-1, Figure 6-2, and Figure 6-3.

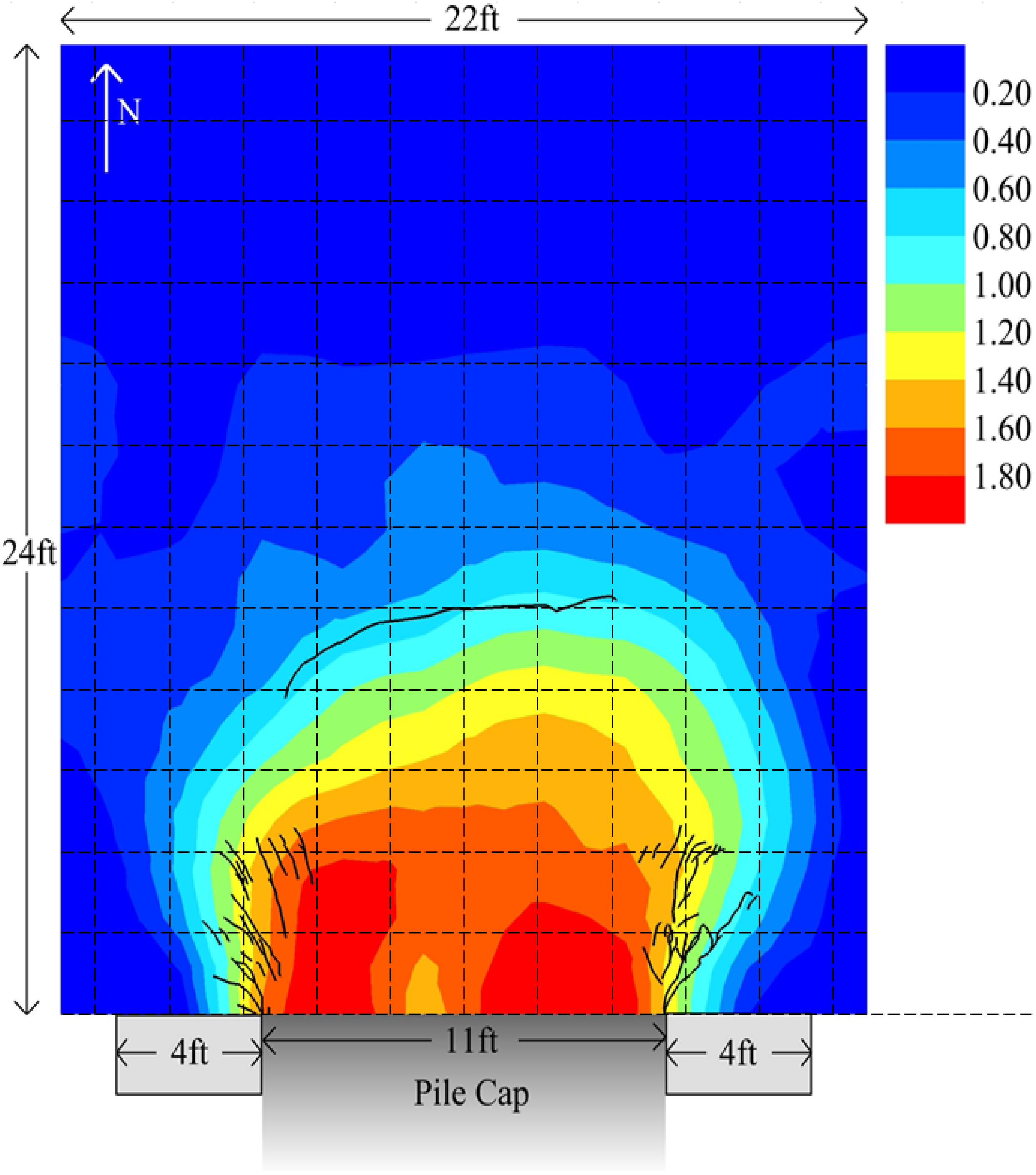

Figure 6-1: Backfill heave contours (in inches) and surface cracks for the 0° skew test (Note: grids are 2 ft by 2 ft (0.61 m by 0.61 m)

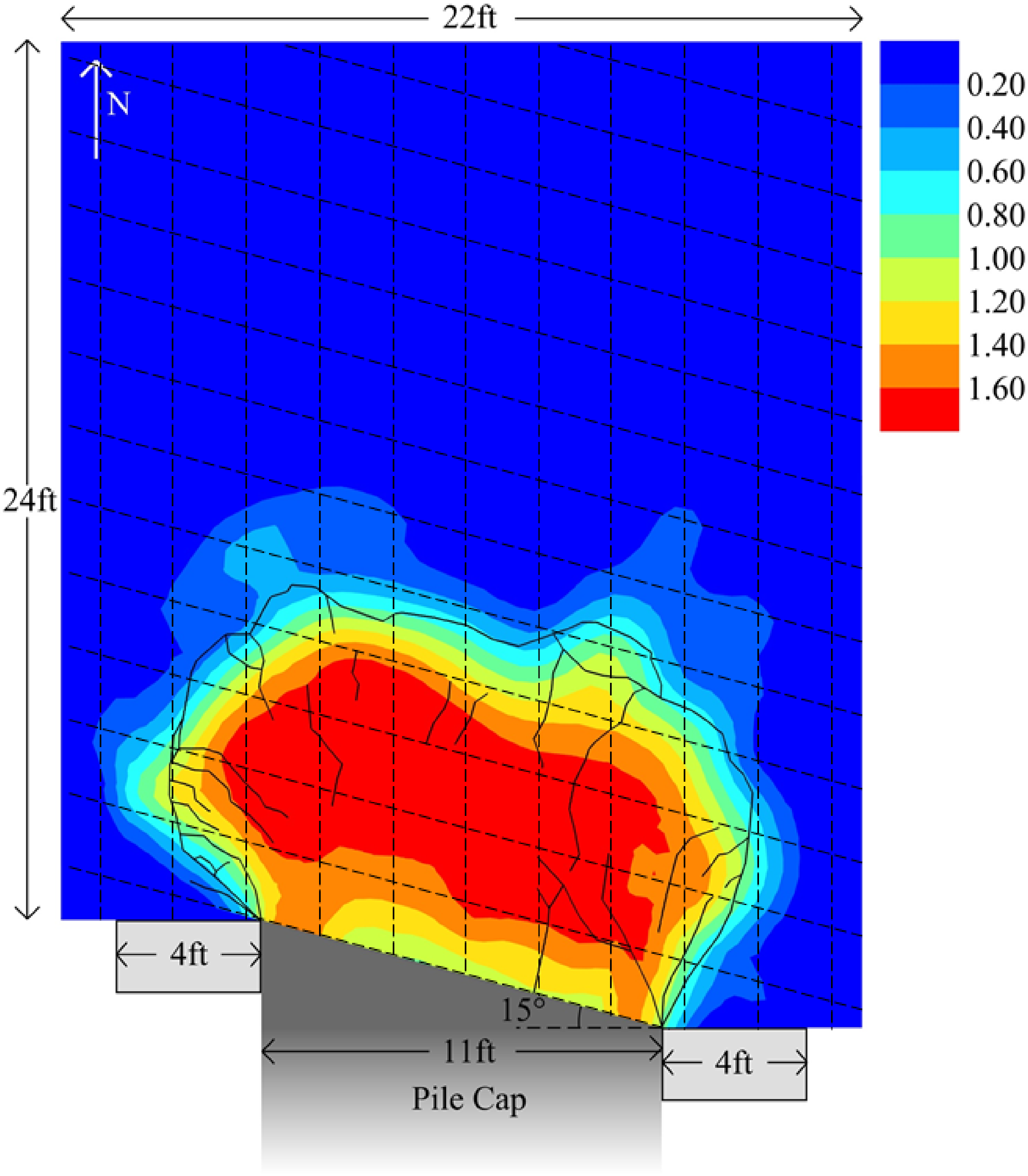

Figure 6-2: Backfill heave contours (in inches) and surface cracks for the 15° skew test (Note: grids are 2 ft by 2 ft (0.61 m by 0.61 m)

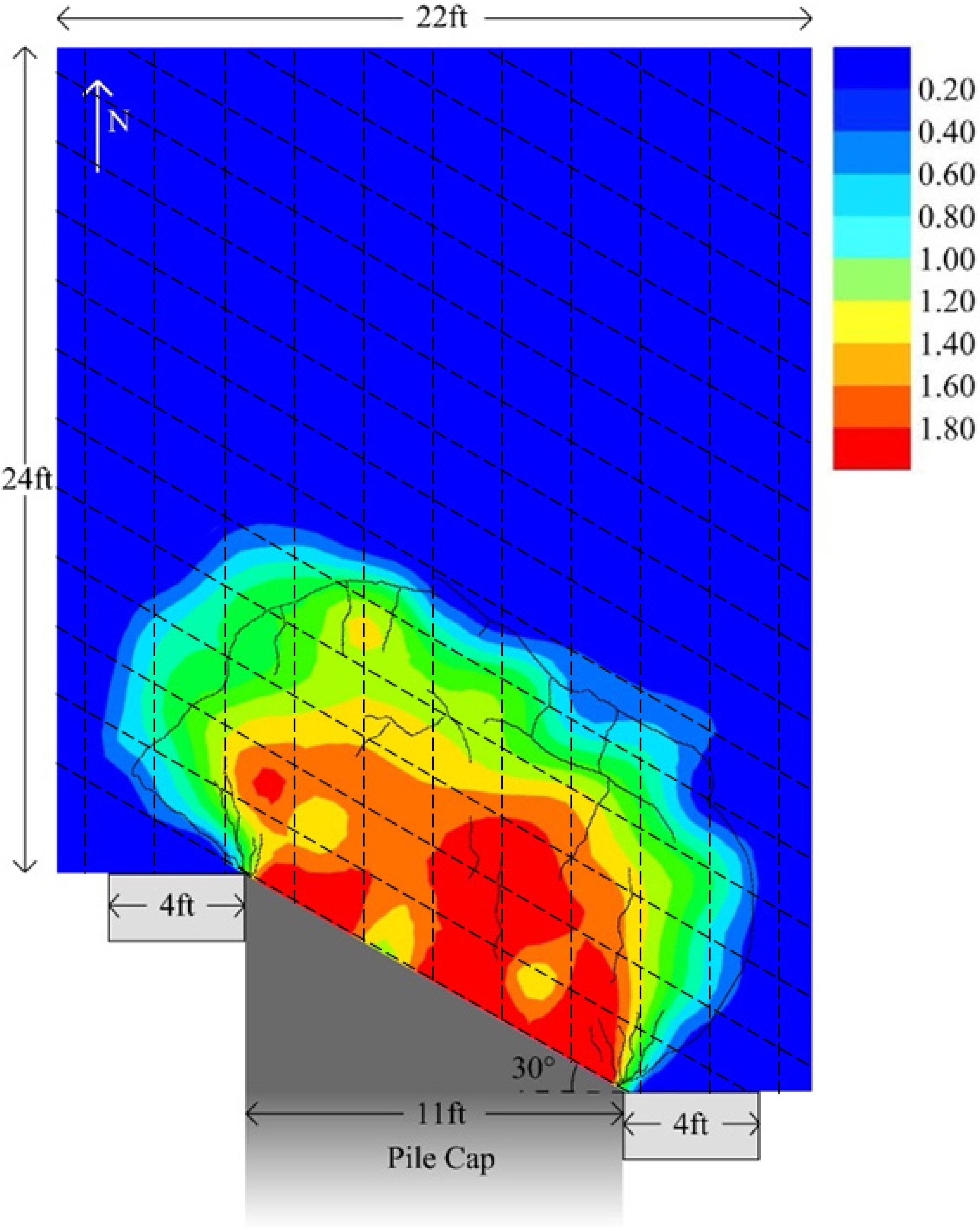

Figure 6-3: Backfill heave contours (in inches) and surface cracks for the 30° skew test (Note: grids are 2 ft by 2 ft (0.61 m by 0.61 m)

As mentioned in Section 4.2, limitations with the supporting piles restricted pile cap displacement, causing insufficient movement for full failure wedge development. However, surface cracks for both the 15° and 30° tests provide complete outlines of both soil wedges (see Figure 6-4). This implies that complete shear failure likely occurred in both backfills. The full development of the failure surface for the 15° and 30° skew tests is consistent with the observation that less movement was required to develop the full passive pressure for the skewed tests than for the 0° skew tests. For both the 15° and 30° skew tests the failure pattern was reasonably consistent. On the acute side, the shear surface initially radiated outward from the corner almost asymptotically to the face of the backwall and then extended at an angle of 10° to 20° relative to the backwall. In contrast, on the obtuse side, the shear surface radiated outward from the corner almost perpendicular to the backwall before extending outward beyond the edge of the cap.

(a) (b)

Figure 6-4: Failure wedge surface for skews of (a) 15° and (b) 30°

6.2 Internal Failure Surfaces

Red dyed sand columns spaced 2 ft (0.61 m) apart enabled the detection of failure planes through identification of offsets in their side profiles. Photographs of the 0°, 15°, and 30° test profiles are shown in Figure 6-5, Figure 6-6, and Figure 6-7, respectively.

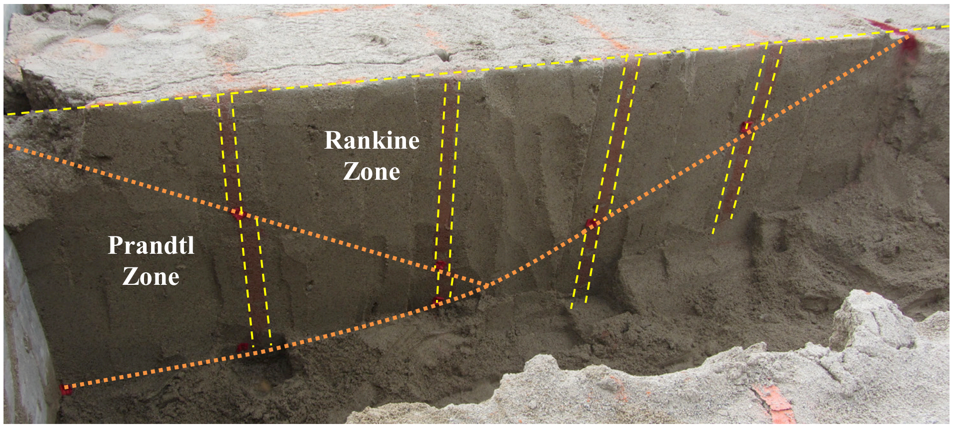

Figure 6-5: Failure surface geometry within sand based on offset in red sand columns for 0° skew test

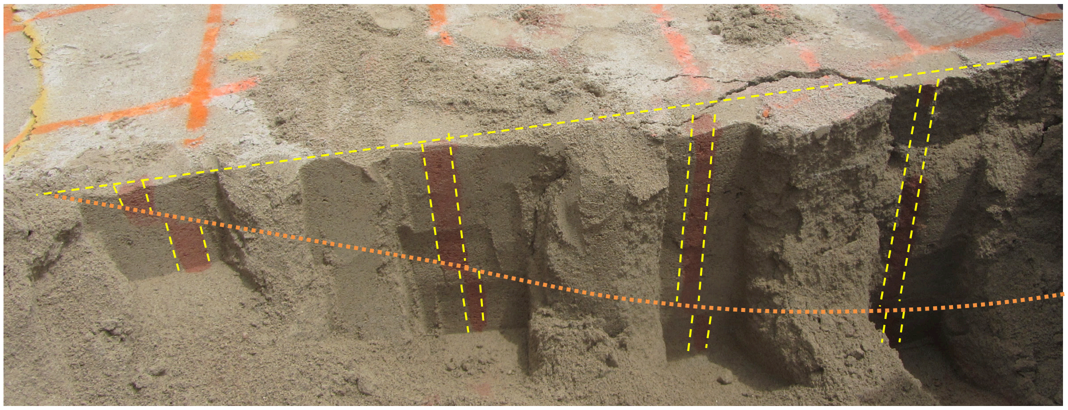

Figure 6-6: Failure surface geometry within sand based on offset in red sand columns for 15° skew test

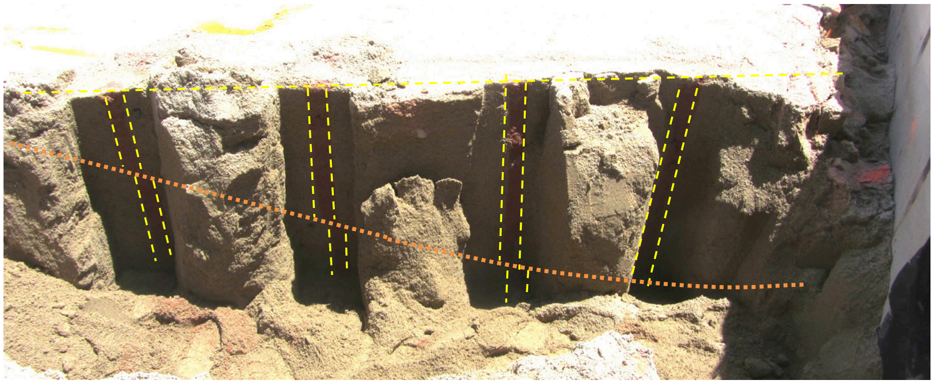

Figure 6-7: Failure surface geometry within sand based on offset in red sand columns for 30° skew test

The sand columns for all three tests indicated a log spiral failure plane, as was predicted by Terzaghi (1943). This plane began with a gradual curve from the base of the pile cap that transitioned into a linear Rankine surface inclined at an approximate angle of $\alpha = 45° - \phi/2$, where α is the angle of inclination of the linear portion of the failure plane and ϕ is the soil friction angle. Additionally, results from the 0° skew test in Figure 6-5 also showed a downward Rankine failure plane connecting the top of the soil at the edge of the backwall to the log spiral plane. Similar behavior was also observed by Nasr and Rollins (2010) in numerical modeling of the failure geometry with Plaxis 2D. The lower left soil wedge, referred to as the Prandtl zone in Figure 2-5, appears to have displaced the furthest, moving downward and to the right. As a result, the right wedge, also called the Rankine zone, was forced upward along the shear failure plane. Although they are difficult to see in Figure 6-6 and Figure 6-7 above, slight offsets of the downward Rankine failure plane were also found in the 15° and 30° tests. Results from all three tests including the failure surface points and heave are plotted in Figure 6-8, Figure 6-9, and Figure 6-10, for the 0°, 15°, and 30° tests, respectively. Comparisons between the actual shear failure planes and those predicted by the Rankine, Coulomb, and Log Spiral methods are discussed in Section 7.3.

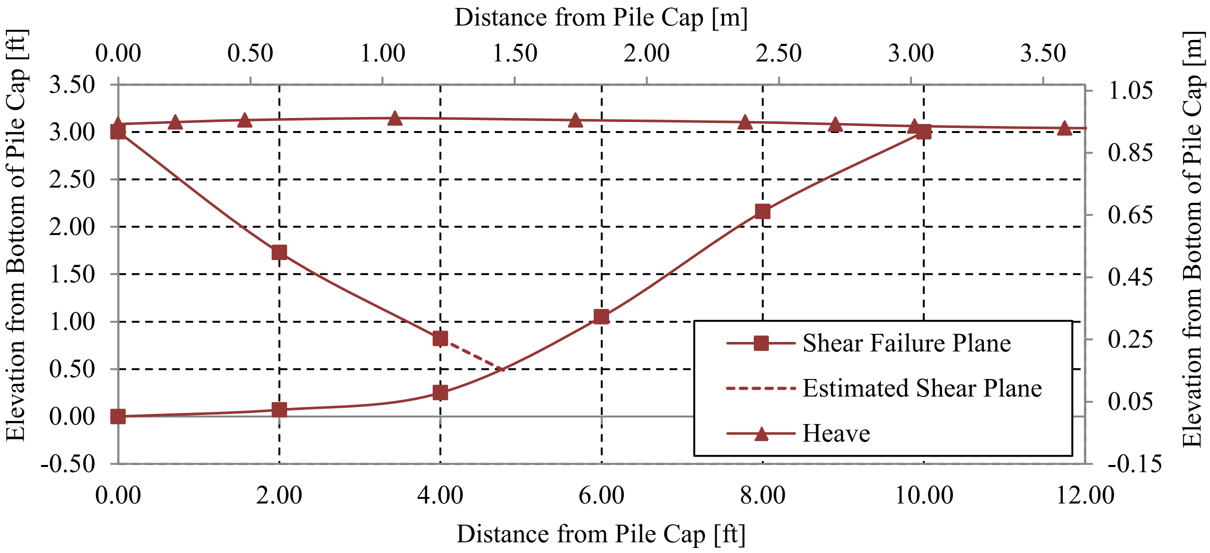

Figure 6-8: 0° skew test profile view of failure geometry

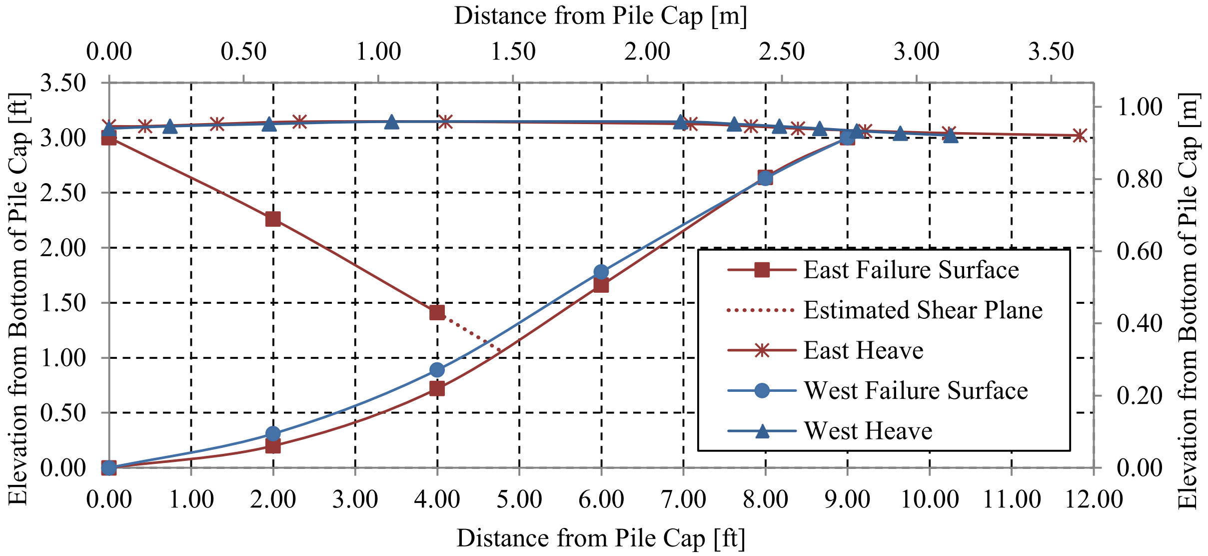

Figure 6-9: 15° skew test profile view of failure geometry

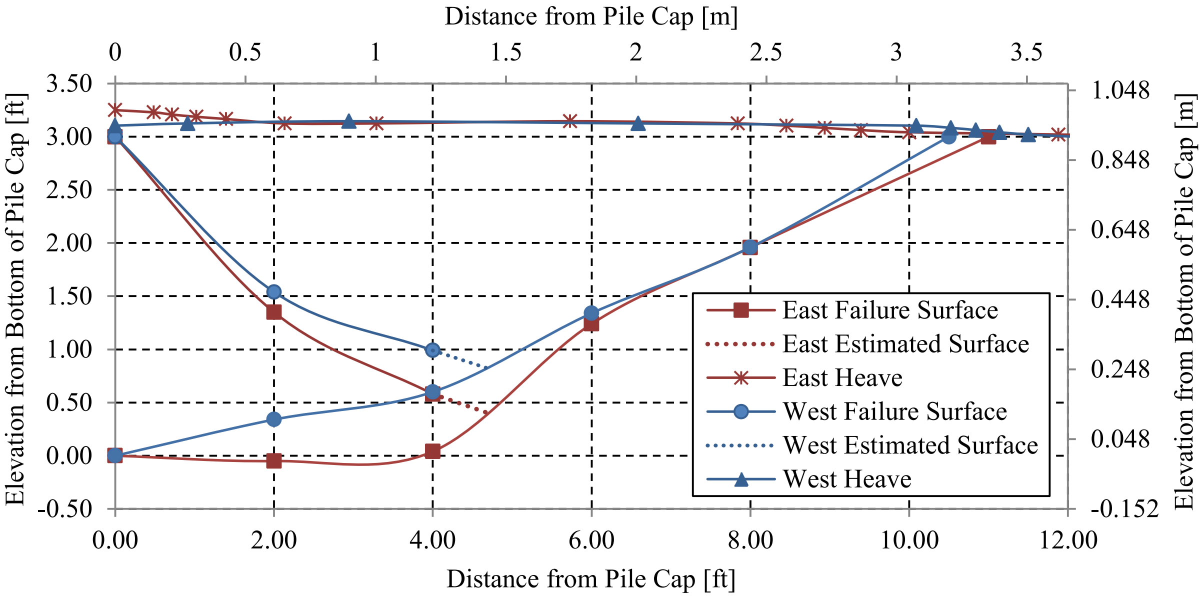

Figure 6-10: 30° skew test profile view of failure geometry

For a skew of 15°, results indicate an upper Rankine failure plane on the obtuse side but not the acute side. However, Rankine failure was identified on both sides of the 30° test. The log spiral failure surface did not extend below the surface of the pile cap for any of the three tests except for a depth of 0.05 in (0.05 in) on the east surface of the 30° test. This type of behavior can be expected for shallower depths of backfill. Strong discrepancies are shown between the east and west failure surface profiles of the 30° test. On the acute side, the failure surface is more linear whereas a log spiral shape can still be identified on the obtuse side.

The shear failure plane inclination, α, for the straight line segment of the failure surface can be estimated using reference points obtained from the red dyed sand columns. The equation $\alpha = 45° - \phi/2$ proposed by Terzaghi (1943) can also be used in conjunction with computer optimization and the program PYCAP created by Duncan and Mokwa (2001) to predict the angle of the failure plane. For this series of tests, the predicted friction angle was approximately 42°, which corresponded to a failure surface inclination of 24°. The actual shear failure plane inclinations for the 0°, 15°, and 30° tests were close to this predicted inclination at values of 26.0°, 22.0°, and 21.3°, respectively.

6.3 Backfill Displacement

As mentioned in Section 3.3.6, seven string potentiometers were used to detect backfill movement at the surface of the fill. These measurements were taken at 2-ft (0.61-m) increments longitudinally from the face of the pile cap. Unfortunately, some uncertainty occurred with the stabilization of some of the grounded stakes as the pile cap moved and shear planes interfered with their stability (see Figure 6-11). These data points were linearized when possible and completely omitted when necessary. However, results still provided sufficient trends to understand the backfill displacement and strain.

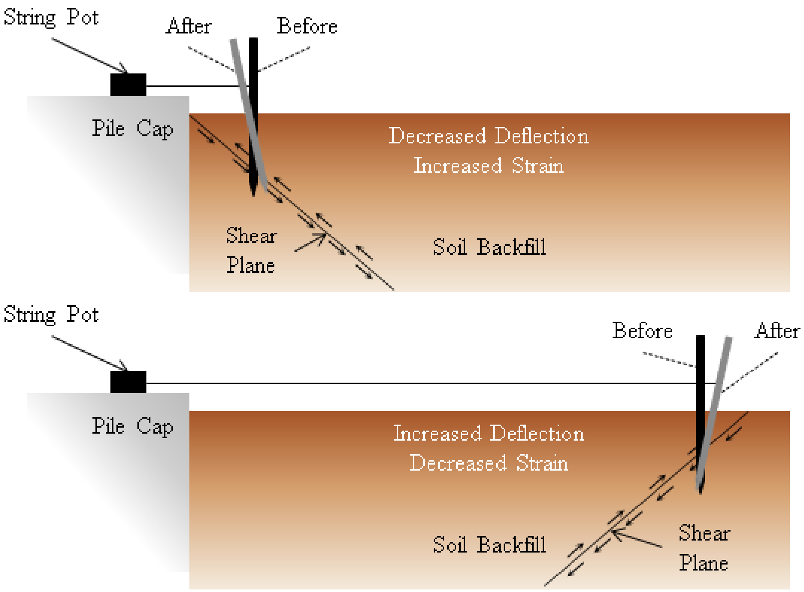

Figure 6-11: Stake-shear plane interaction (Franke, 2013)

Figure 6-12, Figure 6-13, and Figure 6-14 show the total backfill displacement versus backwall movement for the 0°, 15°, and 30° tests. In general, the backfill underwent greater forward movement at closer distances to the pile cap than for locations further away. As stated in Section 6.1, failure wedge surface cracks extended to approximately 10 ft (3.05 m) for the 0° and 15° skew tests and 12 ft (3.66 m) (longitudinally) for the 30° test. All three tests showed a significant drop in backfill deflection either at or immediately following these locations.

For the 0° skew test, the 2-ft (0.61-m) location appeared to cross a downward shear zone. These points were saved through linearization. Unfortunately, all data points above the 0.49 in (1.24 cm) deflection for the 8-ft (2.44-m) location could not be used. Overall, displacements for the 0° test decreased in a relatively uniform fashion with distance until they reached the wedge failure crack, at which point the deflection dropped. As is stated in Section 4.2, maximum passive pressures occurred at a deflection of 1.53 in (3.89 cm). The data in Figure 6-12 correspond well with this information by showing a steeper inclination between locations as the soil failed and displaced at greater magnitudes within the failure wedge.

Both the 2-ft (0.61-m) and 8-ft (2.44-m) points were again disrupted in the 15° skew test. The majority of these points were removed from the analysis. This test did not experience as gradual of a decrease in deflection with distance as did the 0° test. Deflection plateaued between the 4-ft (1.22-m) and 6-ft (1.83-m) data points for all pile cap displacements. These results correspond well with the heave for this test, which showed maximum magnitudes to be within this region of the backfill. The 12 ft (3.66 m) and 14 ft (4.27 m) data also experienced slight increases in deflection. It is possible that the failure wedge pushed this soil outward as it slid upward to the surface. Maximum passive forces for the 15° test occurred at 1.23 in (3.12 cm), although no significant increases in steepness were noted until later in the test. This incident is likely caused by the progressive backfill failure that tends to occur behind skewed abutments. Once full failure occurred, displacement increased at a higher rate.

Several string pots measurements were problematic for the 30° skew test. Fortunately, there was still sufficient data to compare the soil near the pile cap to locations further away. The 8-ft (2.44-m) and 10-ft (3.05-m) locations were linearized, but the 2-ft (0.61-m) location had to be completely dropped. Data point displacements were again unevenly distributed for this test. Some displacements were even noted to increase at the 6-ft (1.83-m) and 8-ft (2.44-m) locations. Although these locations did not correspond to maximum heave locations, they did however, relate to where other surface cracks formed. It is difficult to determine whether this unique behavior actually behaved this way in the study or if it was simply the result of destabilization of the rods. Steeper increases in deflection were again seen after the passive pressure reached a peak at a deflection of 1.02 in (2.59 cm).

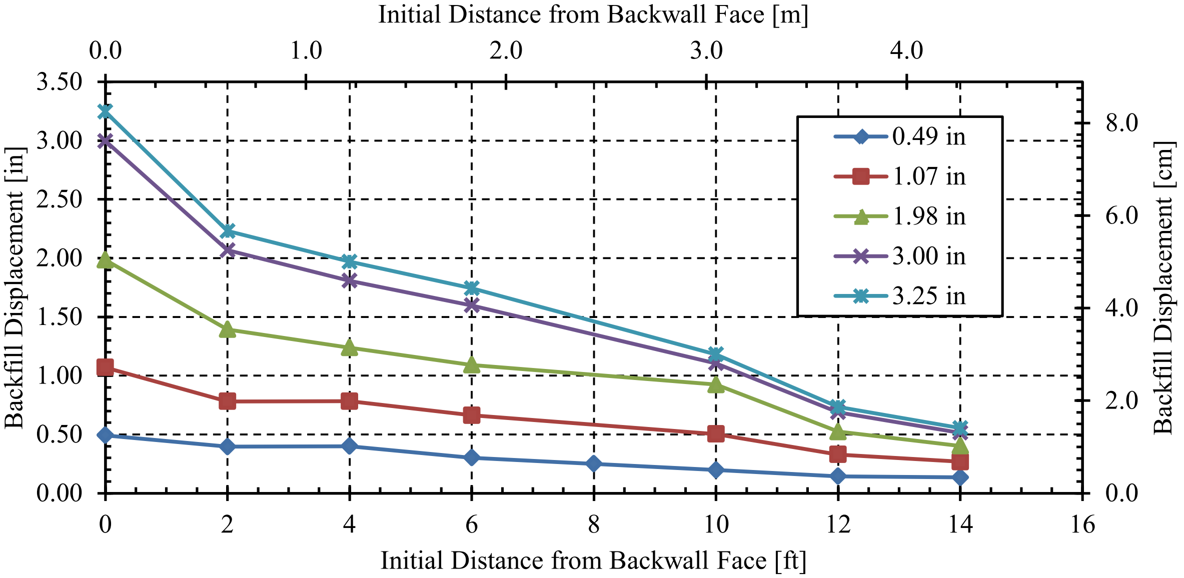

Figure 6-12: Total backfill displacement versus distance from backwall face at selected pile cap displacement intervals for the 0° test

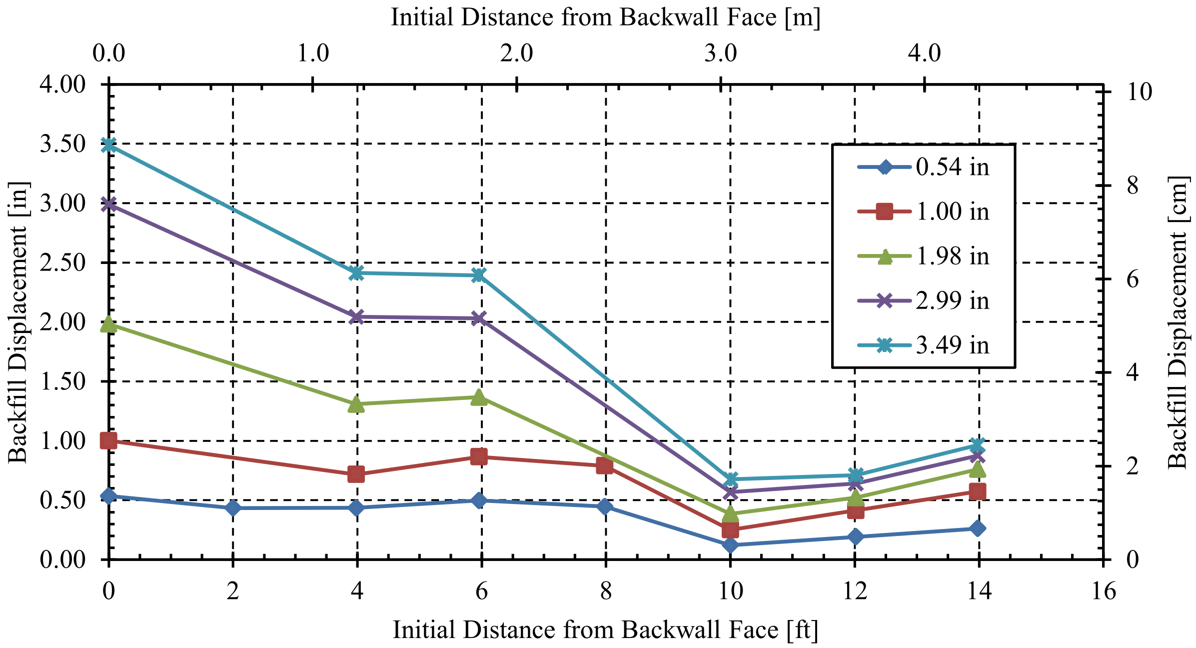

Figure 6-13: Total backfill displacement versus distance from backwall face at selected pile cap displacement intervals for the 15° test

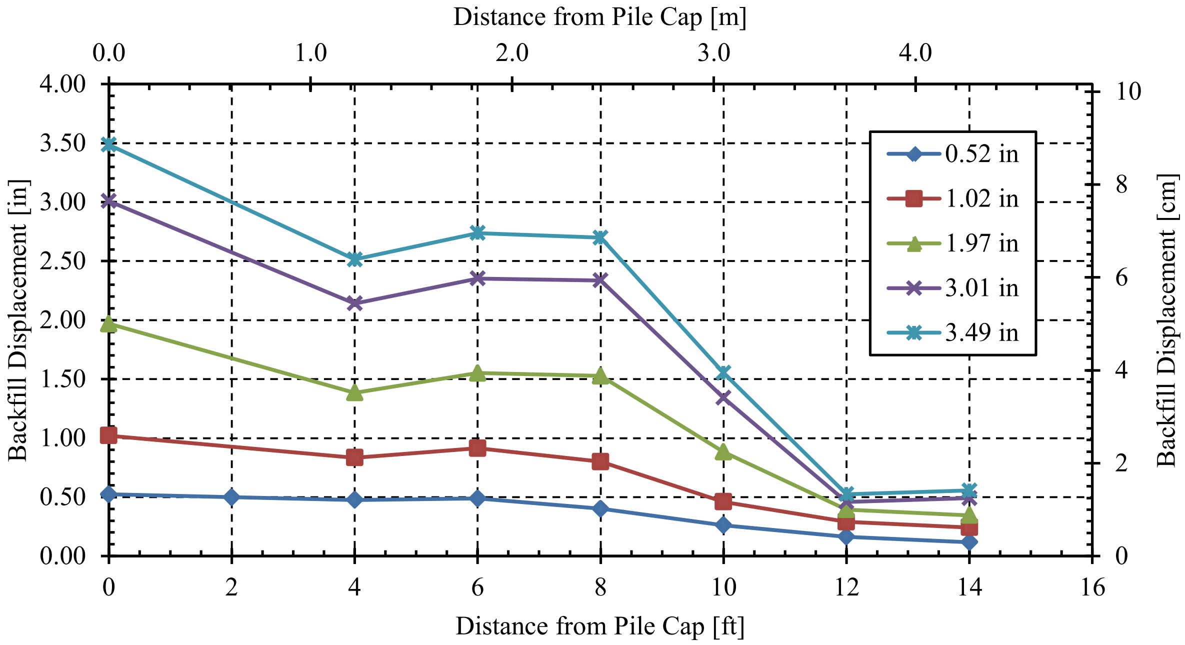

Figure 6-14: Total backfill displacement versus distance from backwall face at selected pile cap displacement intervals for the 30° test

The total backfill displacement versus distance from the backwall at test completion is shown in Figure 6-15 for the 0°, 15°, and 30° skew tests. Initial and final displacements were similar for the three tests; however, the 30° test appears to have displaced the furthest at almost all locations of the driven stakes, with notably larger displacements occurring farther away from the pile cap. According to these trends, as the skew increases, backfill displaces at greater magnitudes and at locations further away from the backwall than for smaller skews. A probable cause could be the shallower shear failure plane inclination that extends to a greater distance and behaves more like a Rankine failure plane than a log spiral failure.

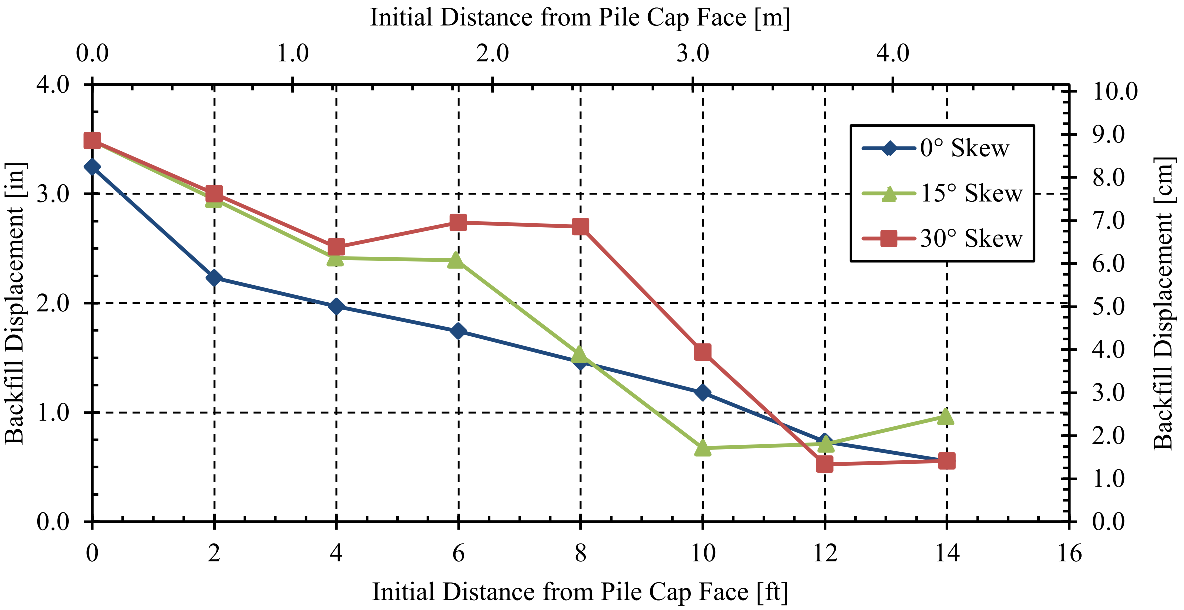

Figure 6-15: Total backfill displacement versus distance from pile cap face for the 0°, 15°, and 30° tests at test completion

6.4 **Backfill Compressive Strain**

Compressive strain vs. longitudinal distance from the backwall for the 0°, 15°, and 30° tests are plotted in Figure 6-16, Figure 6-17, and Figure 6-18, respectively. Strain was measured in 2-ft (0.61-m) increments with the midpoints of these sections being displayed. A maximum compressive strain of 4.2% for the 0° skew test occurred within the first 2 ft (0.61 m) of the backfill. The strain then dropped to approximately 1% and remained relatively constant throughout most of the backfill until it reached a location just beyond the failure wedge. At this point, the failure wedge likely pushed on the adjacent soil, which caused the compressive strain to spike immediately behind the failure surface.

Both the 15° and 30° tests experienced different behavior than in the 0° test. For these two tests, maximum strain occurred directly before the location where shear failure wedge surfaced. Maximum compression strain reached a value of 3.49% for both tests.

The total backfill compressive strain at test completion for all three tests is shown in Figure 6-19. Since the backwall displaced almost exactly the same magnitude for all three tests, differences between the strains can be attributed to the change in backwall geometry. All three tests experienced high compressive strains immediately behind the pile cap that rapidly dropped within 4 ft (1.22 m) of the backwall. Compressive strain then remained relatively low and constant for the within the interior of the failure wedge indicating that the mass was generally displacing as a block in this region. The compressive strain then increased substantially near the location where the shear failure surface day-lighted. These values were measured within 2.5 ft (0.76 m) of the center of the backwall in the transverse direction. Further investigation of locations near the edges of the pile cap would be beneficial in understanding the behavior of the entire 3D soil wedge.

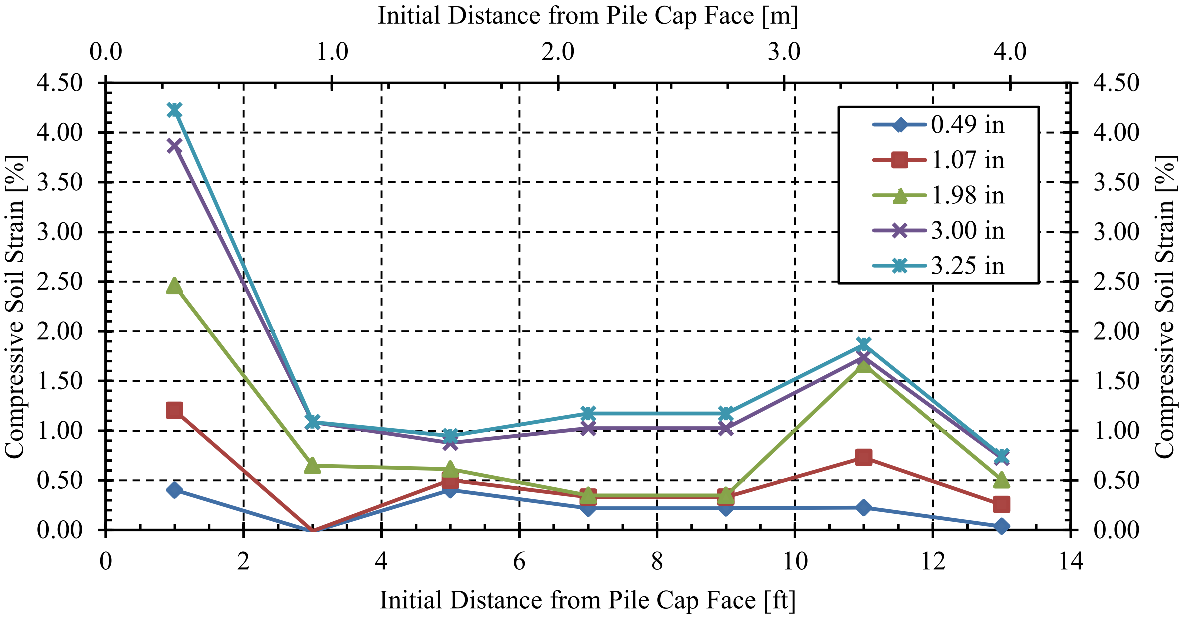

Figure 6-16: Backfill compressive strain versus original distance from backwall at selected displacement intervals for the 0° test

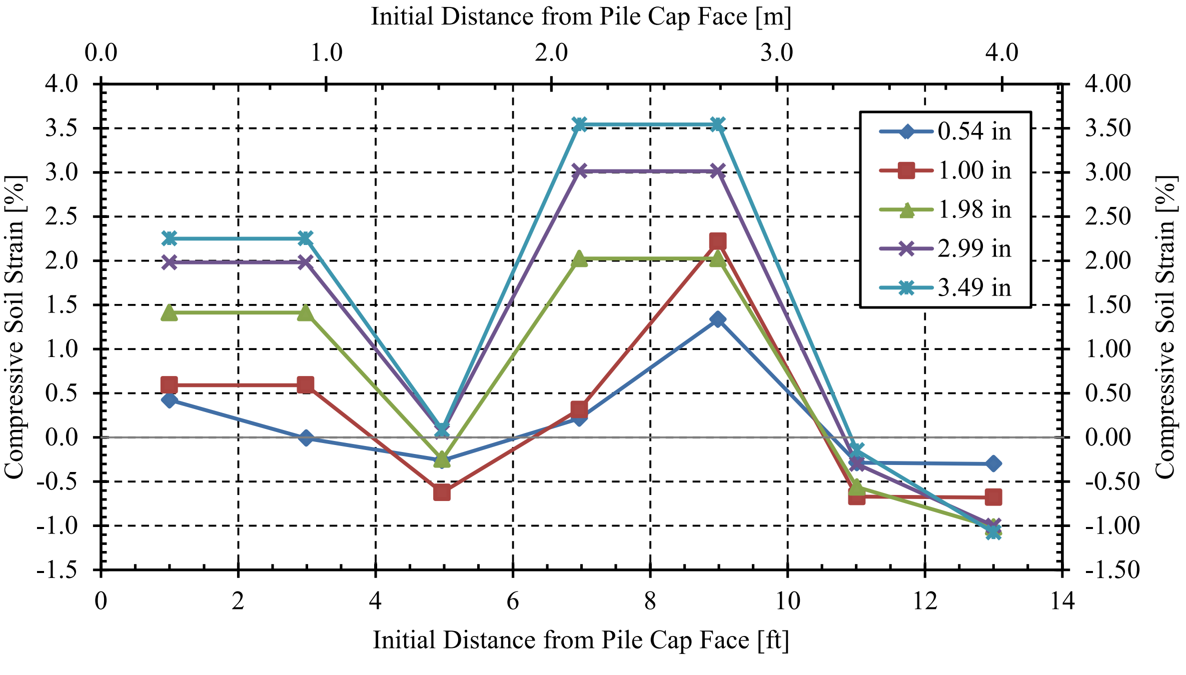

Figure 6-17: Backfill compressive strain versus original distance from backwall at selected displacement intervals for the 15° test

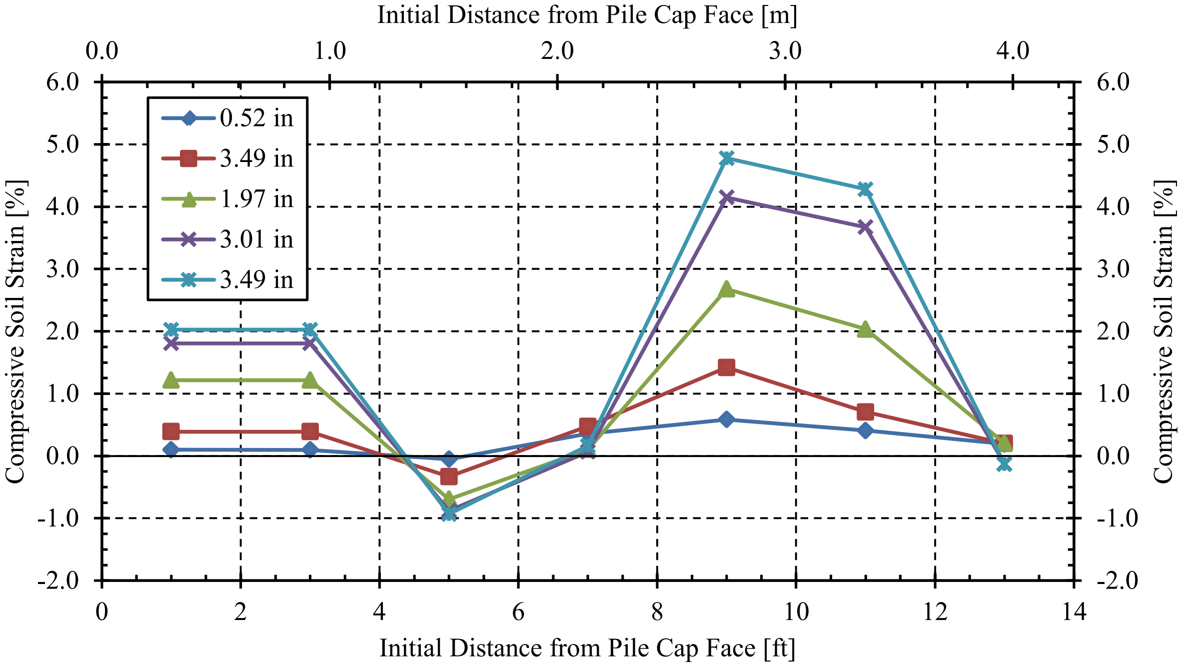

Figure 6-18: Backfill compressive strain versus original distance from backwall at selected displacement intervals for the 30° test

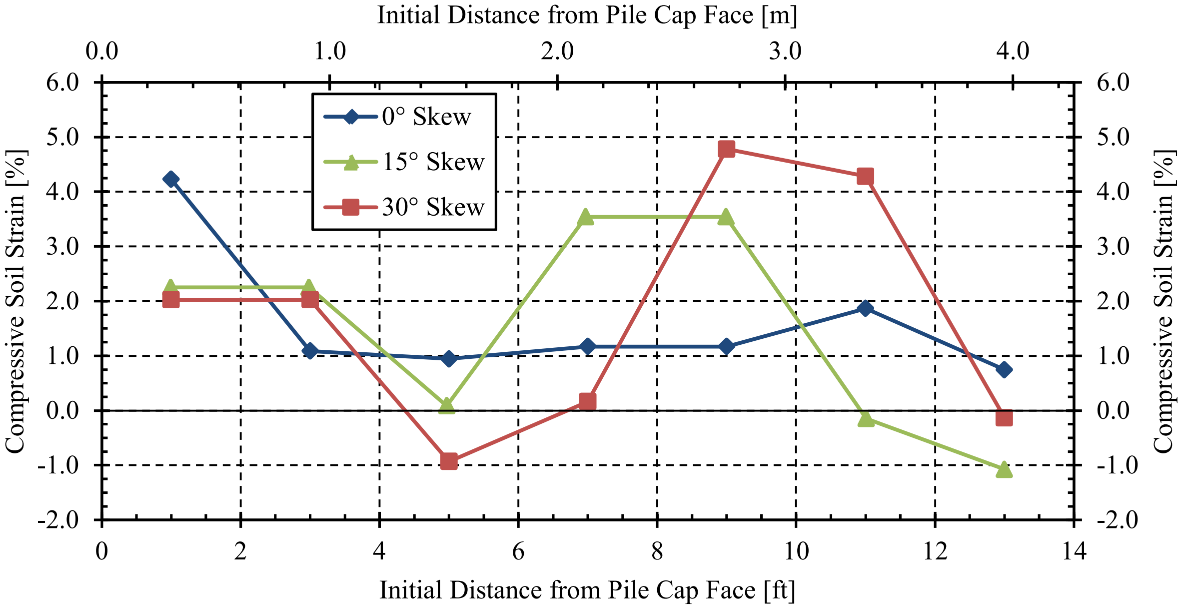

Figure 6-19: Backfill compressive strain versus original distance from backwall for the 0°, 15°, and 30° tests at test completion

6.5 Horizontal Pressure Distribution

As stated in Section 3.3.6, a total of six “Fat Back” pressure cells were installed horizontally across the face of the 30° skew wedge, as shown in Figure 6-20 (a). This instrumentation detected horizontal pressure shifts within the soil as the pile cap moved forward. Unfortunately, pressure plate PP1498 failed to function properly during the first test due to difficulties while removing the concrete pouring form. However, the remaining five pressure plates still produced sufficient data to enable understanding of pressure distribution changes that occurred across the interface of the 30° skew. All figures regarding pressure distribution within this chapter will be presented from the standpoint of the plan view shown in Figure 6-20 (b).

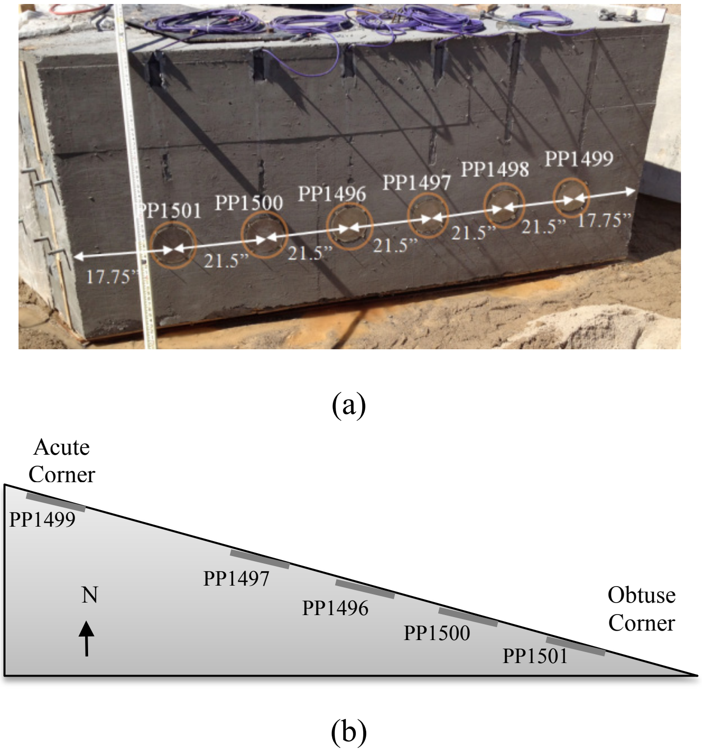

Figure 6-20: (a) Pile cap wedge interface (b) plan view drawing of pressure plates

For the 30° skew 3-ft (0.91-m) unconfined test, results revealed the pressure to be relatively uniform for the first inch (2.54 cm) of displacement, as seen in Figure 6-21 (a). The pressure then shifted in Figure 6-21 (b) to the obtuse end of the pile cap and dropped along the middle portion of the wall. At the displacement of 1.5 in (3.81 cm) shown in Figure 6-21 (c), the passive force reached a maximum pressure and the soil theoretically sheared, causing the pressure to suddenly shift more towards the obtuse end of the pile cap. This distribution corresponds to findings by Apirakyorapinit et al. (2012) which explain that stresses on bridge girders are highest on the obtuse side where the girders are being pushed into the backfill.

As the cap continued to move forward, the overall pressure of the sheared soil and backwall decreased, with the greatest drop being on the obtuse end (see Figure 6-21 (d)). The final distribution had its highest pressures at a locations of 1.3 ft (0.40 m) 7.5 ft (2.29 m) from the acute corner and its lowest pressure in the center of the pile cap (see Figure 6-21 (e)). The complete pressure progression is provided in Figure 6-21 (e) for comparison purposes.

Referring to the displacement of maximum pressures found in Figure 6-21 (c), results from this test also coincide with findings obtained by Sandford and Elgaaly (1993) in that they found the pressure on the obtuse side of a fully functioning bridge abutment to be greater than on the acute side (see Figure 2-14). The higher pressure that developed on the obtuse side of the wall was attributed to possible rotation of the abutment. Pressure distribution results from the 30° skew 3-ft (0.91-m) unconfined test of this study vary from Sandford and Elgaaly on the acute side of the pile cap where pressures were shown to be much greater than in the middle of the pile cap. This is most likely caused by 3D effects exerting an additional pressure on the acute corner of the wedge. However, elastic theory also predicts that the pressure at the corners of wall will be higher than near the center, as shown in Figure 6-22 (Hegger et al., 2007).

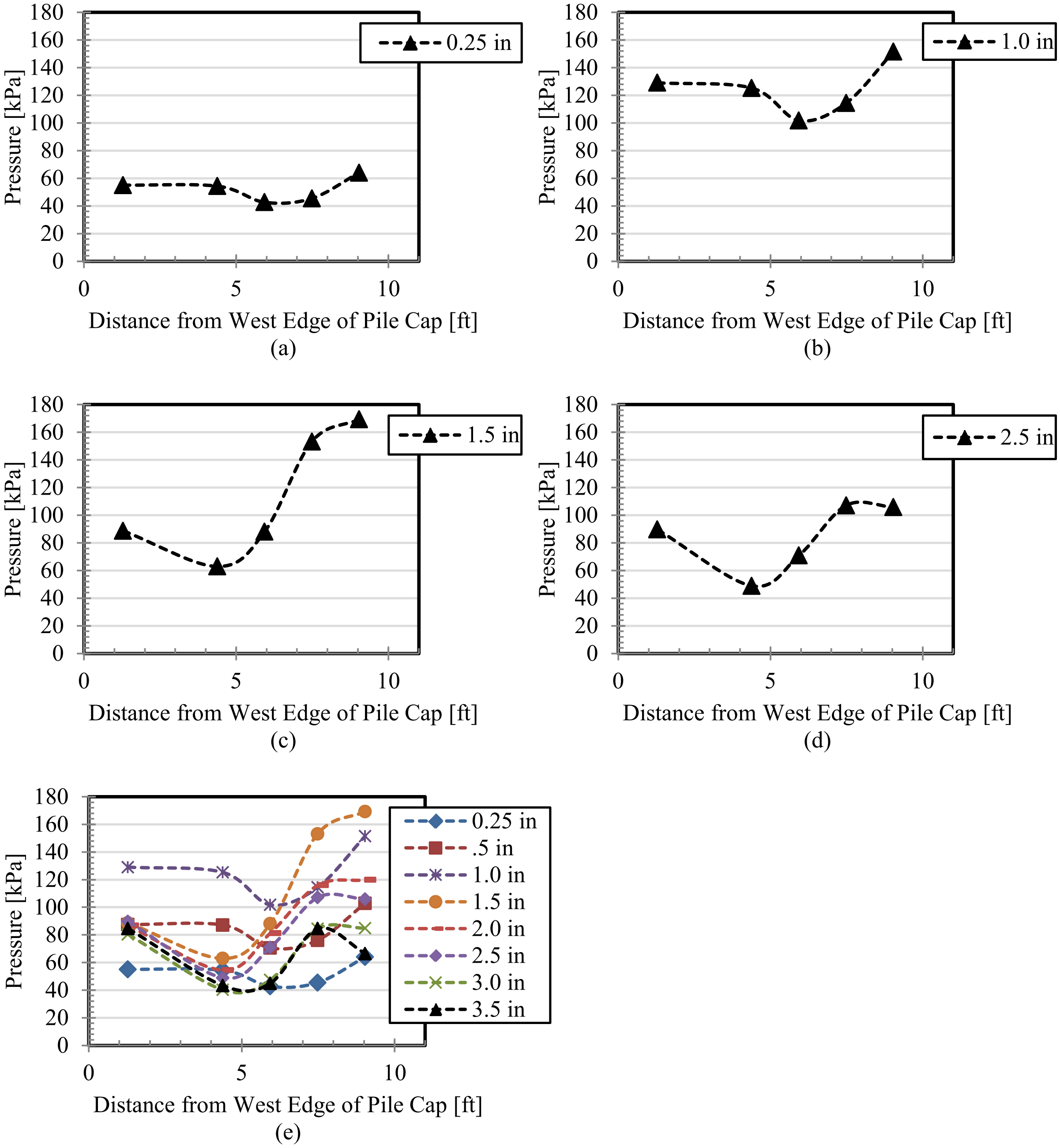

(a) (b) (c) (d) (e)

Figure 6-21: Progression of horizontal pressure distribution with pile cap movement

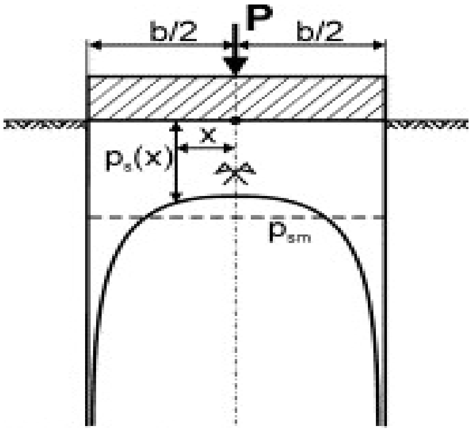

Figure 6-22: Soil pressure distribution under a rigid footing as shown by the elastic theory (Hegger et al., 2007)

Sandford and Elgaaly's study suggest a linear increase between the acute and obtuse corners. Since no instrumentation was installed along the middle portion of the abutment interface in their study, it is possible that their backfill also experienced a similar decrease in pressure within the central portion of the soil distribution profile that was not accounted for because of the scarcity of instrumentation. By selecting pressure values from the 30° skew test (see Figure 6-23 (a)), a pressure distribution can be superimposed to fit the data points obtained in Sandford and Elgaaly's model, as shown in Figure 6-23 (b), which points out the possibility of alternate distributions occurring between Sandford and Elgaaly's two data points.

Since rotation about the longitudinal axis was extremely limited during the 30° skew test by the actuators (see Section 5.3), it can be implied that rotation was not the only cause of the variance in pressure distribution along the soil-backwall interface. Higher pressures can still develop even when the pile cap is restrained. These pressure distributions will only magnify when rotation is incorporated, as was reported by Sandford and Elgaaly. However, care should be taken to maintain an even force distribution of the actuators during testing—small variations in movement rotation of the pile cap could have pronounced effects on the pressure distribution that could lead to false-readings.

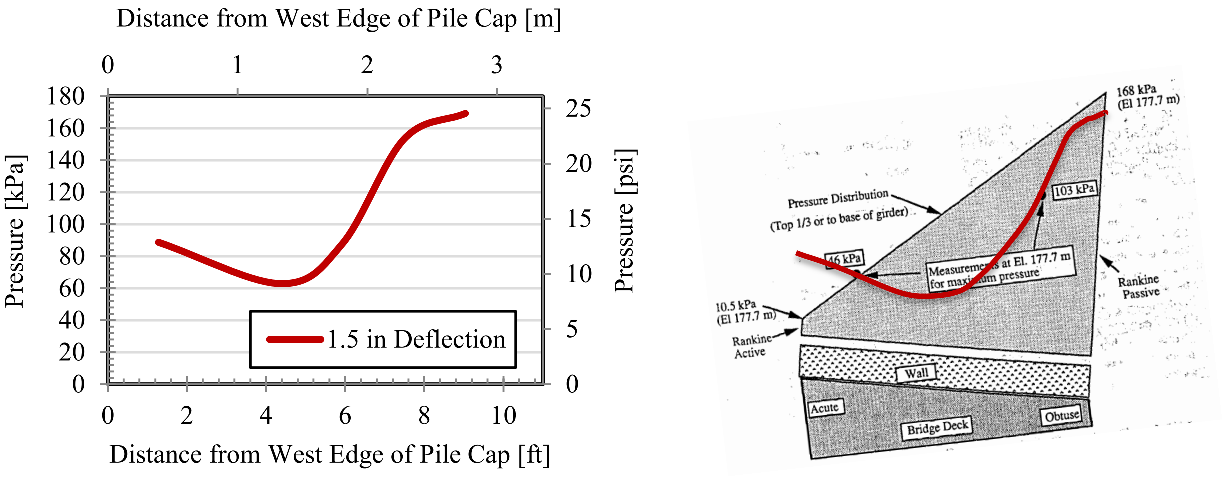

(a) (b)

Figure 6-23: (a) Horizontal pressure distribution for the 30° test 1.5 in (3.81 cm) pile cap deflection, (b) horizontal pressure distribution superimposed onto Sandford and Elgaaly's model from Figure 2-14

The 30° skew horizontal pressure distribution test results correspond well with force calculations from Section 4.5 and heave results presented in Section 6.1. The sudden shift in the pressure distribution towards the obtuse side shown in Figure 6-21 (b) and (c) likely occurred at a moment where the applied shear force overcame the shear resistance which was predicted in Figure 4-17. The uneven heave distribution presented in Figure 6-3 agrees with the pressure distribution in two distinct ways: first, the obtuse side had greater upward heave than other portions of the pile cap, undoubtedly corresponding to the higher pressures noted on that side. Secondly, the effective width extended further outward on the acute side, requiring that additional pressures be placed on that uppermost corner and less in the central region, as was shown in the pressure distribution results.

The total pressure detected by the pressure plates was converted to a force magnitude and compared to test data obtained from the actuators. The total force approximation of the pressure cells was performed by assuming a linear downward pressure distribution, extrapolating to the mid height of the soil, multiplying each cell by its tributary width and soil depth of 3 ft (0.91 m), and summing the forces together. As shown in Figure 6-24 and Table 6-1, the pressure cells appear to have been relatively accurate at the beginning and final test movements; however, the cells overestimated the measured actuator pressure during the middle displacements by a factor as large as 1.6. Although these cells seem to have over-registered the pressure magnitudes, the pressure distributions and movements can still be analyzed to examine the general soil pressure behavior.

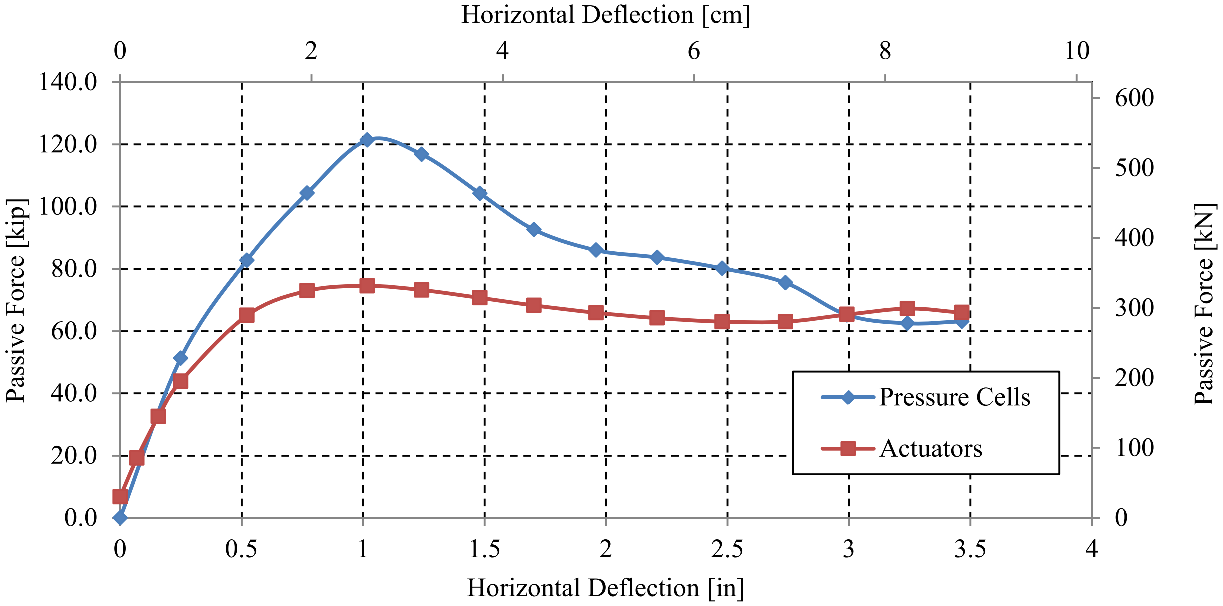

Figure 6-24: Passive force vs. deflection curve as estimated by the pressure cells and recorded by the actuators for the 30° skew test

Table 6-1: Pressure cell tributary widths and predicted passive forces as compared to data recorded by the actuators for the 30° skew test

	PP1499	*PP1497*	*PP1496*	*PP1500*	*PP1501*	*Total*	*Actuators*
Tributary Width [ft]	*3.3*	*2.7*	*1.8*	*1.8*	*2.4*	*11.9*	*11.9*
Deflection [in]	*Force [kip]*	*Force [kip]*	*Force [kip]*	*Force [kip]*	*Force [kip]*	*Force [kip]*	*Force [kip]*
0.00	0.0	0.0	0.0	0.0	0.0	0.0	6.8
0.25	14.5	11.8	6.2	6.6	12.3	51.2	43.9
0.52	23.0	18.9	10.2	11.0	19.7	82.8	65.0
0.77	29.1	23.6	12.7	14.0	24.9	104.3	72.9
1.02	34.0	27.1	14.7	16.5	29.0	121.3	74.5
1.24	26.9	22.9	14.8	19.9	32.3	116.8	73.2
1.48	23.4	13.6	12.7	22.1	32.4	104.2	70.7
1.70	22.0	12.0	11.4	21.4	25.8	92.6	68.3
1.96	22.8	11.8	11.7	16.7	22.9	86.0	65.9
2.21	24.0	11.5	11.1	15.7	21.3	83.6	64.2
2.48	23.6	10.6	10.2	15.5	20.3	80.2	63.0
2.74	23.0	9.7	8.7	14.9	19.2	75.5	63.0
2.99	21.2	8.7	6.9	12.2	16.2	65.2	65.3
3.24	21.7	9.0	6.3	11.8	13.7	62.5	67.2
3.5	22.3	9.4	6.5	12.2	12.7	63.1	65.9

7 ANALYTICAL FINDINGS

This chapter will compare measured passive force-displacement curves from this study to design methods published by (AASHTO, 2011) and (Caltrans, 2010) for approximating passive forces behind an abutment in bridge design. The computer programs PYCAP and ABUTMENT (Duncan & Mokwa, 2001b; Shamsabadi et al., 2007) will also be compared to test results. Backfill shear failure geometries and peak passive forces will then be compared to those predicted by the Log Spiral, Coulomb, and Rankine passive earth pressure theories.

7.1 AASHTO and Caltrans Passive Force versus Backwall Deflection Design Curves

As mentioned in Section 2.4.2, the AASHTO (2011) design manual gives the option of estimating the passive lateral earth pressure coefficient, k_p through Figure 3.11.5.4-2 of their design manual, or by means of the trial procedure given by Terzaghi et al. (1996) if a situation outside their given conditions exists. In using the AASHTO design manual, a passive soil pressure coefficient of 17.0 was calculated.

Figure 7-1 shows the predicted passive force vs. deflection curves calculated by both the AASHTO (2011) and Caltrans (2010) methods as compared to the 0°, 15°, and 30° skew unconfined backfill tests. As previously shown in Table 3-3, the directed shear tests for this study produced a soil friction angle that ranged between 40.4° and 42.3° depending upon which soil conditions were applied. Using computer optimization within PYCAP, the best-fitting soil friction value for this study was approximately 42°. Using this parameter, along with the other optimum soil parameters found using PYCAP, the AASHTO method appeared to reasonably estimate the passive force on the conservative side with a predicted passive force of 92% of the peak passive force found in the field. However, both methods greatly over-predict the passive force for skew angles of 15° and 30°, thus implying the need for a passive force reduction factor. A complete list of the parameters used within the AASHTO curve is provided in Table 7-1. The Ovesen (1964) 3D correction factor was included for direct comparison purposes.

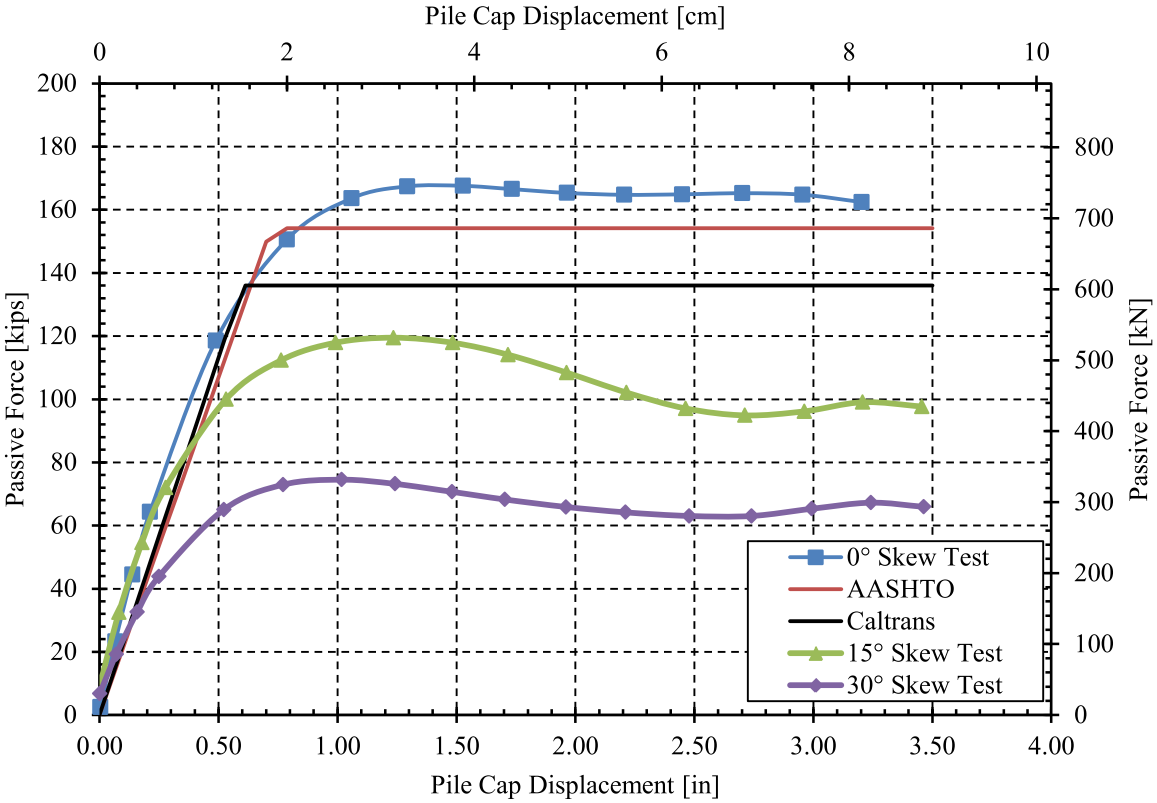

Figure 7-1: Comparison of Caltrans and AASHTO design curves with the passive force vs. backwall deflection curve for the 0°, 15°, and 30° tests

Table 7-1: AASHTO Soil and Wall Parameters

Parameter	*Value (ϕ=42)*	*Units*
Soil Friction Angle, ϕ	42	Degrees
Soil Unit Weight, γ_s	117 (18.4)	lbf/ft^3 (kN/m^3)
Abutment Width, w_2	11 (3.35)	ft (m)
Ovesen-Brinch Hansen 3D Width Correction Factor	1.511	–
Effective Width of Failure Wedge, w_1	16.62 (5.07)	ft (m)
Soil Cohesion, c	100 (4.79)	lbf/ft^2 (kN/m^2)
Abutment Height, H	3 (0.91)	ft (m)
Interface Friction Angle, δ	28.8	Degrees
Coefficient of Passive Earth Pressure, K_P	17.0	–

For the AASHTO design method, soil stiffness is dependent upon the assumed pile cap deflection at failure in relation to the height of the backwall. This method assumes failure at a deflection of 5% the height of the backwall. Although 5% is a reasonable estimate given that the actual failure deflection occurred at a distance of 4.2% the height of the backwall, a smaller value of 2.0% was used to obtain reasonable stiffness estimations. This parameter is still within the range suggested by the AASHTO design manual in Table C3.11.1-1. Decreasing the predicted deflection at failure was also appropriate because the hyperbolic nature of a true passive force-deflection curve implies a transitioning stiffness slope before failure is obtained. A bilinear curve can compensate for its simplicity by reducing the estimated failure deflection and creating a curve that better suites the initial stiffness of the hyperbolic shape.

Although the Caltrans method underestimated the peak passive force by an even greater amount, this bilinear curve provided relatively good agreement for the initial stiffness without making adjustments. The backfill soil stiffness parameter, Kabut = 50 kip/in/ft (28.7 kN/cm/m) was selected since this test fit the granular soil specifications given by Caltrans. The predicted peak passive force for Caltrans method was approximately 81.1% of the peak passive force found in the field, a decrease of more than 10% from AASHTO predictions. Parameters used in the Caltrans method design curve can be viewed in Table 7-2.

Table 7-2: Caltrans Soil and Wall Parameters

Parameter	*Value*	*Units*
Initial Backfill Stiffness, K_i	50 (28.7)	kip/in/ft (kN/mm/m)
Projected Wall Width, w	11 (3.35)	ft (m)
Ovesen-Brinch Hansen 3D Width Correction Factor	1.511	–
Effective Wall Width, w_e	16.62 (5.07)	ft (m)
Abutment Stiffness, K_{abut}	453 (79.4)	kip/in (kN/mm)
Wall Height, h	3 (0.91)	ft (m)
Effective Backwall Area, A_e	49.9 (4.63)	ft^2 (m^2)

7.2 Comparison of Results to Computer Programs PYCAP and ABUTMENT

Unlike the bilinear curves developed by the AASHTO and Caltrans methods, computer programs PYCAP and ABUTMENT (Duncan & Mokwa, 2001b; Shamsabadi et al., 2007) generated passive force vs. deflection curves with a hyperbolic shape. Figure 7-2 presents these two curves in comparison to actual test results from the 0° skew test. Computer optimization techniques enabled very accurate predictions for the PYCAP curve. All parameters lie within suggested range values provided by Duncan and Mokwa (2001b), AASHTO (2011) , and soil parameter tests performed in this study (Section 3.4.2). These values are shown in Table 7-3.

Soil strength parameters for the passive force-deflection curve produced by ABUTMENT are included in Table 7-4. These values are similar to those used in PYCAP except for a lower soil friction angle, a lower wall friction angle, the addition of the strain at 50% of the maximum load, ε_{50} and the failure ratio, R_f. Abutment adhesion was assumed to be negligible. The

ABUTMENT curve was developed using the "Log Spiral Composite Forces Method" with a 3D setting. Although this curve is shallower than the curve provided by field data, the initial stiffness and maximum passive pressure have decent agreement with actual test results. The ε_{50} of 0.0045 is higher than recommendations for clean sand (0.002-0.003), but Shamsabadi et al. (2007) also required a higher value than this range (0.0035) in their study as well.

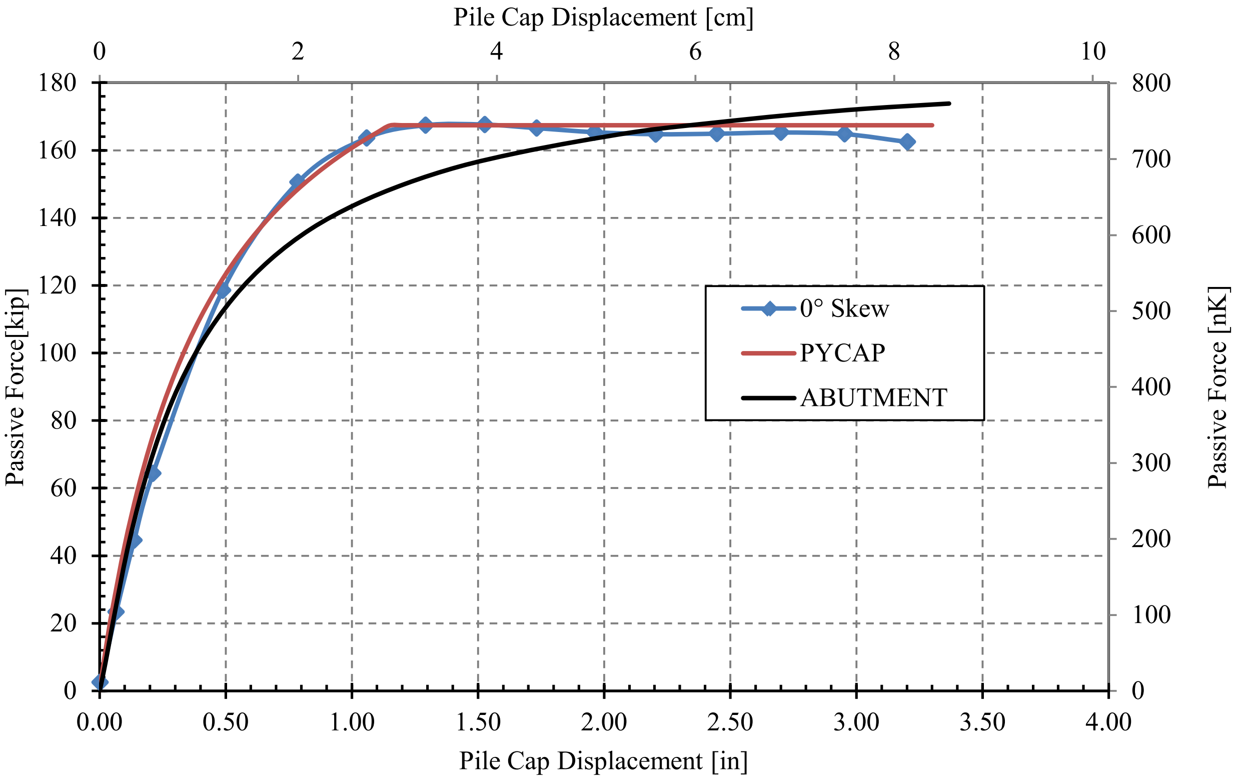

Figure 7-2: Comparison of PYCAP and ABUTMENT design curves with the passive force vs. backwall deflection curve for the 0° test

Table 7-3: PYCAP Soil and Wall Strength Parameters

Soil Strength Parameter	*Value*	*Units*
Cap Width, b (ft)	11.0 (3.35)	ft (m)
Cap Height, H (ft)	3.0 (0.91)	ft (m)
Cohesion, c	100 (4.79)	lbf/ft^2 (kN/m^2)
Soil Friction Angle, ϕ	42	Degrees
Wall Friction Angle, δ	28.8	Degrees
Initial Soil Modulus, E_i	415 (19,870)	kip/ft^2 (kN/m^2)
Poisson's Ratio, ν	0.25	–
Soil Unit Weight, γ_m	117 (18.4)	lbf/ft^3 (kN/m^3)
Adhesion Factor, α	1.0	–
Δ_{max}/H at Failure	0.032	–

Table 7-4: ABUTMENT Soil and Wall Strength Parameters

Soil Parameter	*Value*	*Units*
Friction Angle, ϕ	40.8	Degrees
Interface Friction Angle, δ	28	Degrees
Soil Density, γ	117 (18.4)	lbf/ft^3 (kN/m^3)
Cohesion, c	100 (4.79)	lbf/ft^2 (kN/m^2)
Strain at 50% of Max Load, ε_{50}	0.0045	–
Poisson's Ratio, ν	0.25	–
Failure Ratio, R_f	0.98	–

7.3 Comparison of Results to Rankine, Coulomb, and Log Spiral Methods

As stated in Section 2.3, the three most common methods for predicting total passive pressures are the Rankine, Coulomb, and Log Spiral methods. Their predicted total passive pressures for this study are provided in Table 7-5 along with actual test results from the 0° skew test (k_p values for each theory were obtained using PYCAP). As was expected, the Rankine method produced significantly lower predictions than actual test results. The resulting passive force was 61.3% less than the peak passive pressure. The Coulomb method is known to be well above the actual passive pressure. This also held true with an over-prediction of 75.0%. Both methods included the Ovesen (1964) 3D correction factor of 1.511 obtained in PYCAP.

The Log Spiral estimation also included the Ovesen (1964) 3D correction factor. Neglecting this factor would have significantly under-predicted the passive pressure, even with the high width to height ratio of this study. The Log Spiral method including 3D effects obtained a prediction within 0.10% of actual findings, thus making it the most accurate method.

Table 7-5: Comparison of Measured Total Passive Force for 0° Test to Values Predicted by Log Spiral, Coulomb, and Rankine Methods

Method	*Calculated Passive Force kip/ft (kN/m)*	*Total Passive Force kips (kN)*	*Total Passive Force Percent Error*
Log Spiral	10.1 (147.0)	167.4 (744.7)	-0.10%
Coulomb	17.6 (257.5)	293.2 (1304)	75.0%
Rankine	3.90 (56.9)	64.8 (288.3)	-61.3%
Test Results	15.2 (222.3)	167.6 (745.5)	N/A

Rankine, Coulomb, and Log Spiral methods can also be used to predict failure surface geometry within the soil backfill. Figure 7-3 compares predicted failure geometries of the various methods to the failure surface measured in the field. For the 0° skew test, the Log Spiral method most closely estimated the failure plane of the backfill. The Log Spiral failure plane followed a similar shape throughout the soil before surfacing within 10.4% of actual results. As predicted, the Rankine method underestimated the failure plane while the Coulomb method overestimated at values of -32.6% and 85.9% from the actual surfacing distance.

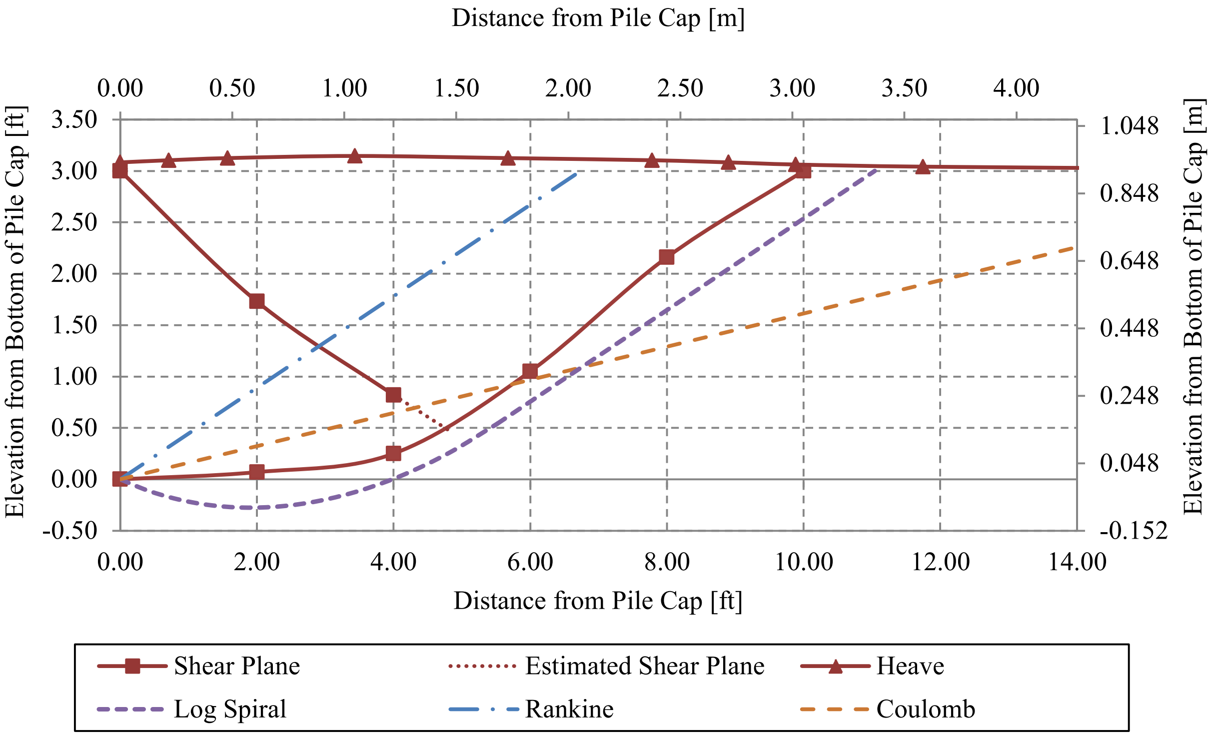

Figure 7-3: Actual and predicted failure surface geometry for the 0° skew test

8 CONCLUSION

This thesis presented results from laterally loaded, large-scale pile cap tests with densely compacted sand at a width of 11 ft (3.35 m) and a height of 3 ft (0.91 m). The backwall interface was adjusted to fit three various skew angles including: 0°, 15° and 30°. The behavior of both the pile cap and adjacent soil backfill were monitored under these conditions, and the following conclusions and recommendations are made:

8.1 Conclusions

1. Increasing the skew angle has little effect on initial stiffness but significantly reduces the peak passive force. This reduction is not accounted for in current bridge design methods but is consistent with previous studies performed by Franke (2013), Marsh (2013), Jessee (2012), and Shamsabadi et al. (2006).
2. The force reduction factor proposed by Rollins and Jessee (2012) provides relatively good agreement for the 3-ft (0.91-m) unconfined backfill tests. Therefore, increasing the width to height ratio of a backwall (specifically from 2:1 to 3.7:1) appears to have little effect on the strength reduction ratio. This is consistent with numerical analysis results performed by Shamsabadi et al. (2006) with a width to height ratio of 13.6:1.

3. The peak passive pressure is achieved at deflections between 2 and 5% of the backwall height. This is consistent with research from non-skewed abutments (Rollins & Sparks, 2002). However, tests in this study indicate that this deflection decreases with increased skew.
4. As the skew angle increases, the pile tends to deflect exhibiting more transverse displacement and rotation. During this movement, the pile cap rotates away from the acute corner of a skew and into the obtuse corner.
5. Both bridge deck rotation and underestimations of the passive force cause significant damage to skewed bridges, causing them to underperform and even fail during earthquakes. Thermal expansion can also induce damage on skewed bridges.
6. As predicted by Shamsabadi et al. (2006), the effective width in relation to the orientation of the backwall decreases with increased skew angle. Results from this study found the decrease to be approximately 26% between skews of 0° and 30°. However, the effective width in the longitudinal direction were unaffected by skew angle.
7. The Log Spiral method is more accurate than the Rankine and Coulomb methods in predicting the peak passive force and internal failure plane. The Rankine method greatly underestimates the passive resistance and failure plane while the Coulomb theory considerably overestimates them.
8. The governing failure plane for skewed bridges follows a log spiral curve that transitions into a linear plane, as proposed by Terzaghi (1943). This failure plane

becomes more linear as skew angle increases, specifically on the acute side of the pile cap, which is similar to findings by Marsh (2013).

9. Design methods published by AASHTO (2011) and Caltrans (2010) both underestimate the peak passive force for wide non-skewed bridge abutments with AASHTO being more accurate. Additionally, the failure deflection of 5% of the backwall height recommended by AASHTO produces extremely low soil stiffness values. A deflection of 2.0% was required to obtain a reasonable soil stiffness.
10. The passive force-deflection curves predicted by computer programs PYCAP and ABUTMENT (Duncan & Mokwa, 2001b; Shamsabadi et al., 2007) provide good agreement with curves obtained in these tests, with PYCAP being the most accurate of the two. However, a higher ε_{50} value of 0.0045 was required to obtain reasonable accuracy with ABUTMENT.
11. Horizontal pressure distribution does not linearly increase for skewed bridges as predicted by Sandford and Elgaaly (1993). Instead, pressure tends to shift unevenly during longitudinal movement with the greatest pressures occurring on the obtuse corner of the pile cap. Additionally, both corners of the pile cap experience higher pressure than in the middle portion as is suggested by the elastic theory.
12. As the skew angle increases, shear resistance decreases and applied shear force increases on the soil-backwall interface until they converge at a skew angle of approximately 30°.
13. Lateral displacement required for shear failure on a soil-backwall interface is smaller for 15° and 30° skews than for the 0° skew recommendations provided

by Duncan and Mokwa (2001b). However, the movement parallel to the skew of the backwall interface is larger for 15° and 30° skews than for the 0° skew recommended values.

14. Piles supporting the pile cap produce very little interference with the lateral forces unaccounted for in longitudinal baseline testing.

8.2 Recommendations

15. Further large-scale testing should be performed at a backfill height of 3 ft (0.91 m) to verify findings presented in this study and the lab-scale tests performed by Rollins and Jessee (2012).
16. Tests should be conducted to examine only 2D effects for backfills with larger width to height ratios and for backfills where embankments aren't capable of fully developing 3D effects.
17. Testing should be performed that allows the pile cap to rotate freely.
18. Surface strain and internal shear failure should be measured in the center, acute corner, and obtuse corner of the backfill to increase understanding of soil behavior.

REFERENCES

AASHTO. (2011). *LRFD Bridge Design Specifications*.

Apirakvorapinit, P., Mohammadi, J., M.ASCE, & Shen, J. (2012). Analytical Investigation of Potential Seismic

Damage to a Skewed Bridge. *American Society of Civil Engineers, 10.1061(ASCE)*(SC.1943-5576.0000094).

Apirakyorapinit, P., Mohammadi, J., & Shen, J. (2012). Analytical Investigation of Potential Seismic Damage to a Skewed Bridge. *Practice Periodical on Structural Design and Construction, 16*(1), 5-12.

Bozorgzahah. (2008). Experimental and Analytical Investigation on Stiffness and Ultimate Capacity of Bridge Abutments.

Burke Jr., M. P. (1996). Semi-Integral Bridges: Movements and Forces. *Transportation Research Record, 1460*.

Burke Jr., M. P., & Gloyd, C. S. (1997). Emergence of Semi-Integral Bridges. *Transportantion Research Record*, 1594-1603.

Caltrans. (2001). *Seismic Design Criteria Version 1.2*. Sacramento, California: California Department of Transportation.

Caltrans. (2010). *Seismic Design Criteria Version 1.6*. Sacramento, California: California Department of Transportation.

Christensen, D. S. (2006). *Full Scale Static Lateral Load Test of a 9 Pile Group in Sand.* M.S. Thesis, Brigham Young University, Provo, UT.

Cummins, C. (2009). *Behavior of a Full-Scale Pile Cap with Loosely and Densely Compacted Clean Sand Backfill Under Cyclic and Dynamic Loadings.* M.S. Thesis, Brigham Young University, Provo, UT.

Danisch, L. A., Lowery-Simpson, M., & Abdoun, T. (2005).

Dicleli, M., & Erhan, S. (2010). Effect of soil bridge interaction on the magnitude of internal forces in integral abutment bridge components due to live load effects. *Engineering Structures, 32*, 129-145.

Duncan, J. M., & Mokwa, R. L. (2001a). Experimental Evaluation of Lateral-Load Resistance of Pile Caps. *Journal of Geotechnical and Geoenvironmental Engineering, ASCE, 127*(2), 185-192.

Duncan, J. M., & Mokwa, R. L. (2001b). Passive Earth Pressures: Theories and Tests. *Journal of Geotechnical and Geoenvironmental Engineering*(March 2001), 248-257.

Elnashai, A. S., Gencturk, B., Kwon, O., Al-Qadi, I. L., Hashash, Y., Roesler, J. R., . . . Valdivia, A. (2010). The Maule (Chile) Earthquake of February 27, 2010: Consequence Assessment and Case Studies (pp. 190): Department of Civil and Environmental Engineering, University of Illinois at Urbana-Champaign.

FHWA. (2011). Postearthquake Reconnaissance Report on Transportation Infrastructure Impact of the February 27, 2010, Offshore Maule Earthquake in Chile. In T.-F. H. R. Center (Ed.). McLean, VA.

Franke, B. (2013). *Passive Force on Skewed Abutments with Mechanically Stabilized Earth (MSE) Wingwalls Based on Large-Scale Tests".* M.S. Thesis, Brigham Young University, Provo, UT.

Hassiotis, S., & Xiong, K. (2007). Deformation of Cohesionless Fill Due to

Cyclic Loading. Hoboken, N.J.: Stevens Institute of Technology.

Hegger, J., Ricker, M., Ulke, B., & Ziegler, M. (2007). Investigations on the Punching Behaviour of Reinforced Concrete Footings. *Engineering Structures, 29*(9), 2233 - 2241

Jessee, S. (2012). *Passive Force-Deflection Curves for Skewed Abutments.* Thesis, Brigham Young University, Provo, UT.

Johnson, S. R. (2003). *Static Lateral Load Testing of a Full-Scale Pile Group Spaced at 5.65 Pile Diameters.* M.S., Brigham Young University, Provo, UT.

Kumar, J., & Subba Rao, K. S. (1997). Passive pressure coefficients, critical failure surface and its kinematic admissibility. *Geotechnique, 47*(1), 185-192.

Kunin, J., & Alampalli, S. (1999). Integral Abutment Bridges: Current Practice in the United States and Canada (N. Y. S. D. o. Transportation, Trans.). In G. E. Pataki (Ed.), *Special Report 132*. Albany, New York: Transportation Research and Development Bureau.

Lee, K. L., & Singh, A. (1971). Relative Density and Relative Compaction. *Journal of Soil Mechanics and Foundations Design, 97*(7), 1049-1052.

Lemnitzer, A., Ahlberg, E., R., N., Shamsabadi, A., Wallace, J., & Stewart, J. (2009). Lateral Performance of Full-Scale Bridge Abutment Wall with Granular Backfill. *Journal of Geotechnical and Geoenvironmental Engineering, 135*(4), 8.

Levesque, C. (2012, December 16, 2012). [M.Sc.E., Measurand Inc.].

Marsh, A. K. (2013). *Evaluation of Passive Force on Skewed Bridge Abutments with Large-Scale Tests.* M.S. Thesis, Brigham Young University Provo, UT.

Nasr, A., & Rollins, K. M. (2010). *Numerical Analysis of Limited Width Dense Gravel Backfills for Plane Strain Conditions*. Paper presented at the 2011 Pan-Am CGS Geotechnical Conference.

Nichols, S. (2012). [Principal Geotechnical Engineer at the FHWA Office of Bridge Technology].

Ovesen, N. K. (1964). Anchor Slabs, Calculation Methods and Model Tests (Vol. Bulletin No. 16). Copenhagen: The Danish Geotechnical Institute.

Rollins, K. M., & Cole, R. T. (2006). Cyclic Lateral Load Behavior of a Pile Cap and Backfill. *Journal of Geotechnical and Geoenvironmental Engineering, ASCE, 132*(9), 1143-1153.

Rollins, K. M., Gerber, T., Cummins, C., & Herbst, M. (2009). *Monitoring Displacement vs. Depth in Lateral Pile Load Tests Using Shape*

Accelerometer Arrays. Paper presented at the 17th International Conference on Soil Mechanics & Geotechnical Engineering, Alexandria, Egypt.

Rollins, K. M., Gerber, T. M., Cummins, C. R., & Pruett, J. M. (2010). Dynamic Pressure on Abutments and Pile Caps. In B. Y. University, U. D. o. Transportation & F. H. Administration (Eds.), *Report No. UT-10.18* (pp. 255): Utah Department of Transportation.

Rollins, K. M., & Jessee, S. (2012). Passive Force-Deflection Curves for Skewed Abutments. *Journal of Bridge Engineering, 17*(5).

Rollins, K. M., King, R., Synder, J. L., & Johnson, S. R. (2005). *Full-Scale Lateral Load Tests of Pile Groups and Drilled Shafts in CLay*. Paper presented at the Intl. Conf. on Soil-Structure Interaction, Calculation Methods and Engineering Practice, Moscow.

Rollins, K. M., & Sparks, A. E. (2002). Lateral Load Capacity of a Full-Scale Fixed-Head Pile Group. *Journal of Geotechnical and Geoenvironmental Engineering, ASCE, 128*(9), 711-723.

Sandford, T. C., & Elgaaly, M. (1993). Skew Effects on Backfill Pressures at Frome Bridge Abutments. *Field Performance of Structures and Nondestructive Evaluation of Subsurface Infrastructure*, 1-11.

Shamsabadi, A., Kapuskar, M., & Zand, A. (2006). *Three-Dimensional Nonlinear Finite-Element Soil-Abutment Structure Interaction Model for Skewed Bridges*. Paper presented at the 5th National Seismic Conference On Bridges and Highways, San Francisco, CA.

Shamsabadi, A., Rollins, K. M., & Kapaskur, M. (2007). Nonlinear Soil-Abutment-Bridge Structure Interaction for Seismic Performance-Based Design. *Journal of Geotechnical and Geoenvironmental Engineering, ASCE, 133*(6), 707-720.

Shehu, J. (2009). *Evaluation of the Foundation and Wingwalls of Skewed Semi-Integral Bridges with Wall Abutments.* Master of Science, Ohio University.

Soubra, A.-H. (2000). Static and seismic passive earth pressure coefficients on rigid retaining structures. *Canadian Geotechnical Journal, 37*(2), 463-478.

Steinberg, E., & Sargand, S. (2010). Forces in Wingwalls from Thermal Expansion of Skewed Semi-Integral Bridges *Report No. FHWA/OH-2010/16* (pp. 87). Athens, OH: Prepared by Ohio University for Ohio Department of Transportation.

Taylor, A. J. (2006). *Full-Scale-Lateral-Load Test of a 1.2 m Diameter Drilled Shaft in Sand.* M.S., Brigham Young University, Provo, Utah.

Terzaghi, K. (1943). *Theoretical Soil Mechanics*. New York: John Wiley and Sons, Inc.

Terzaghi, K., Peck, R. B., & Mesri, G. (1996). Soil Mechanics in Engineering Practice, 3rd Ed. New York: John Wiley & Sons.

Toro, F., Rubilar, F., Hube, M. A., Santa-María, H., & Cabrera, T. (2013). *Statistical Analysis of Underpasses Damaged During 2010 Chile Earthquake*. Paper presented at the National Seismic Conference on Highways and Bridges.

Unjohn, S. (2012, March 1-4). *Repair and Retrofit of Bridges Damaged by the 2010 Chile, Maule Earthquake.* Paper presented at the International Symposium on Engineering Lessons Learned from the 2011 Great East Japan Earthquake, Tokyo, Japan.

Watanabe, G., & Kawashima, K. (2004). *Effectiveness of Cable-Restrainer for Mitigating Rotaion of a Skewed Bridge Subjected to Strong Ground Shaking*. Paper presented at the 13th World Conference on Earthquake Engineering, Vancouver, B.C., Canada.

Zhu, D. Y., & Qian, Q. (2000). Determination of Passive Earth Pressure Coefficient by the Method of Triangular Slices. *Canadian Geotechnical Journal, 37*(2), 485-491.